A METHODOLOGY FOR LINING DESIGN OF CIRCULAR MINE SHAFTS IN DIFFERENT ROCK MASSES

A THESIS SUBMITTED TO
THE GRADUATE SCHOOL OF NATURAL AND APPLIED SCIENCES
OF
MIDDLE EAST TECHNICAL UNIVERSITY

BY

ERDOĞAN GÜLER

IN PARTIAL FULFILLMENT OF THE REQUIREMENTS
FOR
THE DEGREE OF MASTER OF SCIENCE
IN
MINING ENGINEERING

JANUARY 2013

Approval of the thesis:

A METHODOLOGY FOR LINING DESIGN OF CIRCULAR MINE SHAFTS IN DIFFERENT ROCK MASSES

submitted by ERDOĞAN GÜLER in partial fulfillment of the requirements for the degree of **Master of Science in Mining Engineering Department, Middle East Technical University** by,

Prof. Dr. Canan Özgen
Dean, Graduate School of **Natural and Applied Sciences** _____

Prof. Dr. Ali İhsan Arol
Head of Department, **Mining Engineering** _____

Asst. Prof. Dr. Hasan Öztürk
Supervisor, **Mining Engineering Dept., METU** _____

Examining Committee Members:

Prof. Dr. Celal Karpuz
Mining Engineering Dept., METU _____

Asst. Prof. Dr. Hasan Öztürk
Mining Engineering Dept., METU _____

Assoc. Prof. Dr. Levend Tutluoğlu
Mining Engineering Dept., METU _____

Assoc. Prof. Dr. Hakan Başarır
Mining Engineering Dept., METU _____

Asst. Prof. Dr. Mehmet Ali Hindistan
Mining Engineering Dept., Hacettepe University _____

Date 30.01.2013

I hereby declare that all information in this document has been obtained and presented in accordance with academic rules and ethical conduct. I also declare that, as required by these rules and conduct, I have fully cited and referenced all material and results that are not original to this work.

Name, Last name : Erdoğan Güler

Signature :

ABSTRACT

A METHODOLOGY FOR LINING DESIGN OF CIRCULAR MINE SHAFTS IN DIFFERENT ROCK MASSES

Güler, Erdoğan
M.Sc., Department of Mining Engineering
Supervisor: Asst. Prof. Dr. Hasan Öztürk
January 2013, 72 pages

The objective of this thesis is to predict lining thickness inside circular mine shafts. A numerical study with different rock mass strengths and different in-situ non-hydrostatic stresses are carried out in 2D shaft section models to predict pressures that develop on lining support. An iterative process of applying support pressure until observing no failure zone around shaft is used to simulate lining support pressure for each individual model. Later, regression and fuzzy logic analyses are carried out to find a pressure equation for all of the models. Finally, the pressure equation derived is used in elastic "thick-walled cylinder" equation to calculate the lining thickness required to prevent the development of a failure zone around shafts. At the end of this research, a computer program "Shaft 2D" is developed to simplify the lining thickness calculation process.

Keywords: Lining Thickness, Shaft Support, Shaft, Non-Hydrostatic Stresses

ÖZ

FARKLI KAYA KÜTLELERİNDEKİ DAİREDEL MADEN KUYULARININ TAHKİMAT TASARIMI İÇİN BİR YÖNTEM

Güler, Erdoğan
Yüksek Lisans, Maden Mühendisliği Bölümü
Tez Yöneticisi: Yrd. Doç. Dr. Hasan Öztürk
Ocak 2013, 72 sayfa

Bu tezin amacı dairesel kesitli maden kuyularının duraylı kalabilmesi için gerekli tahkimat kalınlığını tahmin etmektir. Tahkimat desteğinin üzerinde gelişen basınçları tahmin etmek için, 2B kuyu kesiti örneklerinde, farklı kaya kütlesi dayanımları ve farklı arazi yüklemeleri için tasarlanmış bir sayısal çalışma yapılmıştır. Her bir farklı durumun tahkimat basıncını modellemek için, kuyunun etrafında kırılmış bölge kalmayana kadar destek basıncı uygulamanın döngüsel bir süreci kullanılmştır. Daha sonra, destek basıncına uygun bir eşitlik bulmak için regresyon ve bulanık mantık çözümlemeleri yapılmştır. Son olarak, kuyuların çevresinde kırılmış bir bölgenin oluşumunu önlemek için, bulunan basınç eşitliği "kalın duvarlı silindir" eşitliğinde kullanıldı. Bu çalışmanın sonucunda, tahkimat kalınlığı hesaplama surecini kolaylaştırmak için bir bilgisayar yazılımı olan “Shaft 2D” geliştirilmiştir.

Anahtar Kelimeler: Tahkimat kalınlığı, Kuyu Tahkimatı, Kuyu, Hidrostatik Olmayan Gerilmeler

ACKNOWLEDGMENTS

I would like to thank my supervisor Asst. Prof. Dr. Hasan Öztürk for his supervision, recommendations, criticism, and vision during the course of this research.

I also wish to express my sincere gratefulness to Prof. Dr. Celal Karpuz, Assoc. Prof. Dr. Levend Tutluoğlu, Assoc. Prof. Dr. Hakan Başarır and Asst. Prof. Dr. Mehmet Ali Hindistan for their suggestions, comments guidance and valuable contributions during various stages of the research and for serving in the M.Sc. Thesis committee.

TABLE OF CONTENTS

LIST OF FIGURES

FIGURES

LIST OF TABLES

TABLES

LIST OF SYMBOLS

The main symbols used in this study are listed below, together with their descriptions. Besides, symbols introduced for any equation are also defined 'locally' after those equations.

Symbol	Description	Unit
a	Hoek-Brown Constant	
d	Diameter of Shaft	m
D	Disturbance Factor	
E_c	Modulus of Concrete or Shotcrete	MPa
E_i	Modulus of Intact Rock	MPa
f_c	Compressive Strength of Concrete or Shotcrete	MPa
ϕ	Internal Friction Angle	
G	Shear Modulus	GPa
GSI	Geological Strength Index	
J	Cost Function	
k	Horizontal Stress to Vertical Stress	
k1	1st Horizontal Stress to Vertical Stress	
k2	2nd Horizontal Stress to Vertical Stress	
m_i	Hoek-Brown Constant	
m_b	Reduced Value of m_i	
σ_1	Major Effective Principal Stress	MPa
σ_3	Minor Effective Principal Stress	MPa
σ_h	Horizontal Stress	MPa
σ_{h1}	1st Horizontal Stress	MPa
σ_{h2}	2nd Horizontal Stress	MPa
σ_{rr}	Radial Stress	MPa
$\sigma_{\theta\theta}$	Tangential Stress	MPa
$\tau_{r\theta}$	Shear Stress	MPa
σ_z	Vertical Stress	MPa
σ_{ci}	Compressive Strength of Intact Rock	MPa
p_i	Support Pressure	MPa
p_o	Outer Pressure	MPa
r	Radius of Shaft	m
r_o	Outer Radius of Lined Shaft	m
R	Questioned Distance	m
RMSE	Root Mean Square Error	
s	Hoek-Brown Constant	
t_c	Thickness of Lining	m
u_r	Radial Displacement	mm
u_θ	Tangential Displacement	mm
γ	Unit Weight of Rock	MN/m^3
ν	Poisson's Radio	
z	Depth of Shaft Section	m

CHAPTER 1

INTRODUCTION

1.1. General Remark

The purpose of the engineered structures influences their design. For example, stabilization measures required for an excavation will depend on whether it is to be a permanent structure for a civil engineering project or a temporary structure for a mine. For civil, mining and petroleum engineering, there are different constraints on tolerable disturbance caused by excavation, on rock displacements, on type of instability which can be allowed to occur, on type of support that may be installed, etc. An engineer has to consider what types of instability might be expected. Is it the instability of rock blocks defined by pre-existing fractures, stress-induced failure of intact rock, or a combination of them? The consequences of interaction between high stresses and rock mass structure may result in a considerable amount of displacement of the individual rock blocks and the significant distortion of installed support (Harrison & FREng, 2000).

Lining of shafts works for two purposes: support for shaft equipment and support for walls of excavations. Although, in shafts having short life span sunk in competent rock, a rectangular shape with timber support is still commonly used, in modern and large shafts, concrete lining is used almost completely. Circular shape reduces airflow resistance, facilitates the sinking process and permits taking full advantage of the structural features of concrete. Concrete lining with its numerous advantages may be used over formerly popular materials such as brick and concrete blocks. Its placement is mechanized, resulting in high sinking rates as well as lower cost. Moreover, concrete strength may be adjusted according to need (for instance, 20 to 50 MPa) and water tightness of the lining can be achieved within aquifers with moderate head (Unrug, 1992).

1.2. Problem Statement

The term support generally means procedures and materials used to improve stability and preserve load-carrying capability of rocks near the boundaries of underground excavations. The main objective of support application is to mobilize and protect the inherent strength of rock masses so that they become self-supporting. To sum up, support is applied as a reactive force against surface of an excavation and includes practices like timber, fill, shotcrete, mesh, steel, concrete sets, reinforced concrete and liners.

The determination of lining thickness around shafts may be done by using one of the three ways: numerical, empirical or analytical methods. Analytical methods are assume that rock and liner material behave elastically and the pressure acting on the liner is hydrostatic. In reality, rock mass and liner material behaves elasto-plastic, which means that the material will behave plastically if it is over stressed. This kind of behavior can only be modeled with numerical modeling. It should also be noted that hydrostatic stress around the shaft perimeter is not always the case and also shaft is sunk through different rock mass layers with different material behaviors.

1.3. Objectives

The ultimate objective of this study is to compute lining thickness needed to support circular mine shafts in jointed weak to hard rock mass. For this reason, a numerical study including different rock mass strengths and different in-situ non-hydrostatic stress states is carried out in 2D shaft section models.

In the numerical modeling work, support pressure applied to the opening walls simulates lining support for circular mine shafts. In order to simulate support pressure for each shaft section model, an iterative process of applying support pressure is utilized until no failure region around the shaft section detected. Therefore, deriving an accurate for shaft support pressure in different rock masses and in different in-situ stress cases is another objective of this study.

Regression and fuzzy logic analyses are carried out to find the most proper support pressure equation for all of the models. At the end of the study, a lining thickness equation is generated by integrating the pressure equation obtained from the numerical study to the elastic "thick-walled cylinder" solution. In addition, a user friendly computer software package with graphical interface based on the lining thickness equation is developed to make the tedious lining thickness computation process easier for users.

1.4. Outline of the Thesis

Introduction of the thesis gives some main point about the thesis. Then, literature survey chapter presents commonly used analytical, empirical and numerical studies of support pressures and lining thickness calculations for mine shafts. In numerical modeling chapter, the numerical analysis method used to calculate support pressure is explained in detail. In this section, also the results of the parametric studies are given. In regression analysis chapter, the results of the parametric studies are used to obtain a regression equation for support pressure with minimum error. In evaluation of the regression result with fuzzy logic chapter, regression equations found for support pressure are compared in terms of their consistency. In lining support design chapter, lining thickness is given and it is integrated to the computer program "Shaft 2D". Also, a number of examples are presented. Finally, in the last chapter, conclusions and recommendations are presented.

CHAPTER 2

LITERATURE SURVEY

In this chapter, some procedures for shaft design, analytical studies in elastic theory, numerical and empirical methods for shaft lining design are explained.

2.1. Shaft Design

2.1.1. Shaft Radius

The radius of the shaft may be determined by considering the followings (Unrug, 1992):

- Lateral dimensions of hoisting conveyances, other installations like a ladder way and adequate distances between each and lining,
- Designed amount of airflow to satisfy ventilation necessities.

2.1.2. Shaft Collar

The shaft collar is the upper part of the shaft extending to the first footing and must be anchored in competent rock. The dimensions of a collar, for example, its depth, cross section and thickness depend on shaft functions, character of over-burden rocks, hydrologic conditions, resulting water, ground pressures, sinking method and additional loading conditions when appropriate. Sinking and construction shaft collar depend on geo-mechanical and hydrologic conditions. A collar is required for a shaft or raise entry used by an underground mine. In addition to providing a mine entrance, a shaft collar of a production shaft implements the followings (Unrug, 1992):

- Keeping shaft watertight,
- Providing a top anchor for shaft sets and plumb lines necessary for shaft surveying,
- Providing space for shaft sinker to install equipment before main excavation initiates,
- Supporting a portion of headframe.

Also, collars are essential for ventilation shafts, service shafts and all raises reaching surface. Constructing collars in a rock outcrop or shallow overburden is comparatively straightforward. However, constructing collars may be a major task for deep and particularly water bearing soil overburdens. The same is true of a portal, but, for deep and water bearing overburdens, construction may be harder or even impractical. Shaft and raise collars are usually lined by concrete (Unrug, 1992).

The collar of a production shaft generally has 24 inches concrete lining in overburden and 18 inches concrete lining in weathered bedrock. The collar of a ventilation shaft generally has 18 inches concrete lining in overburden and 12 inches concrete lining in weathered bedrock. A concrete shaft collar has minimum 92 feet depth. If a long round jumbo is used to sink, it is 120 feet (Vergne, 2003).

2.1.3. Shaft Lining

The type of lining mostly depends on the followings (Unrug, 1992):

- Hydrogeological conditions,
- Function of shaft,
- Intended lifespan of shaft,
- Shape and depth of shaft ,
- Obtainability of building materials and
- Cost of construction.

Geotechnical properties and hydrologic conditions may significantly affect deciding shaft lining. On the other hand, the chemical activity like corrosiveness of the water can also be an important factor. Since modern shafts often have automatically operating hoisting gear sensitive to moisture, they should be dry. Main shafts are usually planned for the entire mine lifespan, so they are constructed according to minimum repairs and maintenance times. There are two kind of support for shaft (Unrug, 1992):

- Temporary support and
- Permanent support.

Temporary supports protect crew and equipment from falling rocks of the exposed shaft wall and they are used while the face is advancing. When the work at the face is postponed, temporary supports are dismantled and a concrete form is located. If the removal of the temporary lining produces safety problems, concrete can be poured over temporary support. One of the most popular types of temporary lining are steel rings (Unrug, 1992).

There are several different permanent lining systems along with shaft design and environmental settings like rock formations. While shotcrete is generally sufficient in strong rocks, a combination of rock bolts with mesh and shotcrete can be applied in fractured zones. Permanent lining for water bearing weak strata can be made of reinforced concrete or steel, as a single (with stiffening rings) or double cylinder with concrete fill between the outer and inner segments. Permanent linings can be listed as follows (Unrug, 1992):

- Timber,
- Brick or concrete blocks,
- Concrete monolithic,
- Reinforced concrete,
- Tubbing (cast iron and precast elements),
- Shotcrete, various systems (e.g., with mesh) and
- Anchor bolts.

Linings of shafts generally consist of a combination of the lining types above. In modern shafts, timber lining is very rarely used. They are only applied in auxiliary shafts with a short lifespan like inter-level blind shafts. Brick lining was popular before the mechanized shaft sinking. Some typical features of brick lining are simplicity and ease of construction, ability to carry load instantly, ease of repairs and resistance to corrosive waters. The latter can be beneficial in certain conditions. The disadvantages of brick lining can be listed as follows (Unrug, 1992):

- Time and labor consuming erection,
- Low strength,
- High cost if employment is expensive and
- Substantial permeability.

Concrete block lining is a type of improved brick lining with a reduced number of seams and a higher strength of a concrete shaft wall. This lining is less labor intensive when compared to brick lining. Monolithic concrete lining is the most popular shaft lining. It has many advantages when compared to other lining types (Unrug, 1992):

- Possibility of complete mechanization of construction with slip or switch forms and by transporting concrete through slicklines,
- Good bond between lining and shaft wall leading to no shaft foundations,
- Reduced labor intensity (3 to 6 times) and costs (30 to 40 %) when compared to brick lining,
- High strength causing less excavation.

The disadvantages of monolithic concrete lining are as follows (Unrug, 1992):

- Less resistance to corrosive waters
- Sensitivity to movement of rock masses
- Inability to immediately take load after settlement and
- Difficulty to repair.

There are several technologies to construct monolithic concrete lining. After sinking in series, short segments of shaft, 4 to 5 m in length, are lined with a collapsible steel form, which is relocated after concrete sets. This type of lining is not a monolith but consists of segments with seams. When the shaft is sunk in long lifts, a sliding concrete form can be applied. Then, longer sections of monolithic lining are obtained (Unrug, 1992)

Other than standard monolithic concrete liner, there are liners joining a steel plate into their design (Vergne, 2003):

- Steel plate and concrete composite ("sandwich liner"),
- Perforated steel liner ("leaky liner") and
- Steel hydrostatic liner (water-tight).

The sandwich liner benefits from strength of steel and inertia of concrete. For the composite to act together, there should be a near equality of the ratios of strength to stiffness for each of the components. Shear connectors help ensure composite action. These liners are seldom come across but still applied to shafts in hard rock (Vergne, 2003).

Leaky liners have occasional use where wall rock of shaft or raise must be kept from unraveling. Upon installation, annulus between liner and rock is filled, usually with pea gravel. Perforations ensure that no pressure builds up because of ground water. Design of leaky liners only concern the minimum necessary thickness for handling. Handling is not as severe a problem as it is for the hydrostatic liner. A plate thickness equal to the radius/144 is generally suitable (Vergne, 2003).

Steel hydrostatic liners have numerous uses in hard rock mine shafts having severe groundwater circumstances. Usual hydrostatic liners are made of a cylindrical steel shell reinforced with stiffening rings. A shell is intended for compressive strength and rings deliver extra resistance to buckling. Mild steel is suggested because it is least affected by residual stresses. (Vergne, 2003).

Shotcrete lining can used as regular shotcrete, shotcrete with rock bolts, reinforced concrete and reinforced concrete with bolts. Shotcrete is mostly applicable in dry shafts in rocks having good strength. Particularly, shotcrete is very suitable for blind shafts of smaller diameter where use of concrete methods is restricted. Shotcrete has several very pretty features like very good binding with rock, tightness and high strength because of low water to cement ratio. However, shotcrete is mostly used in combination with rock bolts and mesh. These are usually installed as a temporary support, before or after the first shotcreting. Lastly, shotcrete covers mesh pinned to shaft wall with bolts and makes a strong but thin shell of lining (Unrug, 1992).

Rock bolt lining is used mainly in salt mine shafts. Salt has creep features and exert too much pressure on a rigid shaft lining by flowing toward opening. Two main systems may be used in such situations. If salt rock has good shape, no lining is required for ground control. If there are laminations and a general trend to weathering creating worse conditions, rock bolts and mesh made from synthetic materials such as plastic (not corroding) are used (Unrug, 1992).

2.2. Elastic Theory

Stress concentration around excavations in rock can be explained by determining the distribution of stresses in a thick-walled cylinder subject to uniformly distributed radial pressures inside and outside. As the outer radius of the cylinder goes to infinity, the problem reduces to the determination of stress about a circular opening in a medium of indefinite extent.

Stresses around a thick-walled cylinder subjected to support pressure p_i and outer pressure p_o, as shown in Figure 2.1 are given in terms of polar coordinates.

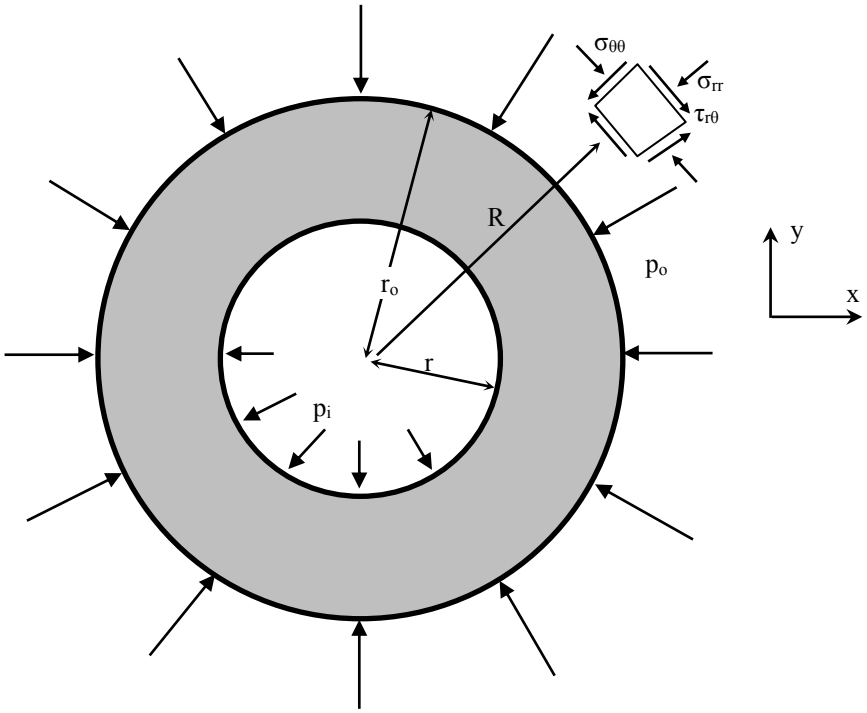

Figure 2.1 A thick-walled cylinder in elastic condition.

The radial stress around the opening given by Brady and Brown (2005) in Figure 2.1 is

$$\sigma_{rr} = \frac{r^2 r_o^2 (p_i - p_o)}{R^2 (r_o^2 - r^2)} + \frac{p_o r_o^2 - p_i r^2}{(r_o^2 - r^2)} \quad (1)$$

The tangential stress for the opening is

$$\sigma_{\theta\theta} = -\frac{r^2 r_o^2 (p_i - p_o)}{R^2 (r_o^2 - r^2)} + \frac{p_o r_o^2 - p_i r^2}{(r_o^2 - r^2)} \quad (2)$$

The shear stress acting on the tangential-radial plane is

$$\tau_{r\theta} = 0 \quad (3)$$

where r is inner radius of the opening; r_o is outer radius of the opening; p_i is pressure at inner surface; p_o is pressure at outer surface; and R is the questioned distance where the stresses above take place.

The complete solutions for distribution of stresses and displacements around a circular opening in an elastic opening are given by Kirsch. Figure 2.2 shows the circular cross section of a long excavation in a medium subject to biaxial stress: $p_{yy} = p_o$ and $p_{xx} = k*p_o$ where k is the stress ratio.

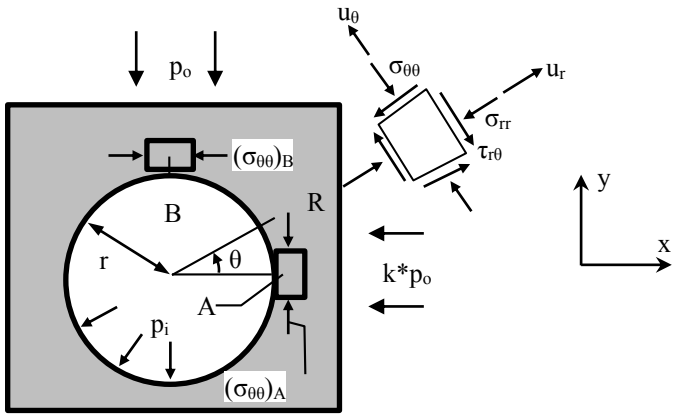

Figure 2.2 Stresses around a circular opening (Brady & Brown, 2005).

The following Kirsch equations give the stress distribution around a circular opening (Brady & Brown, 2005).

$$\sigma_{rr} = \frac{p_o(k+1)}{2}\left(1-\frac{r^2}{R^2}\right) + \frac{p_o(k-1)}{2}\left(1-4\frac{r^2}{R^2}+3\frac{r^4}{R^4}\right)\cos 2\theta + p_i\frac{r^2}{R^2} \tag{4}$$

$$\sigma_{\theta\theta} = \frac{p_o(k+1)}{2}\left(1+\frac{r^2}{R^2}\right) - \frac{p_o(k-1)}{2}\left(1+3\frac{r^4}{R^4}\right)\cos 2\theta - p_i\frac{r^2}{R^2} \tag{5}$$

$$\tau_{r\theta} = -\frac{p_o(k-1)}{2}\left(1+2\frac{r^2}{R^2}-3\frac{r^4}{R^4}\right)\sin 2\theta \tag{6}$$

where σ_{rr}, $\sigma_{\theta\theta}$ and $\tau_{r\theta}$ are total stresses after generation of the opening; and R is a questioned distance from the center of the opening. Assuming that the opening is unsupported, p_i is taken as zero.

The displacements induced by the opening are given by the following equations (Brady & Brown, 2005).

$$u_r = -\frac{p_o r^2}{4GR}\left[(1+k)-(1-k)\left(4(1-\nu)-\frac{r^2}{R^2}\right)\cos 2\theta\right] \tag{7}$$

$$u_\theta = -\frac{p_o r^2}{4GR}\left[(1-k)\left(2(1-2\nu)+\frac{r^2}{R^2}\right)\sin 2\theta\right] \tag{8}$$

where u_r and u_θ are displacements in polar coordinates; G is shear modulus; and ν is Poisson's ratio.

By putting R = r in Equations (4), (5) and (6), the stresses on the excavation boundary are given as

$$\sigma_{rr} = 0 \tag{9}$$

$$\sigma_{\theta\theta} = p_o(k+1) - 2p_o(k-1)\cos 2\theta \tag{10}$$

$$\tau_{r\theta} = 0 \tag{11}$$

Equations (9), (10) and (11) define the condition of stress on the boundary of a circular excavation in terms of the coordinate angle θ. Among these equations, only non-zero stress component is the circumferential component $\sigma_{\theta\theta}$.

For $\theta = 0$ and infinitely large r

$$\sigma_{rr} = kp_o \tag{12}$$

$$\sigma_{\theta\theta} = p_o \tag{13}$$

$$\tau_{r\theta} = 0 \tag{14}$$

Boundary stresses in the side wall ($\theta = 0$) and roof ($\theta = \pi / 2$) of the excavation according to Figure 2.2 are defined by the following:

$$\theta = 0 \text{ at A} \rightarrow (\sigma_{\theta\theta})_A = p_o(3 - k) \tag{15}$$

$$\theta = \frac{\pi}{2} \text{ at B} \rightarrow (\sigma_{\theta\theta})_B = p_o(3k - 1) \tag{16}$$

When $k = 0$, the boundary stresses are

$$\sigma_A = 3p_o \tag{17}$$

$$\sigma_B = -p_o \tag{18}$$

These values define upper and lower limits for stress concentration at the boundary. For $k > 0$, the sidewall stress is less than $3p_o$ and the roof stress is greater than $-p_o$.

For a hydrostatic stress field ($k = 1$), Equation (60) becomes

$$\sigma_{\theta\theta} = 2p_o \tag{19}$$

The boundary stress takes the value $2p_o$, independent of the coordinate angle θ. Equations (4), (5) and (6) are simplified for a hydrostatic stress field:

$$\sigma_{rr} = p_o\left(1 - \frac{r^2}{R^2}\right) \tag{20}$$

$$\sigma_{\theta\theta} = p_o\left(1 + \frac{r^2}{R^2}\right) \tag{21}$$

$$\tau_{r\theta} = 0 \tag{22}$$

For the analysis of circular shafts, cylindrical coordinates are preferred as shown in Figure 2.3. The opening is considered long enough and variations with z are negligible, so that derivatives with respect to z are zero. In particular, the z direction strains are zero and the analysis is plane strain (Pariseau, 1992).

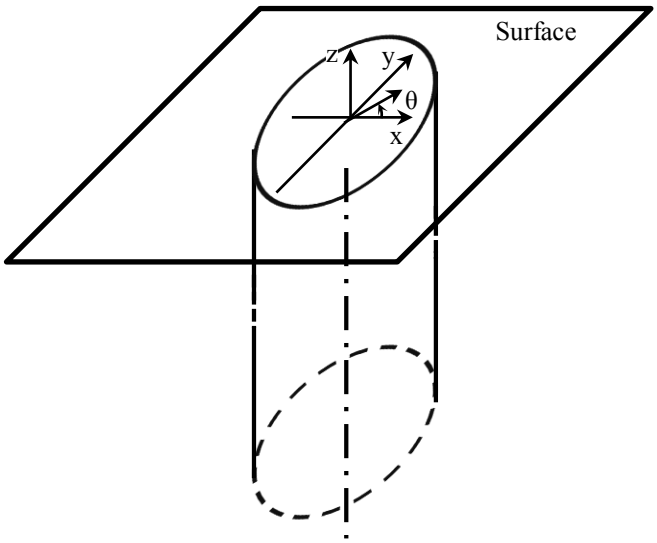

Figure 2.3 A circular shaft with coordinates (Pariseau, 1992).

The stresses around the shaft in Figure 2.3 after excavation are given by

$$\sigma_{rr} = \sigma_h \left[1 - \frac{r^2}{R^2}\right] \tag{23}$$

$$\sigma_{\theta\theta} = \sigma_h \left[1 + \frac{r^2}{R^2}\right] \tag{24}$$

$$\sigma_z = \gamma z \tag{25}$$

$$\sigma_h = k\sigma_z \tag{26}$$

where σ_{rr} and $\sigma_{\theta\theta}$ are post-excavation stresses in the radial and circumferential (tangential) directions, respectively. σ_h and σ_z are pre-excavation horizontal and vertical stresses related by the constant k (horizontal to vertical stress ratio); z is depth; γ is specific weight of rock; r is the shaft radius; and R is a questioned distance from the center of the opening.

Concrete and shotcrete are among the existing support liners for circular excavations as shown in Figure 2.4. A concrete cylinder subjected to a uniform pressure (radial) around its outer circumference will develop an internal compressive stress tangential to its circumference. If the pressure is applied suddenly, the concrete will react elastically and the stress near the interior wall of the lining will be greatest and gradually reduce towards the outer wall (Vergne, 2003). For this case, Lamé's thick wall formula gives the maximum support pressure of concrete or shotcrete (Brady & Brown, 2005):

$$p_{sc\,max} = \frac{f_c}{2}\left[1 - \frac{r^2}{(r + t_c)^2}\right] \tag{27}$$

where f_c is uniaxial compressive strength of concrete or shotcrete in MPa; r is radius of opening in meter and t_c is lining thickness in meter.

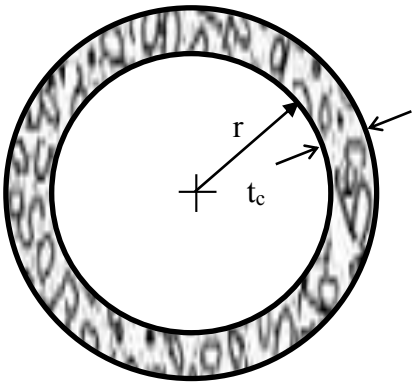

Figure 2.4 Concrete or shotcrete lining for a circular excavation.

From Equation (27), the thickness of concrete or shotcrete is estimated as

$$t_c = r\left(\sqrt{\frac{f_c}{f_c - 2p_{sc\,max}}} - 1\right) \tag{28}$$

If the pressure is great and applied slowly, the concrete may react plastically and the stresses will tend to redistribute themselves evenly across the thickness of the concrete wall. Among a number of formulae developed to account for this plastic or visco-elastic property of concrete or shotcrete, the best one is Huber's formula (Vergne, 2003):

$$p_{sc\,max} = \frac{f_c}{\sqrt{3}}\left[1 - \frac{r^2}{(r + t_c)^2}\right] \tag{29}$$

Then, the thickness of concrete or shotcrete is

$$t_c = r\left(\sqrt{\frac{f_c}{f_c - \sqrt{3}p_{sc\,max}}} - 1\right) \tag{30}$$

And support stiffness of concrete or shotcrete is given by

$$k_c = \frac{E_c[(r + t_c)^2 - r^2]}{(1 + \nu_c)[(1 - 2\nu_c)(r + t_c)^2 + r^2]} \tag{31}$$

where E_c is Young's modulus of concrete or shotcrete; ν_c is Poisson's ratio for concrete or shotcrete.

2.3. Empirical Studies

There are a number of studies calculating lining thickness and pressure on lining. For instance, the thickness of the shaft lining t_c in meter may be found from the following relation (Unrug, 1992):

$$t_c = r\left(\sqrt{\frac{f_c}{f_c - \sqrt{3}np_o}} - 1\right) \tag{32}$$

where r_i is radius of shaft in meter, f_c is allowable compressive stress of the concrete in MPa, n is coefficient of lining work conditions; and p_o is calculated outside pressure acting on the lining in MPa. From this equation, Figure 2.5 can be built to determine the concrete thickness. Unrug (1992) provides details about the parameters in Equation (32).

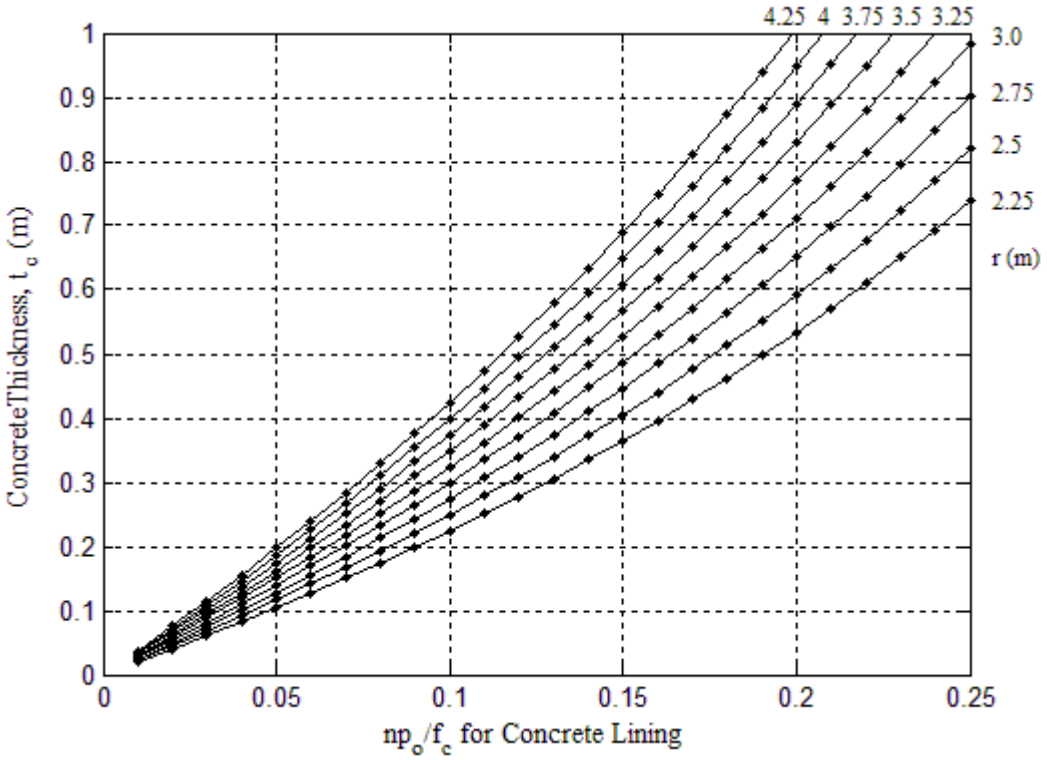

Figure 2.5 Diagram of Equation (32) for the thickness of concrete.

Arıoğlu (1982) suggested the following formula to calculate the lining thickness inside circular shafts.

$$t_c = r\left(e^{2.04p_o/f_c} - 1\right) \tag{33}$$

where t_c is concrete lining thickness (m); r is radius of shaft (m); p_o is radial pressure (MPa) and f_c is uniaxial compressive strength of concrete (MPa).

Poland's Branch Standard (Kopex Corporation, 1998) gives pressure on lining for different depths h, in meter as

$$p_o = 0.013 * z \text{ MPa for saturated sand} \tag{34}$$

$$p_o = 0.017 * z \text{ MPa for clays} \tag{35}$$

Protodjakonow's pressure theory (Arıoğlu, 1970) gives the radial pressure (MPa) on lining as

$$p_o = \gamma z \tan^2 \frac{90 - \phi}{2} \tag{36}$$

where γ is average unit weight of rocks around shaft (MN/m^3); z is depth of shaft (m) and ϕ is internal friction angle of rocks passing through. ϕ is calculated as arc tan ($f_{average}$) where f is hardness coefficient.

Heise's equation (Arıoğlu, 1970) gives the thickness of lining in m as

$$t_c = \frac{p_o r}{f_c} \tag{37}$$

where p_o is radial pressure on lining in MPa; r is radius of shaft (m); f_c is compressive strength of lining material MPa.

Also, Haynes (Vergne, 2003) gives the ultimate strength (maximum support pressure) $p_{sc\ max}$ of the concrete as

$$p_{sc\ max} = f_c \left(2.17 \frac{t_c}{d} - 0.04 \right) \tag{38}$$

where d is diameter of shaft (m).

2.4. Rules of Thumb

Lastly, the following rule of thumbs give useful suggestions for designing concrete lining in shafts:

- The minimum and the maximum lining thickness for poured concrete are 200 mm and 800 mm, respectively (Unrug, 1992).
- The minimum and the maximum lining thickness for shotcrete are 25 mm and 150 mm for various rock masses, respectively (Hoek, 2012).
- The circular concrete lining is generally designed for the minimum practical thickness (Vergne, 2003).
- A concrete lining may not be satisfactory in the long run for outer pressures exceeding 3.5 MPa (Vergne, 2003).
- Concrete lining in circular shafts develops greater strength than that of standard concrete cylinder tests as it is laterally constrained. Tri-axial tests specify that increase up to 20% (Vergne, 2003).
- Substituting 25 to 35% fly ash for cement in high strength concrete may cut permeability by more than half and extends the life of concrete (Vergne, 2003).
- Although, compressive strength of concrete lining may be increased by addition of reinforcing steel, this technique is inefficient. It is usually easier and less expensive to merely employ concrete with higher strength (Vergne, 2003).
- Concrete strength is generally 20 to 25 MPa in underground applications and for most purposes rarely exceeds 50 MPa (Kendorski & Hambley, 1992).

2.5. Numerical Studies

2D or 3D numerical software packages can be used to model shaft sections or three dimensional shafts. Also 2D axisymmetric models can be used to simulate shafts in 3D but axisymmetric models would not work for non-hydrostatic stress case. Therefore the only way of modeling shafts in 3D for non-hydrostatic stresses is possible with 3D software packages.

Öztürk (2000) numerically modeled broken zone radius and lining thickness around circular shafts. In this approach, numerical and empirical, rock-load height, methods were also integrated.

In literature, Emir and Önce (2002) numerically modeled the 540 m deep shaft with 3.25 m radius in GLI deep coal zone in Phases (an older version of Phase2 by Rocscience Inc.) to predict the lining thickness and gave 30 cm lining thickness for the interval 36 to 390 m.

CHAPTER 3

NUMERICAL MODELING

In this chapter, the numerical study carried on different horizontal shaft sections are explained. The idea behind this study is to model shaft sections in different rock masses subjected to Hoek-Brown failure criterion and non-hydrostatic stress state. Circular shaft sections are firstly modeled without any support pressure and then if any failure zone develops around the shaft, iterative support pressure (simulating lining support) is applied to the shaft wall until the plastic zone around the shaft disappears. The numerical study carried out in Phase2 6.0 (Rocscience Inc., 2005) are explained below.

3.1. Geometry of Models

It is very important to well define the geometry of the models because this thesis is based on this geometry. Figure 3.1 shows a 3D graphic of a shaft opened in a rock mass. In Figure 3.1, there are three in-situ field stresses represented by σ_z, σ_{h1} and σ_{h2} around the shaft section which is much below the surface. σ_z denotes the vertical stress on z direction; σ_{h1} denotes the first horizontal stress on x direction; and σ_{h2} denotes the second horizontal stress on y direction.

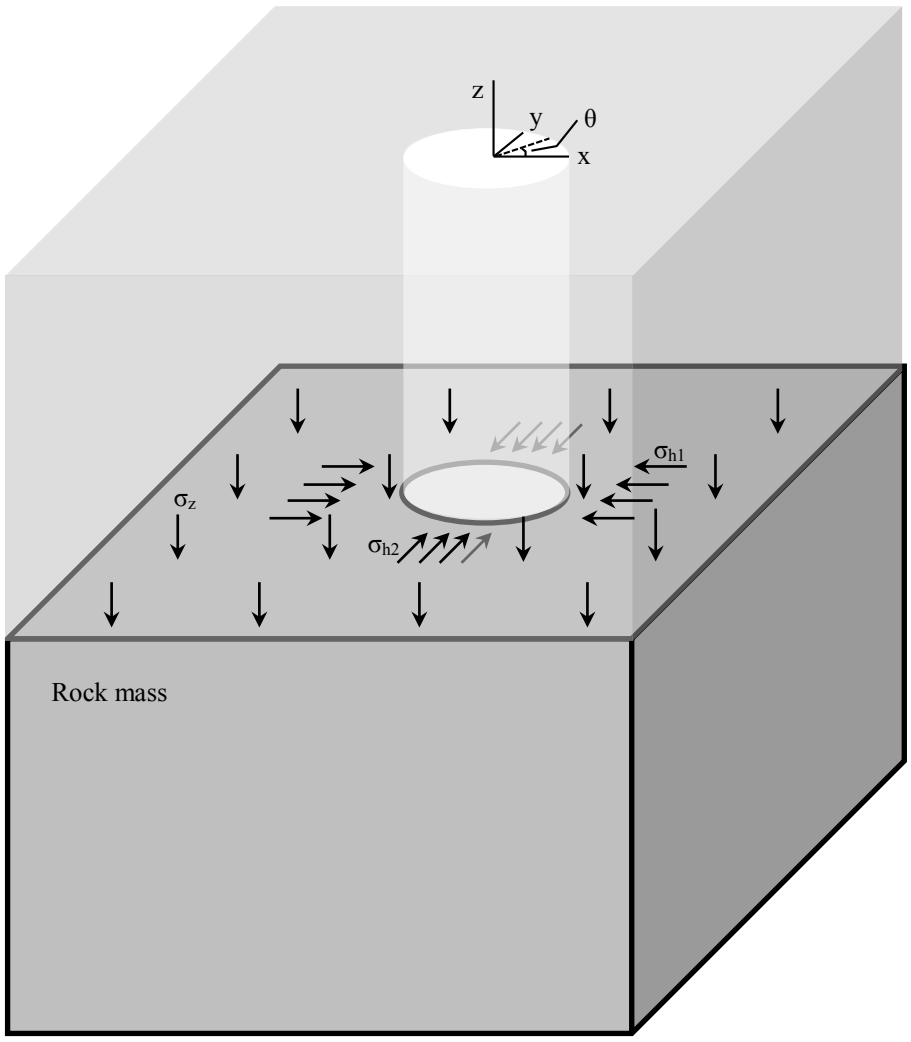

Figure 3.1 The position of the field stresses around a shaft.

3.2. Phase2 Models

Phase2 shaft sections models in 2D with applied in-situ stress state is presented in Figure 3.2.

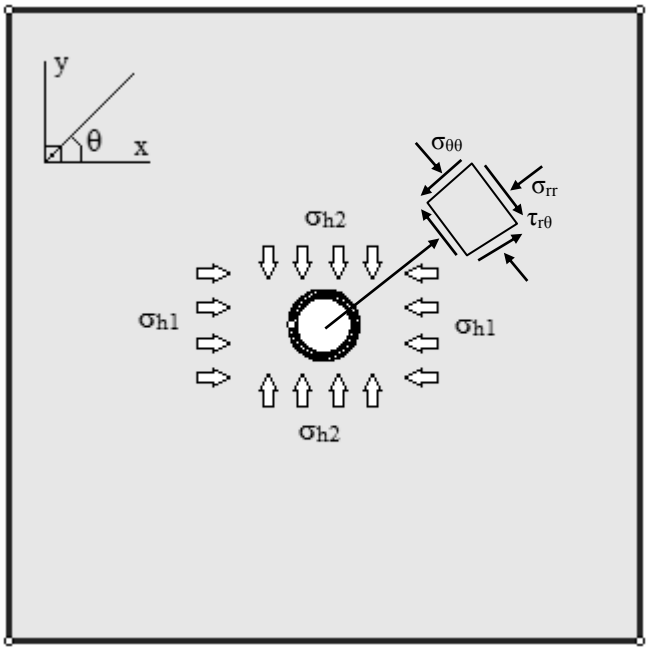

Figure 3.2 Direction of field stresses for shaft sections modeled in Phase2. σ_z is normal to x-y plane.

It should be noted that σ_{h1} is always greater or equal to σ_{h2} in Phase2. After discretizing, meshing the models and restricting the external boundaries, the geometry of the model like in Figure 3.3.

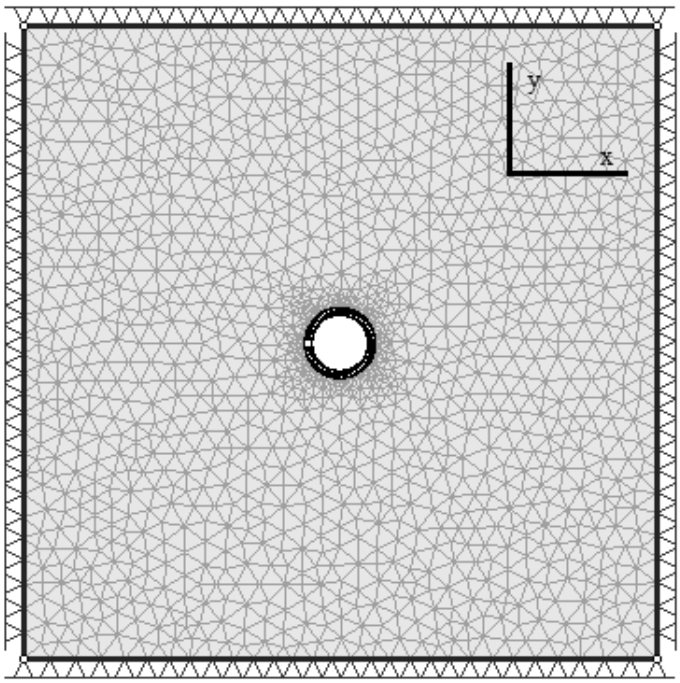

Figure 3.3 Shaft section model after mesh setup and restricting external boundaries in Phase2.

A close-up view of a fine triangulated Phase2 shaft excavation is seen in Figure 3.4.

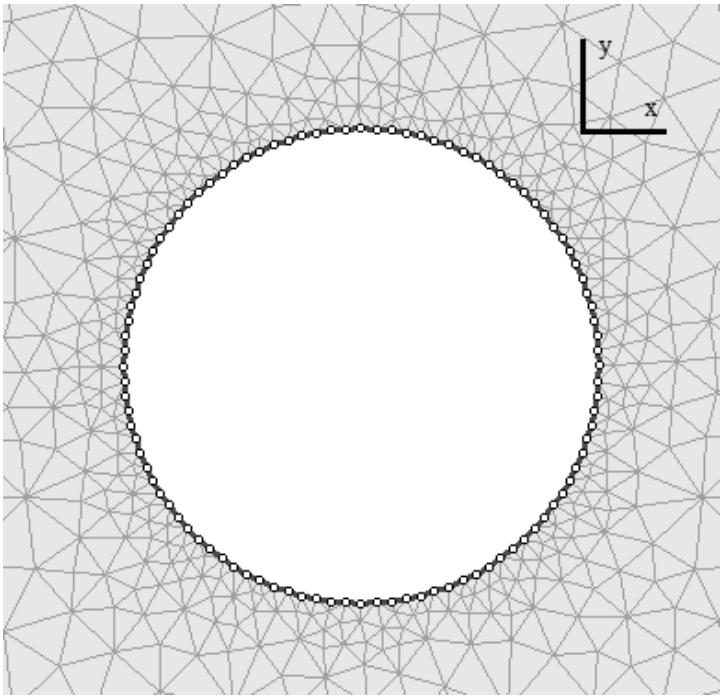

Figure 3.4 The close-up view of a shaft boundary in Phase2.

Discretization around the boundary is very important. Therefore fine meshing is made on the external boundary and it is increased gradually to the shaft boundary to get more accurate results in the numerical modeling.

The shaft circle and the surrounding area in Figure 3.3 have the following properties in Table 3.1. It should be noted that the shaft is opened in the 2nd stage.

Table 3.1 Properties of the shaft circle and surrounding area in Phase2.

Radius of shaft circle	2 m
Number of segments on the shaft circle	100
External Boundary	40 m x 40 m
Number of elements on stage 1	3604
Number of nodes on stage 1	1861
Number of elements on stage 2	3048
Number of nodes on stage 2	1632

The mesh is contiguous in all the models. Moreover, all the mesh elements in the models are of good quality. In a finite element mesh, generally it is wanted to avoid elements of high aspect ratio (i.e. long "thin" elements that may cause numerical problems).

The general setup for the shaft models utilizing the properties in Table 3.1 is shown in Figure 3.5.

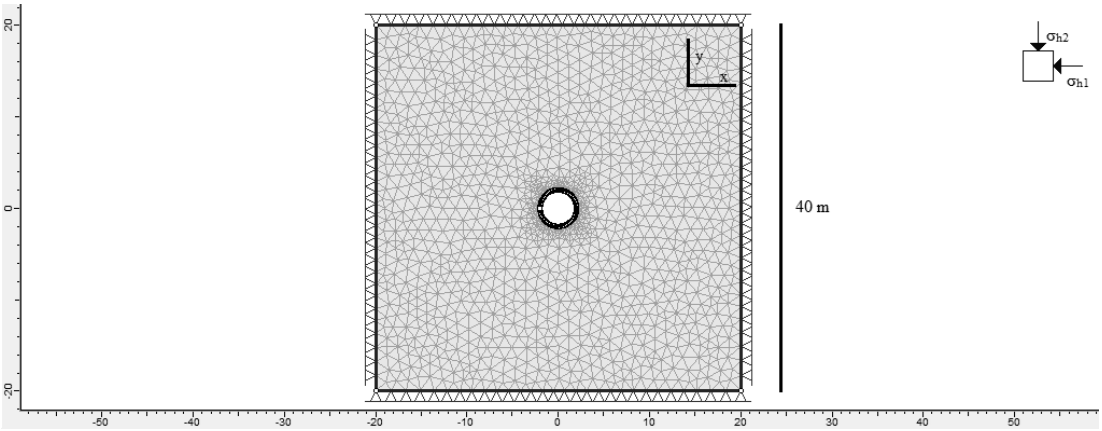

Figure 3.5 The general geometry of the shaft sections in Phase2.

3.3. Generalized Hoek-Brown Failure Criterion

Since the rock mass is assumed to behave as elastic-perfectly plastic and Hoek-Brown medium, the generalized Hoek-Brown failure criterion is used.

Generalized Hoek-Brown failure criterion (Hoek, Carranza-Torres, & Corkum, 2002) is given by

$$\sigma_1 = \sigma_3 + \sigma_{ci}\left(m_b\frac{\sigma_3}{\sigma_{ci}} + s\right)^a \tag{39}$$

where σ_1 and σ_3 are major and minor effective principal stresses at failure; σ_{ci} is uniaxial compressive strength of intact rock material; m_b is a reduced value of material constant m_i; s and a are constants for rock mass.

The following equations give m_b, s and a.

$$m_b = m_i * \exp\left(\frac{GSI - 100}{28 - 14D}\right) \tag{40}$$

where D is a disturbance factor caused by blast damage and stress relaxation. It starts from 0 for undisturbed rock masses and finishes at 1 for very disturbed rock masses.

$$m_i = \frac{1}{\sigma_{ci}}\left[\frac{\sum xy - \sum x \sum y/n}{\sum x^2 - (\sum x)^2/n}\right] \tag{41}$$

where x is σ_3 and y is $(\sigma_1 - \sigma_3)^2$.

$$s = \exp\left(\frac{GSI - 100}{9 - 3D}\right) \tag{42}$$

$$a = \frac{1}{2} + \frac{1}{6}\left(e^{-GSI/15} + e^{-20/3}\right) \tag{43}$$

In the equations above, GSI denotes geological strength index and provides a number used for approximating the decrease in rock mass strength for different geological conditions. This index can be used for blocky, heterogeneous, molassic rocks and ophiolites (Hoek, 2012).

3.4. Parameters of the Numerical Study

The numerical study is carried out in Phase2 with the help of Rocklab 1.0 (Rocscience Inc., 2007) by changing the independent variables once at a time and observing the change in the plastic zone developing around the shaft. The dependent variable support pressure is changed iteratively until the plastic zone around the shaft disappears totally. The independent variables of the models are as follows:

- Uniaxial compressive strength of intact rock, σ_{ci} (MPa)
- Geologic strength index, GSI
- σ_{h1} to σ_z ratio, k_1
- σ_{h2} to σ_z ratio, k_2
- Depth of shaft section, z (m)

The independent variables and their input values for the models are given in Table 3.2.

Table 3.2 Assumed values of the independent variables.

σ_{ci} (MPa)	25	50	100	200
GSI	20	40	60	80
k_1	1	1	1	1
k_2	0.5	1	1.5	2
z (m)	100	300	600	

According to Hoek (2012), the variables that are dependent on σ_{ci} are these:

- Intact modulus, E_i
- Material constant, m_i

Hoek (2012) provides a table for uniaxial compressive strength of intact rocks that gives fairly accurate intervals for the strength of rock types. Rock types with their approximate strength group are shown in Table A.9 in Appendix A. Since E_i and m_i are dependent on σ_{ci}, Table A.9 is utilized to approximate E_i and m_i. Therefore, a number of calculations based on σ_{ci} (25 MPa, 50 MPa, 100 MPa and 200 MPa) were made to estimate E_i and m_i, and their estimated values were rounded off to the following values in Table 3.3 to increase the interval. The calculations are explained in Appendix A.

Table 3.3 Values of dependent variables on σ_{ci}.

E_i (MPa)	12500	25000	50000	100000
m_i	7	14	21	28

Poisson's ratio is taken as 0.2; and unit weight is taken as 0.027 MN/m^3. Then, the vertical stress, σ_z is calculated by

$$\sigma_z = 0.027 * z \tag{44}$$

Equation (44) is used for shaft sections at different depths and the vertical stress is calculated as shown in Table 3.4.

Table 3.4 Vertical stresses around the shaft section models.

Depth of shaft section, z	100 m	300 m	600 m
σ_z	2.7 MPa	8.1 MPa	16.2 MPa

Table 3.5 Parameters and their values used to model shafts in Phase2.

Zipped Models	σ_{ci} (MPa)	E_i (MPa)	m_i	GSI	r (m)	ν	z (m)	σ_z (MPa)	σ_{h1} (MPa)	σ_{h2} (MPa) k2 = 0.5	σ_{h2} (MPa) k2 = 1	σ_{h2} (MPa) k2 = 1.5	σ_{h2} (MPa) k2 = 2
1	25	12500	7	20	2	0.2	100	2.7	2.7	1.35	2.7	4.05	5.4
2	25	12500	7	20	2	0.2	300	8.1	8.1	4.05	8.1	12.15	16.2
3	25	12500	7	20	2	0.2	600	16.2	16.2	8.1	16.2	24.3	32.4
4	25	12500	7	40	2	0.2	100	2.7	2.7	1.35	2.7	4.05	5.4
5	25	12500	7	40	2	0.2	300	8.1	8.1	4.05	8.1	12.15	16.2
6	25	12500	7	40	2	0.2	600	16.2	16.2	8.1	16.2	24.3	32.4
7	25	12500	7	60	2	0.2	100	2.7	2.7	1.35	2.7	4.05	5.4
8	25	12500	7	60	2	0.2	300	8.1	8.1	4.05	8.1	12.15	16.2
9	25	12500	7	60	2	0.2	600	16.2	16.2	8.1	16.2	24.3	32.4
10	25	12500	7	80	2	0.2	100	2.7	2.7	1.35	2.7	4.05	5.4
11	25	12500	7	80	2	0.2	300	8.1	8.1	4.05	8.1	12.15	16.2
12	25	12500	7	80	2	0.2	600	16.2	16.2	8.1	16.2	24.3	32.4
13	50	25000	14	20	2	0.2	100	2.7	2.7	1.35	2.7	4.05	5.4
14	50	25000	14	20	2	0.2	300	8.1	8.1	4.05	8.1	12.15	16.2
15	50	25000	14	20	2	0.2	600	16.2	16.2	8.1	16.2	24.3	32.4
16	50	25000	14	40	2	0.2	100	2.7	2.7	1.35	2.7	4.05	5.4
17	50	25000	14	40	2	0.2	300	8.1	8.1	4.05	8.1	12.15	16.2
18	50	25000	14	40	2	0.2	600	16.2	16.2	8.1	16.2	24.3	32.4
19	50	25000	14	60	2	0.2	100	2.7	2.7	1.35	2.7	4.05	5.4
20	50	25000	14	60	2	0.2	300	8.1	8.1	4.05	8.1	12.15	16.2
21	50	25000	14	60	2	0.2	600	16.2	16.2	8.1	16.2	24.3	32.4
22	50	25000	14	80	2	0.2	100	2.7	2.7	1.35	2.7	4.05	5.4
23	50	25000	14	80	2	0.2	300	8.1	8.1	4.05	8.1	12.15	16.2
24	50	25000	14	80	2	0.2	600	16.2	16.2	8.1	16.2	24.3	32.4
25	100	50000	21	20	2	0.2	100	2.7	2.7	1.35	2.7	4.05	5.4
26	100	50000	21	20	2	0.2	300	8.1	8.1	4.05	8.1	12.15	16.2
27	100	50000	21	20	2	0.2	600	16.2	16.2	8.1	16.2	24.3	32.4
28	100	50000	21	40	2	0.2	100	2.7	2.7	1.35	2.7	4.05	5.4
29	100	50000	21	40	2	0.2	300	8.1	8.1	4.05	8.1	12.15	16.2
30	100	50000	21	40	2	0.2	600	16.2	16.2	8.1	16.2	24.3	32.4
31	100	50000	21	60	2	0.2	100	2.7	2.7	1.35	2.7	4.05	5.4
32	100	50000	21	60	2	0.2	300	8.1	8.1	4.05	8.1	12.15	16.2
33	100	50000	21	60	2	0.2	600	16.2	16.2	8.1	16.2	24.3	32.4
34	100	50000	21	80	2	0.2	100	2.7	2.7	1.35	2.7	4.05	5.4
35	100	50000	21	80	2	0.2	300	8.1	8.1	4.05	8.1	12.15	16.2
36	100	50000	21	80	2	0.2	600	16.2	16.2	8.1	16.2	24.3	32.4
37	200	100000	28	20	2	0.2	100	2.7	2.7	1.35	2.7	4.05	5.4
38	200	100000	28	20	2	0.2	300	8.1	8.1	4.05	8.1	12.15	16.2
39	200	100000	28	20	2	0.2	600	16.2	16.2	8.1	16.2	24.3	32.4
40	200	100000	28	40	2	0.2	100	2.7	2.7	1.35	2.7	4.05	5.4
41	200	100000	28	40	2	0.2	300	8.1	8.1	4.05	8.1	12.15	16.2
42	200	100000	28	40	2	0.2	600	16.2	16.2	8.1	16.2	24.3	32.4
43	200	100000	28	60	2	0.2	100	2.7	2.7	1.35	2.7	4.05	5.4
44	200	100000	28	60	2	0.2	300	8.1	8.1	4.05	8.1	12.15	16.2
45	200	100000	28	60	2	0.2	600	16.2	16.2	8.1	16.2	24.3	32.4
46	200	100000	28	80	2	0.2	100	2.7	2.7	1.35	2.7	4.05	5.4
47	200	100000	28	80	2	0.2	300	8.1	8.1	4.05	8.1	12.15	16.2
48	200	100000	28	80	2	0.2	600	16.2	16.2	8.1	16.2	24.3	32.4

It should be noted that when k2 is greater than 1, σ_{h2} gets larger than σ_{h1}. Therefore, in Phase2, σ_{h2} is defined as σ_{h1} when k2 is greater than 1.

As a result, the 48 zipped models in Table 3.5 show the combinations of the parameters of the numerical study. Since, each of 48 models include four k2 (σ_{h2} / σ_z) values, there will be four σ_{h2} values. This leads to 48 * 4 = 192 models for Phase2 in total.

In order to find the support pressure (p_i) which balances the outer pressure, uniform pressure in terms of MPa is distributed inside the shaft as shown in Figure 3.6. If there is no support pressure inside the shaft, there will be yielded zones (elements) around the shaft when the rock is not strong enough. Therefore, to prevent yielding, enough support pressure must be exerted on the inside walls of the shaft.

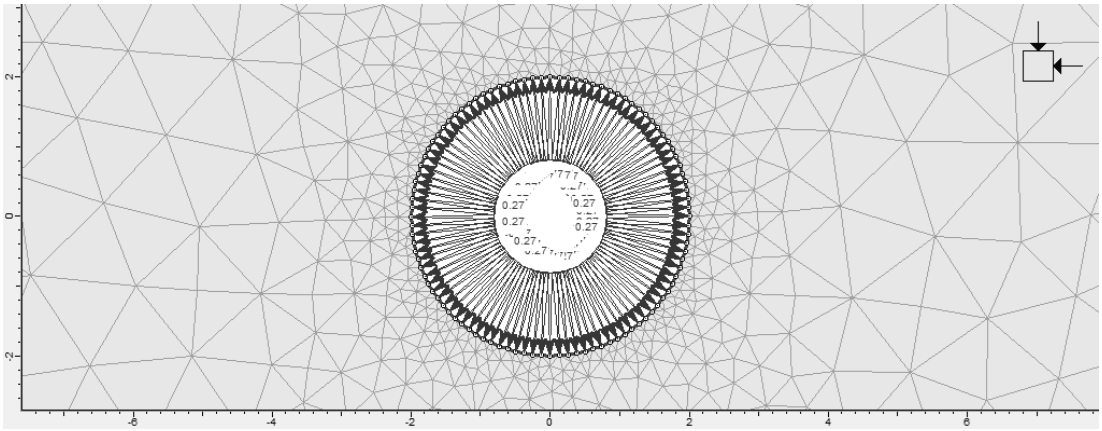

Figure 3.6 Support pressure p_i (shown as black arrows) is exerted on the inside walls of the shaft.

3.5. Comparison of Numerical Modeling to Kirsch's Solution

In order to check the validity of the Phase2 models, closed form Kirsch solutions (Equations (4) and (5)) for hydrostatic stress state were compared to Phase2 solutions. It is essential to recall that θ is described in x-y plane in Figure 3.2.

When σ_{h1} is 8.1 MPa; σ_{h2} is 8.1 MPa; σ_z is 0 MPa; r is 2 m; and θ is 0°, the comparison of the elastic solutions by Kirsch and Phase2 are given in Figure 3.7.

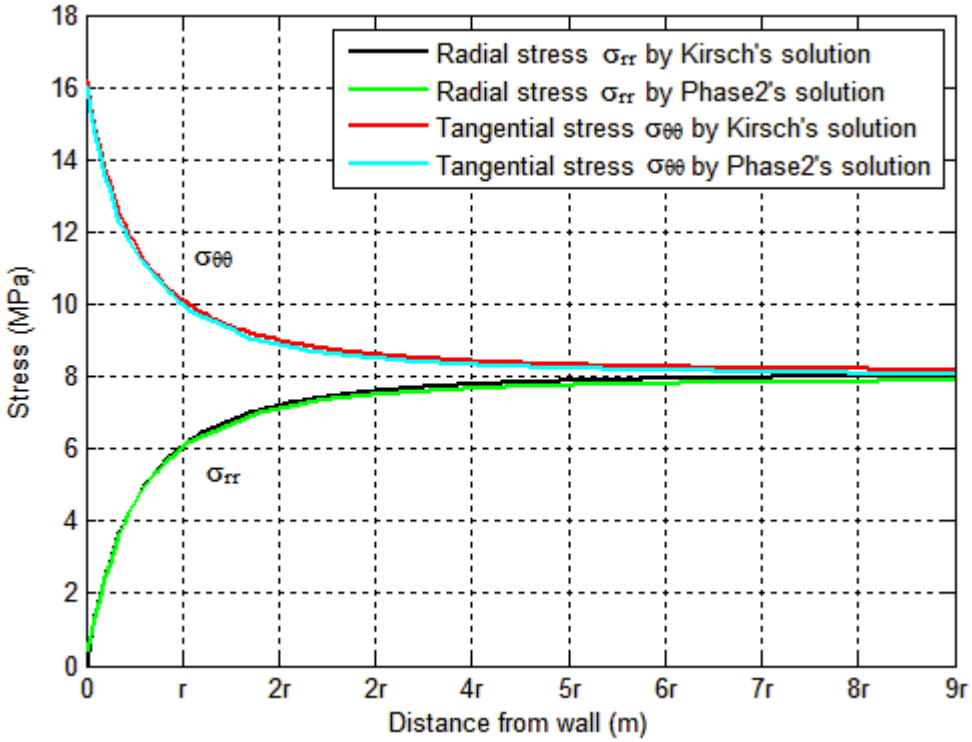

Figure 3.7 Comparison of Kirsch's and Phase2's solution for elastic condition.

As can be seen in Figure 3.7, Kirsch's and Phase2's solutions give almost the same stress distribution around the shaft. Besides, variation of σ_z does not change the results of Phase2 for elastic conditions if all mesh elements are of good quality. However, in plastic condition, the effect of σ_z on the solutions of Phase2 is shown in Figure 3.8 when σ_{h1} is 8.1 MPa; σ_{h2} is 8.1 MPa; σ_z is 0 and 8.1 MPa; r is 2 m; and θ is 0°.

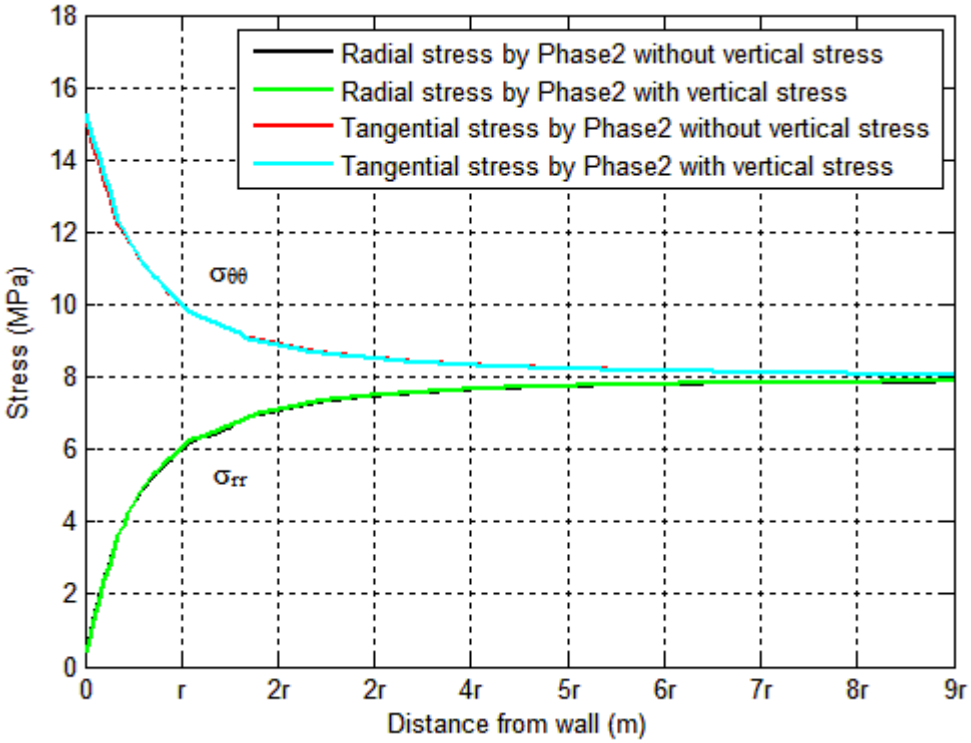

Figure 3.8 Comparison of Phase2's results with and without σ_z.

Although the results seem nearly same in Figure 3.8, number of yielded elements shows a great difference when σ_z is applied in plastic condition with generalized Hoek-Brown failure criterion.

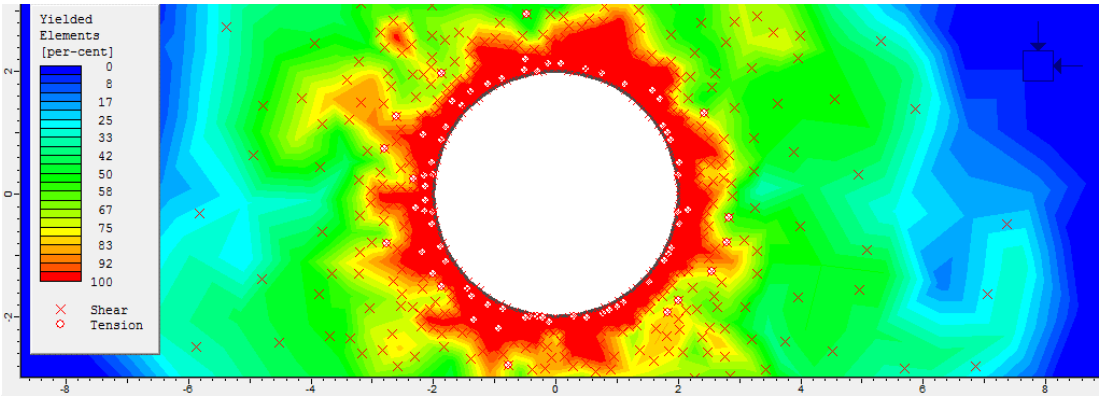

Figure 3.9 σ_z = 0 MPa; σ_{h1} = 8.1 MPa; σ_{h2} = 8.1 MPa; r = 2 m There are 796 yielded elements.

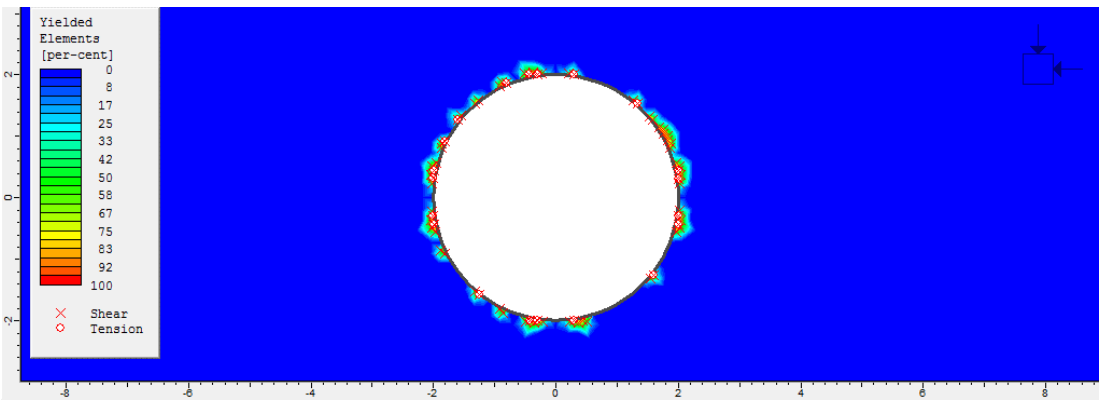

Figure 3.10 σ_z = 8.1 MPa; σ_{h1} = 8.1 MPa; σ_{h2} = 8.1 MPa; r = 2 m. There are 70 yielded elements.

As Figure 3.9 and Figure 3.10 show, inserting vertical stress to the shaft models decreases yielded elements significantly. Thus, even in higher field stresses, it will be possible to model shafts in Phase2.

3.6. Numerical Modeling Results

After each Phase2 modeling, yielded elements are recorded and support pressure is applied until all the yielded elements are eliminated in the second stage of the models. Although, the support pressure is applied in an attempt to eliminate all the yielded elements, there are some unwanted cases where it is impossible to eliminate all the yielded elements. However, in these cases, the support pressure still minimizes the yielded elements. Table 3.6 shows a part of the run results. The outcomes of the numerical modeling are given in Appendix B.

Table 3.6 A part from the modelling results with the change of p_i. Gray numbers show unwanted cases.

		z (m)	100				300				600			
		k2	0.5	1	1.5	2	0.5	1	1.5	2	0.5	1	1.5	2
σ_{ci} (MPa)	**GSI**		p_i (MPa)											
25	40		1.02	0.75	1.71	2.8	4.44	3.75	7.7	13.29	10.35	9.3	18.24	18.9
50	40		0.4	0.28	0.75	1.35	2.61	1.91	4.44	7.44	7.44	5.56	12.07	17.58
100	40		0.13	0.08	0.28	0.57	1.22	0.87	2.24	4.05	4.05	2.93	7.06	12.13
200	40		0	0	0.06	0.19	0.49	0.34	0.99	1.93	1.93	1.37	3.61	6.63
25	60		0.55	0.36	1.05	1.9	3.57	2.64	5.89	9.62	8.4	7.28	15.12	19.98
50	60		0.07	0.01	0.31	0.66	1.48	1.03	2.75	4.95	4.95	3.58	8.54	14.47
100	60		0	0	0	0.1	0.46	0.27	1.06	2.18	2.18	1.5	4.14	7.66
200	60		0	0	0	0	0	0	0.19	0.7	0.7	0.43	1.64	3.44

If Table 3.6 is interpreted, the following results can be obtained:

- If uniaxial compressive strength of intact rock, σ_{ci} increases, p_i decreases.
- If geological strength index, GSI increases, p_i decreases.
- If depth, z increases, p_i increases.
- If horizontal to vertical stress ratio, k2 increases, p_i behaves like a curve.

The model for the relations above may include linear, quadratic, cubic or convex functions. In Table 3.6, the range of the support pressure is minimum when k2 = 1 (hydrostatic case). The range increases when k2 increases. However, when k2 is 0.5, it is less spread than k2 = 1.5 and k2 = 2.

When the practical limits for outer pressures are taken into account, p_i obtained by the numerical modeling may be limited to the interval (0-4) MPa since a concrete based lining may not be satisfactory in the long run for outer pressures exceeding 3.5 MPa (Vergne, 2003). The restricted results of the numerical modeling are tabulated according to row number and can be seen in Appendix C.

CHAPTER 4

REGRESSION ANALYSES

Deriving a formula for the support pressure p_i is the most challenging part of this thesis since there is not a single way to do that. Therefore, limited number of methods were used to obtain the most appropriate formula for p_i. These methods can be summarized as linear and non-linear methods. Also, k-means clustering algorithm was utilized to simplify the formula derivation process for p_i.

4.1. Linear Response of p_i

A regression analysis was made by Minitab 16 (Minitab Inc., 2010) assuming that the response of pi is linear. To get a dimensionally balanced equation, p_i, σ_{ci}, σ_z and σ_{h2} were divided by σ_{ci} and the following equation with a regression coefficient of 74.6 % was generated in Minitab 16.

$$\frac{p_i}{\sigma_{ci}} = 0.0161 - 0.000718 * GSI + 0.241 * \frac{\sigma_z}{\sigma_{ci}} + 0.162 * \frac{\sigma_{h2}}{\sigma_{ci}} \quad (45)$$

where p_i, σ_{ci}, σ_z, σ_{h2} are in MPa; and GSI is dimensionless. The statistical results of this regression are given in Appendix D.

The comparison of the outputs of Equation (45) to the outputs of Phase2 is seen in the following graph.

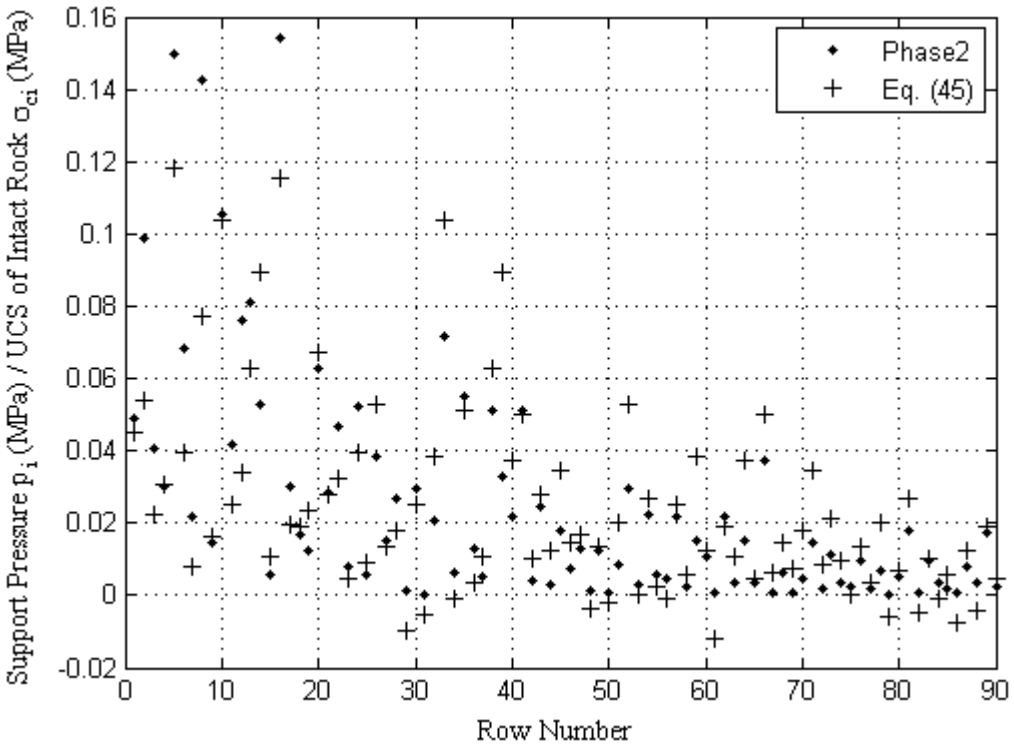

Figure 4.1 Comparison of Equation (45) to Phase2 in terms of p_i/σ_{ci}.

Figure 4.1 shows that Equation (45) produces values similar to those of Phase2 to some extent. The differences of the two method are shown in the range, sign and distribution of data in Figure 4.1. Firstly, while Phase2 gives data with a greater range, Equation (45) provides a smaller range. Secondly, Phase2 does not produce minus values whereas Equation (45) produces minus values. Thirdly, while Phase2

offers randomly distributed data, Equation (45) offers less randomly distributed or more patterned data. If the points (dots and pluses) in Figure 4.1 are plotted against each other, the following graph of linearity is obtained.

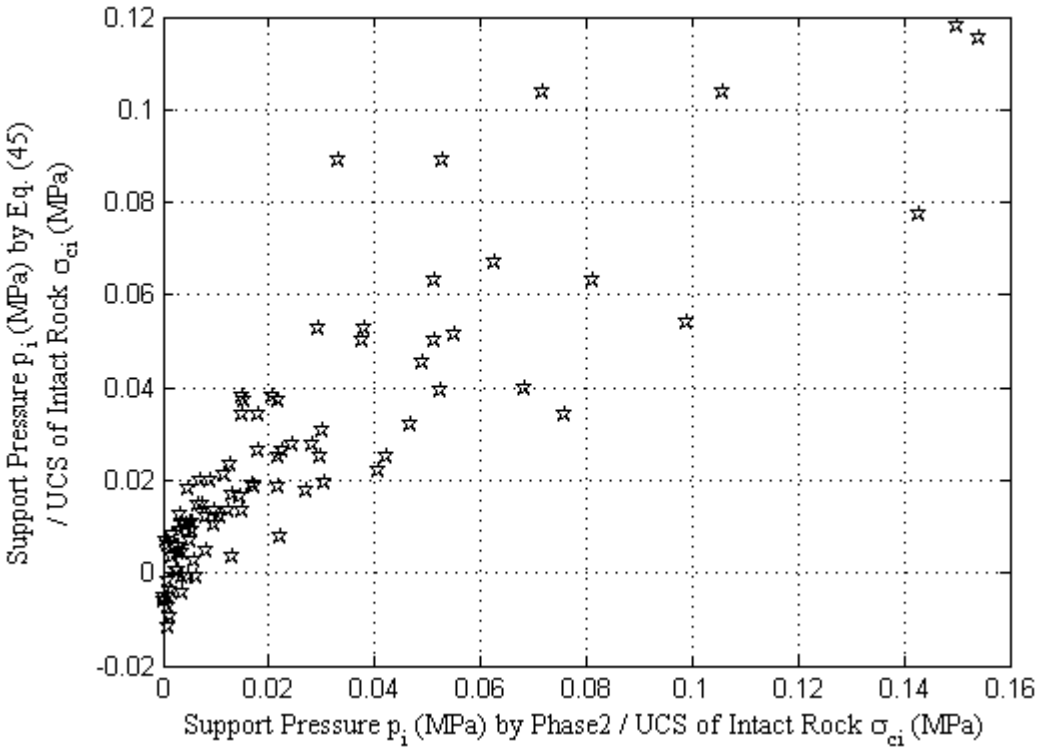

Figure 4.2 p_i/σ_{ci} by Equation (45) vs. p_i/σ_{ci} by Phase2.

The linearity in Figure 4.2 indicates that Equation (45) is not completely capable of producing the values of Phase2 but delivers outputs which are valid to some degree. If a line is drawn staring from (0, 0) point having 45° slope, it is seen that most of the data in Figure 4.2 will be close to the line.

Recall that the second horizontal stress is expressed as

$$\sigma_{h2} = k2 * \sigma_z \tag{46}$$

And inserting Equation (44) into Equation (46) gives

$$\sigma_{h2} = 0.027 * k2 * z \tag{47}$$

Then, Equation (45) is modified to the following equation:

$$\frac{p_i}{\sigma_{ci}} = 0.0161 - 0.000718 * GSI + 0.241 * \frac{0.027 * z}{\sigma_{ci}} + 0.162 * \frac{0.027 * k2 * z}{\sigma_{ci}} \tag{48}$$

Behavior of Equation (48) as surfaces for three different depth is shown in Figure 4.3, Figure 4.4 and Figure 4.5.

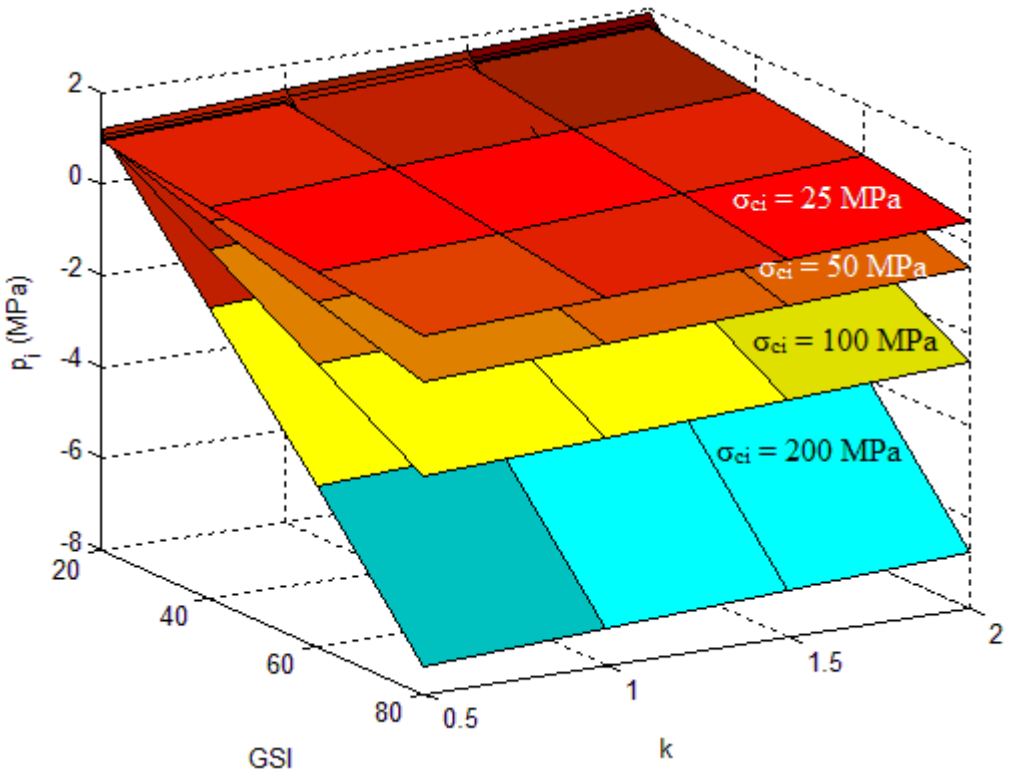

Figure 4.3 Behavior of Equation (48) for z = 100 m.

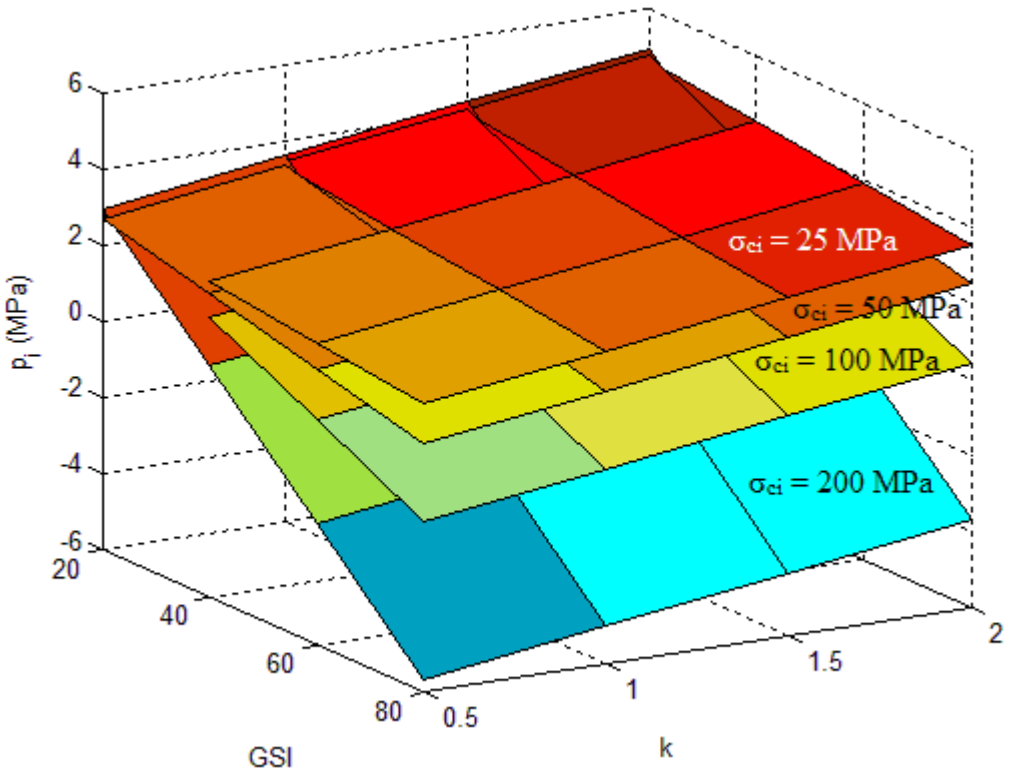

Figure 4.4 Behavior of Equation (48) for z = 300 m.

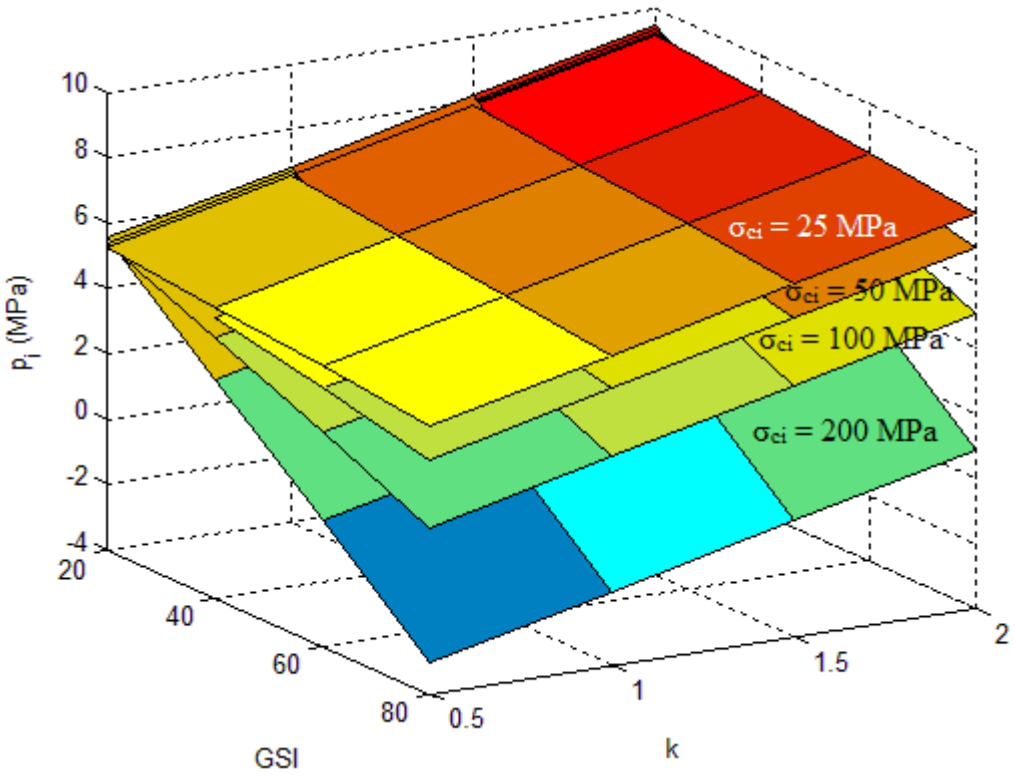

Figure 4.5 Behavior of Equation (48) for z = 600 m.

As can be seen from Figure 4.3, Figure 4.4 and Figure 4.5, p_i decreases as σ_{ci} and GSI increases; and p_i increases as z and k increases. As expected, the response of p_i is linear while the parameters are changing.

4.2. Non-linear Response of p_i

Here, it is assumed that p_i has a non-linear response. As the variables (σ_{ci}, GSI and field stresses) are independent, their effect on p_i can be observed. However, because the range of each variable is large, it is difficult to observe precisely the effect of any variable on p_i, the error increases. Therefore, one of ways to overcome this situation is to cluster the data and then observe the effect of each variable on p_i.

Clustering may be done with any clustering algorithm but k-means algorithm seems more advantageous. Firstly, it is an unsupervised method. Secondly, it is a fast iterative algorithm because in practice it requires only a few iterations to converge and iterations require uncomplicated computations.

4.2.1. Clustering

K-means is the most widely known clustering algorithm and its basis is very simple. In this algorithm, there are parameter vectors θ_j (also called cluster representatives or means) corresponding to points in d-dimensional space, where the vectors of data set (X) are present. It is assumed that the number of clusters, m in X, is already known. The aim is to move the points θ_j, j = 1,..., m, into regions that are dense in terms of data vectors. K-means algorithm has an iterative nature. It starts with a number of initial estimates: $\theta_1(0)$,..., $\theta_m(0)$ for the parameter vectors θ_1,..., θ_m. At each iteration (t), the vectors x_i that lie close to each $\theta_j(t-1)$ are identified and then the new (updated) value of θ_j, $\theta_j(t)$ is computed as the mean of the data vectors that lie closer to $\theta_j(t-1)$. The algorithm terminates when no changes occur in θ_j's, between two successive iterations (Theodoridis & Koutroumbas, 2009).

The algorithm takes the followings as input:

- X is a d*N matrix whose columns contain the data vectors.
- θ_i is a d*m matrix whose columns are the initial estimates of θ_j (the number of clusters, m, is defined by the size of θ_i).

And the algorithm gives the value of the cost function, J for the resulting clustering. K-means algorithm minimizes the cost function:

$$J(\theta, U) = \sum_{i=1}^{N} \sum_{j=1}^{m} u_{ij} \|x_i - \theta_j\|^2 \quad (49)$$

where $\theta = [\theta_1^T, \dots, \theta_m^T]^T$ and $\|.\|$ is Euclidean distance. u_{ij} =1 if x_i lies closest to θ_j; 0, otherwise. To sum up, k-means minimizes the sum of squared Euclidean distances of each data vector from its closest parameter vector. When the data vectors of X form m compact clusters (with no significant difference in size), it is expected that J is minimized and each θ_j is placed (approximately) in the center of each cluster, only if m (number of classes) is known. As a result, the algorithm terminates when the values of the cluster representatives remain unaltered between two successive iterations.

The algorithm takes p_i, σ_{ci}, GSI, σ_z, σ_{h1} and σ_{h2} as d by N matrix, each column of which corresponds to a d-dimensional data vector. Number of classes may change according to initial estimation of the cluster representatives (arbitrary means). Number of classes should be as many as possible to minimize similarity of variable means in each class. The algorithm finds maximum 5 classes. For the classification, all the data obtained by the numerical modeling in Appendix B was used since the algorithm needs many data.

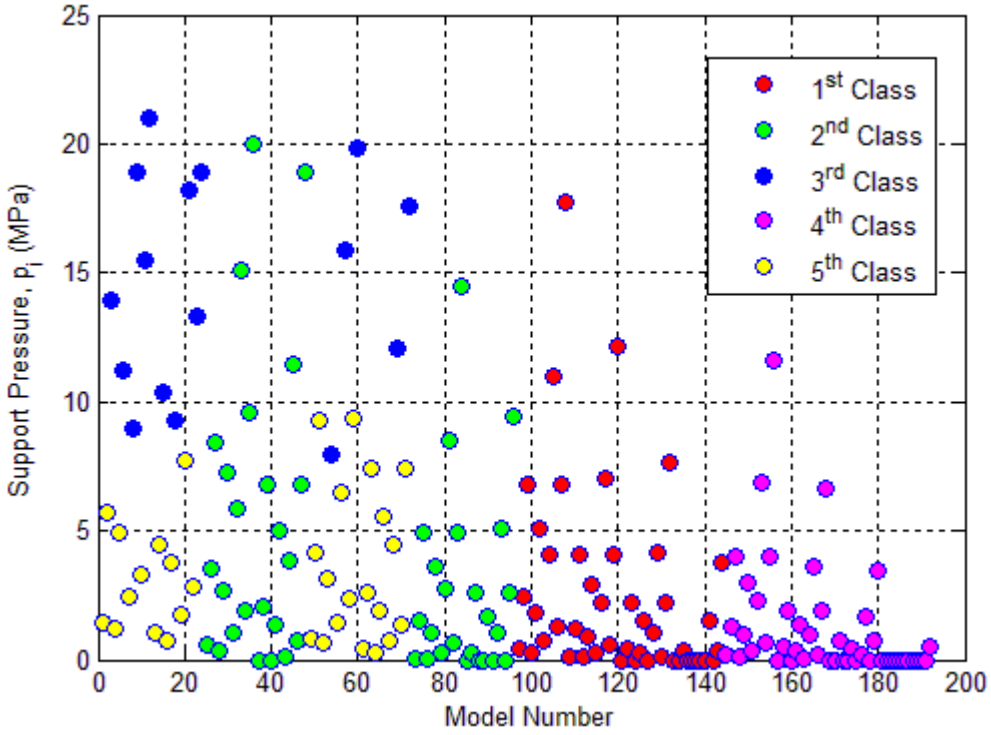

Figure 4.6 The classified data by k-means algorithm.

After classification, mean of each variable in each class is seen in the following table.

Table 4.1 Mean of each variable according to classes.

	1st Class	2nd Class	3rd Class	4th Class	5th Class
p_i (MPa)	2.4929	4.1448	14.5581	1.2627	3.4716
σ_{ci} (MPa)	100	37.5	32.8125	200	39.8438
GSI	50	70	28.75	50	30.625
σ_z (MPa)	9	9	14.6813	9	6.1594
σ_{h1} (MPa)	9	9	14.6813	9	6.1594
σ_{h2} (MPa)	11.25	11.25	21.0094	11.25	6.3703

4.2.2. Checking the Clustered Data

Since the number of data is limited and no real data from fields are present, the result of the clustering should be somehow validated to increase reliability. LOO (leave-one-out or cross validation) is particularly useful in cases where only a limited data set is available. Given N training points, N−1 points are used for training the classifier and the remaining point for testing. The procedure is repeated N times, each time by leaving out a different sample. Finally, the number of errors committed by the N different test points is averaged out. This method is computationally expensive because the classifier has to be trained N times; the same data set is utilized for training, testing; and at the same time, the testing is carried out on points that have not been used in the training (Theodoridis & Koutroumbas, 2009).

To compute error, the class of the training data must be known. As there is no training data collected from the field and the same data is used for both training and testing, the class of data must be assumed. For the cross validation, the classes produced by k-means algorithm were used. The data classified by the cross validation differs from k-means only on five points; that is only five points (their model numbers are 8, 15, 23, 54 and 69) were classified differently by cross validation. Those points were classified as 5th class instead of 3rd. The error rate is 0.026. Consequently, the result of k-means algorithm can be used to model a non-linear response for p_i since the clustered data are validated with a very small error (0.026 or 2.61 %).

4.2.3. Non-linear Response of p_i

If the change in the mean of a variable in Table 4.1 is compared to the change in p_i, the effect of that variable on p_i can be seen. However, initially, the 3rd class is removed to restrict p_i to the interval (0 – 4) MPa; σ_{h2} is also removed since it is equal to σ_z and the results are divided by σ_{ci} to get a dimensionally balanced equation.

Table 4.2 Scaled values for estimating the non-linear response of p_i.

	1st Class	2nd Class	4th Class	5th Class
p_i (MPa) / σ_{ci} (MPa)	0.0249	0.1105	0.0063	0.0871
GSI	50	70	50	30.625
σ_z (MPa) / σ_{ci} (MPa)	0.09	0.24	0.045	0.1546
σ_{h2} (MPa) / σ_{ci} (MPa)	0.1125	0.3	0.0563	0.1599

Then p_i/σ_{ci} vs. GSI, p_i/σ_{ci} vs. σ_z/σ_{ci} and p_i/σ_{ci} vs. σ_{h2}/σ_{ci} graphs are plotted by Minitab, giving the results shown from Figure 4.7 to Figure 4.9, respectively. Statistical results can be seen in Appendix D.

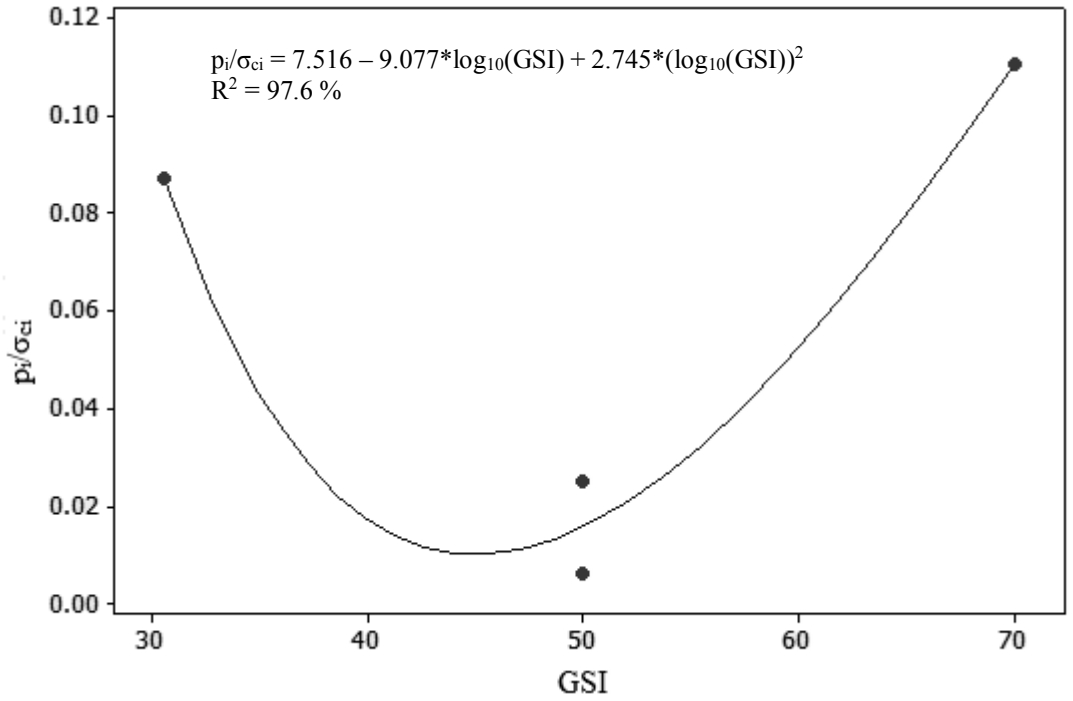

Figure 4.7 p_i (MPa) / σ_{ci} (MPa) vs. GSI.

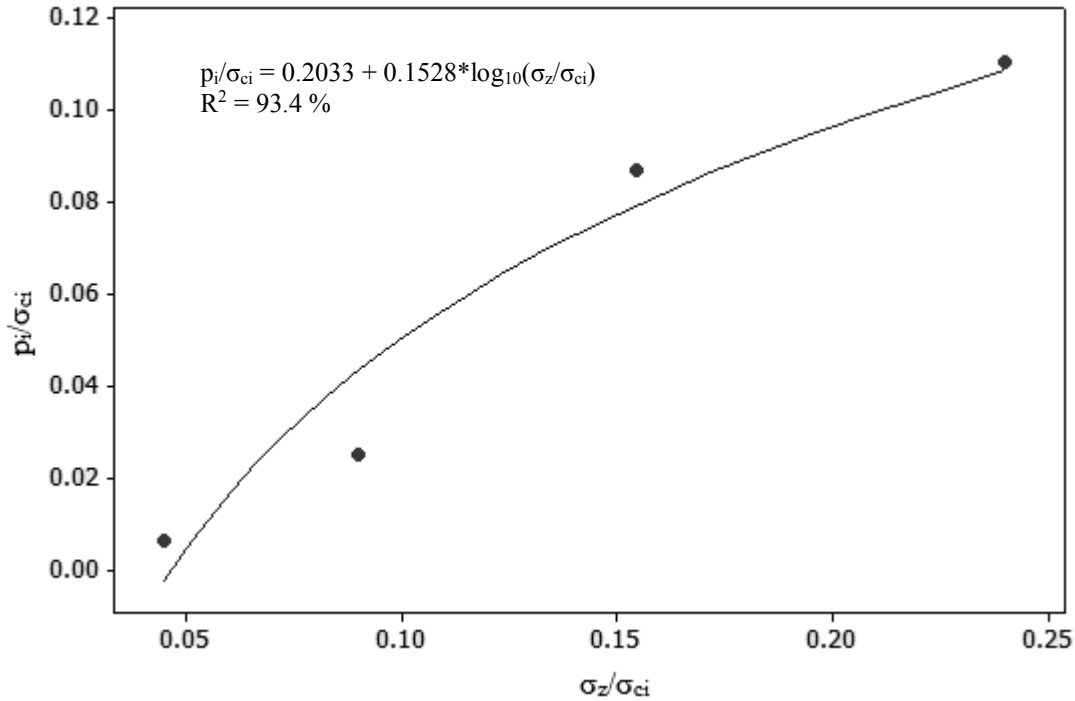

Figure 4.8 p_i (MPa)/σ_{ci} (MPa) vs. σ_z (MPa)/σ_{ci} (MPa).

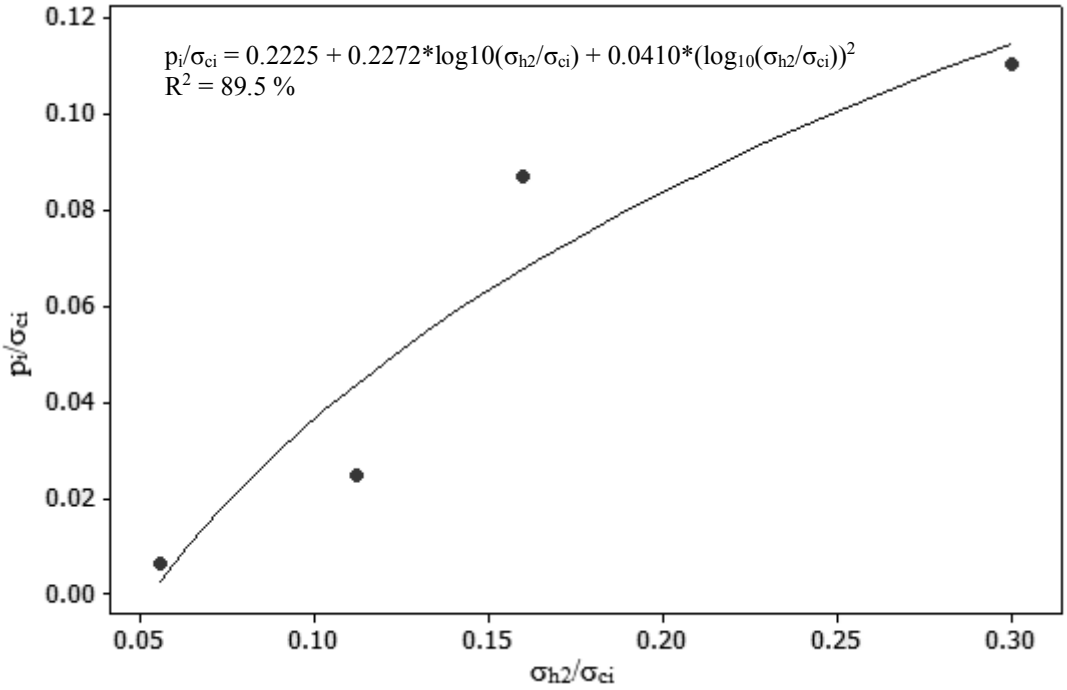

Figure 4.9 p_i (MPa)/σ_{ci} (MPa) vs. σ_{h2} (MPa)/ σ_{ci} (MPa).

Then, the equations above are multiplied to estimate the non-linear response of p_i. Thus, the following formula is obtained:

$$\frac{p_i}{\sigma_{ci}} = N * (7.516 - 9.077 * \log_{10} GSI + 2.745 * (\log_{10} GSI)^2) * (0.2033 + 0.1528 * \log_{10}(\sigma_z/\sigma_{ci})) * (0.2225 + 0.2272 * \log_{10}(\sigma_{h2}/\sigma_{ci}) + 0.0410 * (\log_{10}(\sigma_{h2}/\sigma_{ci}))^2) \quad (50)$$

where, while p_i, σ_{ci} and σ_{h2} are in MPa, GSI is dimensionless. N is a scaling factor to increase the range of the results and may be taken between 25 and 50.

Rearranging Equation (50) gives

$$\frac{p_i}{\sigma_{ci}} = N * (7.516 - 9.077 * \log_{10} GSI + 2.745 * (\log_{10} GSI)^2) * (0.2033 + 0.1528 * \log_{10}(0.027 * z/\sigma_{ci})) * (0.2225 + 0.2272 * \log_{10}(0.027 * k2 * z/\sigma_{ci}) + 0.0410 * (\log_{10}(0.027 * z * k2/\sigma_{ci}))^2) \quad (51)$$

The outputs of Equation (50) are compared to the outputs of Phase2 in the following graph.

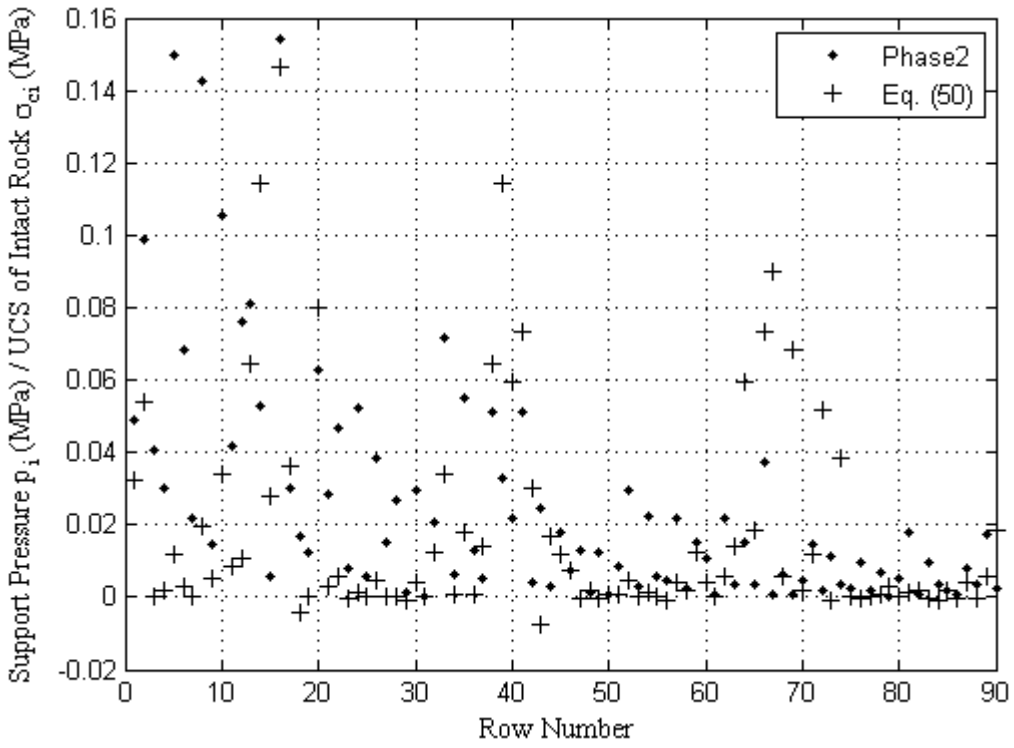

Figure 4.10 Comparison of Equation (50) to Phase2 in terms of p_i/σ_{ci}. N is 40.

Although Equation (50) tries to produce values similar to that of Phase2, it is not as successful as Equation (48) because there is a weak matching in Figure 4.10. If the pluses are plotted against the dots, the following graph of linearity is obtained.

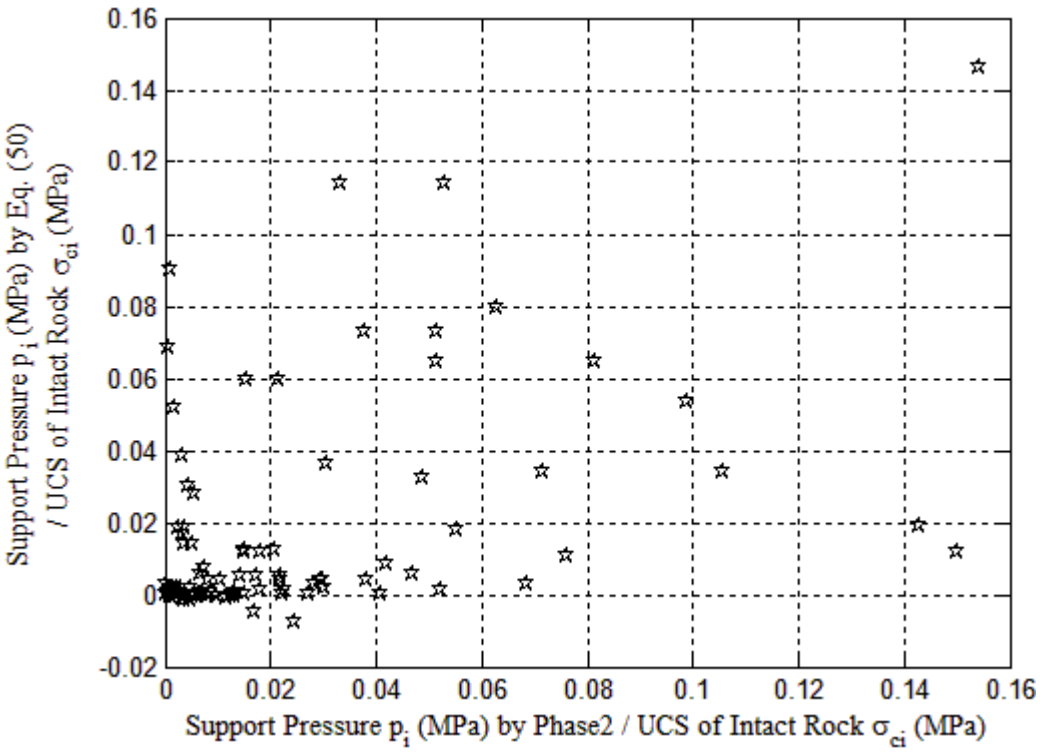

Figure 4.11 p_i/σ_{ci} by Equation (50) vs. p_i/σ_{ci} by Phase2.

As it is seen clearly, there is not a convinced linearity in Figure 4.11. Therefore, Equation (50) does not

well represent the data obtained by Phase2.

4.3. Results

Figure 4.2 gives the most linear match when it is compared to Figure 4.11. Since the linearity is greater in the former, the prediction error of Equation (45) is smaller with respect to Equation (50). Therefore, Equation (45) is better in terms of predicting p_i/σ_{ci}. To summarize, neither Figure 4.2 nor Figure 4.11 give the exact linearity, but the regression equations reproduce the properties of the original Phase2 data.

If a sensitivity analysis of Equation (45) is carried out when σ_{ci} is 50 MPa, GSI is 40, σ_{h2} is 8.1 MPa and σ_z is 8.1 MPa, Figure 4.12 is obtained.

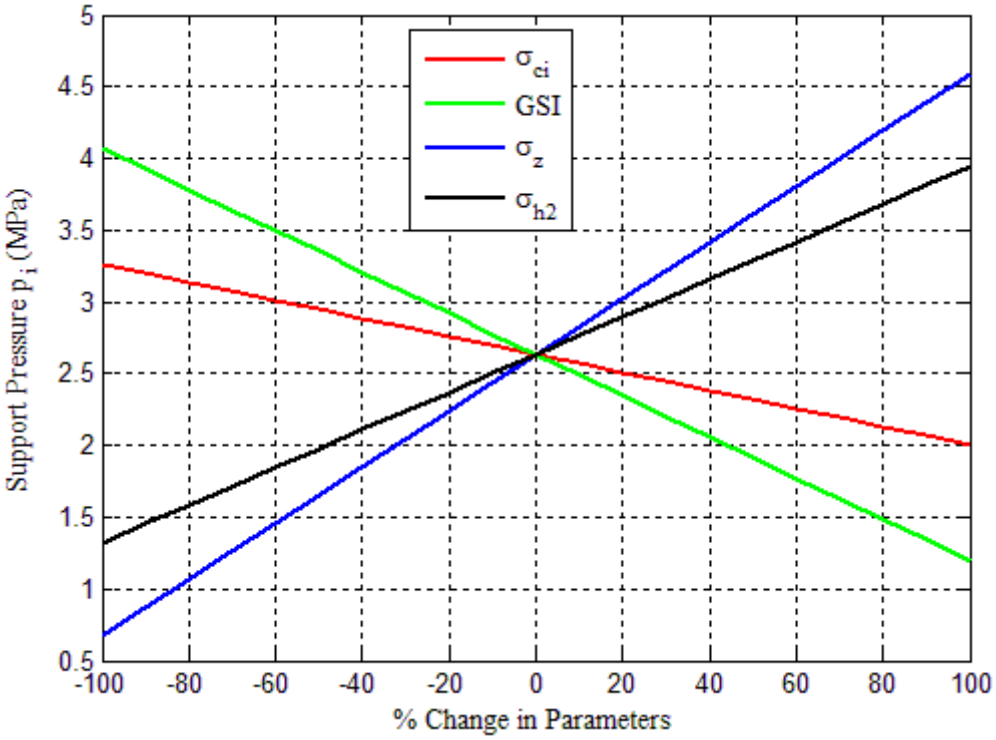

Figure 4.12 Sensitivity of support pressure to the parameters to σ_z, σ_{h2}, σ_{ci} and GSI.

Sensitivity analysis of Equation (45) shows that p_i is more sensitive to σ_z and GSI while less sensitive to σ_{ci} and σ_{h2}. This may stem from that Equation (45) involves the scaling by σ_{ci}. While σ_{ci} and GSI have negative effects, σ_z and σ_{h2} have positive effects on Equation (45).

CHAPTER 5

EVALUATION OF THE REGRESSION RESULTS WITH FUZZY LOGIC

The results of regressions are evaluated by a system named adaptive neuro-fuzzy inference system (anfis). Anfis constructs a fuzzy inference system by using an input-output data set and the results are used to validate that data set and predict its error. In order to understand how anfis works, fuzzy logic should be understood.

Fuzzy logic has mainly those meanings: Firstly, fuzzy logic is a logical system, which is an extension of multivalued logic. Secondly, fuzzy logic is almost identical to the theory of fuzzy sets, a theory which relates to classes of objects with non-sharp boundaries in which membership is a matter of degree. Another basic concept, which plays a central role in most of fuzzy logic applications, is fuzzy if-then rule or fuzzy rule. Fuzzy logic depends on the relative importance of precision: it trades off between significance and precision (The MathWorks, Inc., 2012). The following section provides an introduction to theory and practice of fuzzy logic from Fuzzy Logic Toolbox User's Guide (2012) provided by The MathWorks, Inc.

5.1. Fuzzy Logic

Fuzzy logic maps an input space to an output space, mostly with a list of if-then statements or rules. All rules are evaluated in parallel and their order is unimportant. The rules are useful because they refer to variables and adjectives describing these variables. Before a system that interpreters rules is built, all the terms to be used and the adjectives describe the terms must be defined. For example, to say that the water is hot, a range of temperature must be defined so that the temperature of the water varies at that range. Table 5.1 shows the general description of a fuzzy system on the left and a specific example on the right.

Table 5.1 A general fuzzy system with a specific example (The MathWorks, Inc., 2012).

A General Example			**A Specific Example**		
Input	→	Output	Service	→	Tip
	↓			↓	
	Rules			If service poor, tip cheap If service good, tip average If service excellent, tip generous	
/		\	/		\
Input terms		Output terms	Service is interpreted as poor, good, excellent		Tip is assigned as cheap, average, generous
(Interpret)		(Assign)			

Consequently, fuzzy inference is a method interpreting the values in an input vector and assigning different values as output vector, with the help of some set of rules.

5.1.1. Fuzzy Sets

Fuzzy logic starts with a fuzzy set. A fuzzy set is a set without a crisp and clearly defined boundary. It can contain elements with only a partial degree of membership. A fuzzy set is more easily understood

by considering a classical set. A classical set is a container that wholly includes or excludes any given element. For instance, the set of days in a week includes Monday, Thursday and Saturday and unquestionably excludes everything else. This type of set is called a classical set. According to this logic, opposites (two classes: such as Day and not-Day) should contain the entire universe. Everything falls into either one group or the other. There is not anything that is both a day of the week and not a day of the week.

When it comes to the set of days forming the weekend, most people would agree that Saturday and Sunday belong to weekend. However, there would be doubts about Friday. It is like a part of the weekend, but it should be technically excluded according to classical logic. Thus Friday tries its best by belonging both to workdays and weekend but classical sets do not tolerate such a classification. When individual perceptions are taken into account to define the weekend, yes-no (Boolean) logic with sharp edges does not answer. Then, fuzzy reasoning becomes valuable: the truth of any statement becomes a matter of degree. Any statement can be fuzzy. The major advantage of fuzzy reasoning is its ability to reply to a yes-no question with a not-quite-yes-or-no answer.

Reasoning in fuzzy logic is just a matter of generalizing the familiar yes-no logic. Even if numerical value of 1 is true and numerical value of 0 is false, fuzzy logic permits in-between values like 0.2 and 0.7453. Fuzzy logic leads to multivalued logic that stands in direct contrast to the more familiar concept of two-valued (or bivalent yes-no) logic. Then, a continuous scale time plot of weekend-ness may be designed via multivalued logic as shown in Figure 5.1.

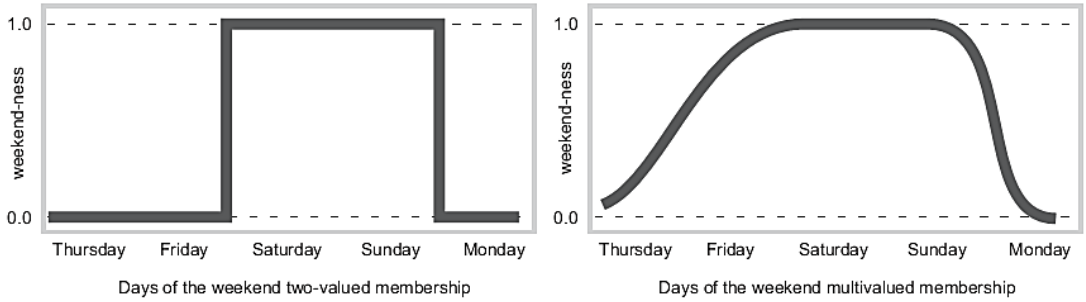

Figure 5.1 Bivalent and multivalued logic for weekend-ness (The MathWorks, Inc., 2012).

By making the plot continuous, it is possible to measure the weekend-ness of any given instant rather than an entire day. In the plot on the left, at midnight on Friday, when the second hand sweeps past 12, the weekend-ness truth value jumps discontinuously from 0 to 1.

The plot on the right shows a smoothly varying curve. There, all of Friday and to a small degree, parts of Thursday, share of the quality of weekend-ness and thus warrant partial membership in the fuzzy set of weekend moments. The curve that defines the weekend-ness of an instant in time is a function that maps the input space (time of the week) to the output space (weekend-ness). Specifically it is known as a membership function (The MathWorks, Inc., 2012).

5.1.2. Membership Functions

A membership function (MF) is a curve that describes how each point in an input space is mapped to a membership value (or degree of membership) between 0 and 1.

For instance, in the set of tall people, the input space is all potential heights (e.g. 3 to 6 feet) and the word tall would correspond to a curve that defines the degree where any person is tall. If the set of tall people is described with a well-defined (crisp) boundary of a classical set, it can be said that any person taller than a certain feet is considered tall. However, such a distinction is clearly ridiculous because everything is relatively defined in real world.

Figure 5.2 shows a smoothly varying curve that defines the transition from not tall to tall. The output axis is the membership value between 0 and 1. The curve is a membership function (μ). While both people in the figure below are tall to some degree, one is clearly less tall than the other.

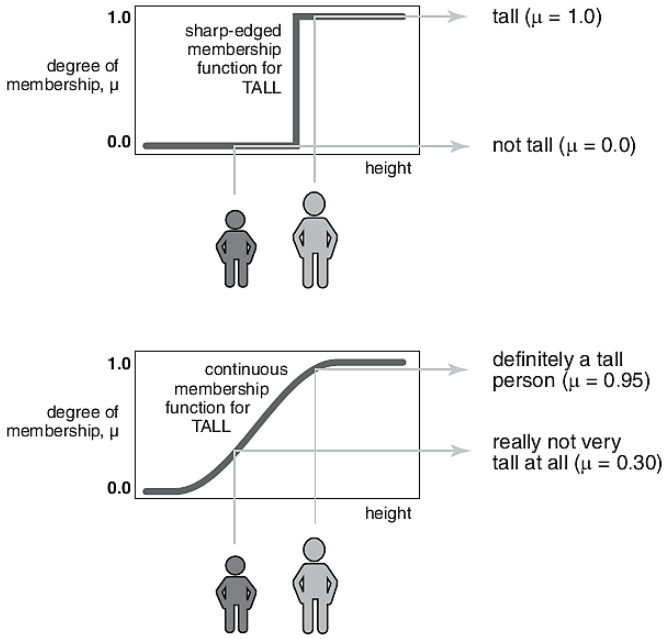

Figure 5.2 Two membership functions (The MathWorks, Inc., 2012).

Subjective interpretations and appropriate units are built into fuzzy sets. Similarly, units are included in the curve. A membership function really satisfies if it varies between 0 and 1. The function can be an arbitrary curve and its shape can be defined according to simplicity, convenience, speed and efficiency.

A classical set might be expressed as

$$A = \{x | x > N\} \tag{52}$$

where N is an arbitrary number.

A fuzzy set is an extension of a classical set. If X is an input space and its elements are denoted by x, then a fuzzy set A in X is defined as a set of ordered pairs.

$$A = \{x, \quad \mu_A(x) | x \quad X\} \tag{53}$$

Above, $\mu_A(x)$ is the membership function of x in A. The membership function assigns each element of X to a membership value between 0 and 1. Membership functions may be built from several basic functions: piece-wise linear functions, Gaussian distribution function, sigmoid curve and quadratic or cubic polynomial curves.

The simplest membership functions are formed using straight lines. The simplest one is the triangular membership function. The trapezoidal membership function has a flat top, indeed it is just a truncated triangle curve. These straight line membership functions have the advantage of simplicity.

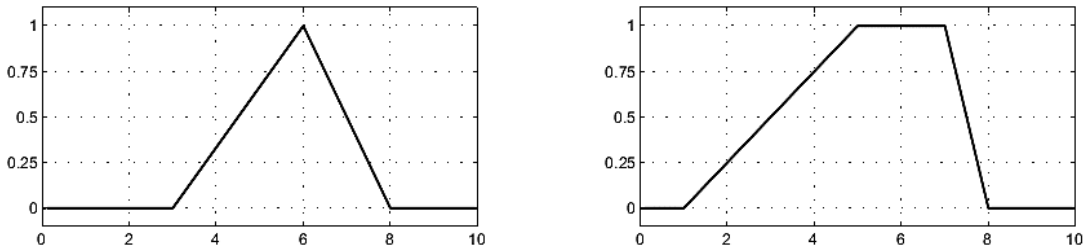

Figure 5.3 Triangular and trapezoid functions (The MathWorks, Inc., 2012).

Also, there are membership functions that are built on the Gaussian distribution curve, a simple Gaussian curve and a two-sided composite of two different Gaussian curves.

The generalized bell membership function is specified by three parameters. The bell membership function has one more parameter than the Gaussian membership function, so it can approach a non-fuzzy set if the free parameter is tuned. Because of their smoothness and concise notation, Gaussian and bell membership functions are popular methods for specifying fuzzy sets. Both of these curves have the advantage of being smooth and nonzero at all points.

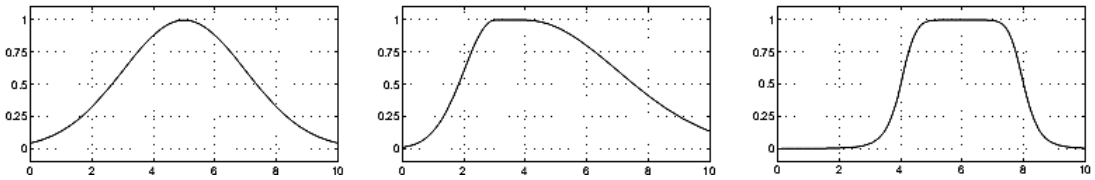

Figure 5.4 Gaussian, another Gaussian and Gaussian bell function (The MathWorks, Inc., 2012).

Although the Gaussian membership functions and bell membership functions achieve smoothness, they cannot specify asymmetric membership functions, which are important in certain applications. Therefore, the sigmoidal membership function is defined, which is either open left or right. Asymmetric and closed (i.e. not open to the left or right) membership functions can be synthesized using two sigmoidal functions: the difference and the product of two sigmoidal functions.

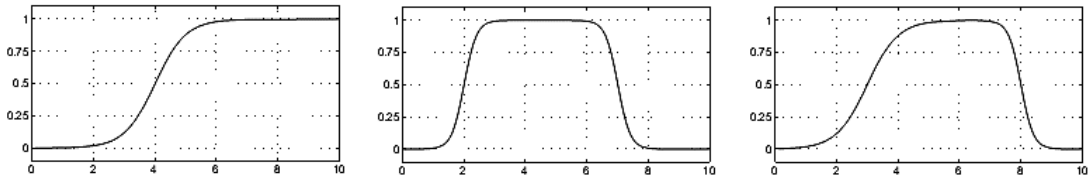

Figure 5.5 Sigmoidal, closed and asymmetric sigmoidal functions (The MathWorks, Inc., 2012).

Polynomial curves account for several of membership functions. Three related membership functions are Z, S, and Pi curves (because of their shape). Z is the asymmetrical polynomial curve open to the left, whereas S is open to the right. Pi is zero on both extremes with a rise in the middle.

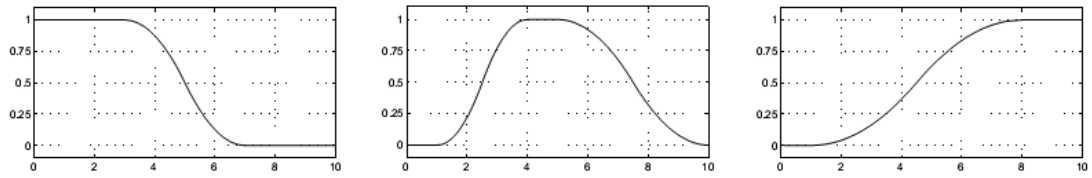

Figure 5.6 Z, Pi and S curves (The MathWorks, Inc., 2012).

The followings summarize fuzzy sets and membership functions:

- Fuzzy sets define uncertain concepts like tall people, hot water or weekend days.
- A fuzzy set utilizes possibility of partial membership. For instance, Friday is sort of a weekend day or the water is rather hot.
- The degree an object belongs to a fuzzy set is denoted by a membership value between 0 and 1. For example, Friday is a weekend day to the degree 0.8.
- A membership function linked to a given fuzzy set assigns an input value to its proper membership value.

5.1.3. Logical Process

Fuzzy logical reasoning is a superset of standard Boolean logic. That is, if fuzzy values are kept at their extremes, 1 (absolutely true) and 0 (absolutely false), standard logical processes are used, Table 5.2 shows an example of the standard truth table for AND, OR and NOT.

Table 5.2 An example for AND, OR and NOT (The MathWorks, Inc., 2012).

A	B	A AND B	A OR B	NOT A
0	0	0	0	1
0	1	0	1	1
1	0	0	1	0
1	1	1	1	0

The inputs and outputs in Table 5.2 may also be represented by some operators. Moreover, input values can be real numbers between 0 and 1 according to fuzzy logic. The operation min preserves both the results of AND process and extends inputs to all real numbers between 0 and 1. The statement A AND B (they are either 0 or 1) is resolved by using min (A, B). Likewise, OR process may be replaced with the operation max, so that A OR B becomes equivalent to max (A, B). Finally, NOT A process becomes equal to the operation 1−A. Thus, the truth table remains unaltered.

Table 5.3 Standard truth table with min and max functions (The MathWorks, Inc., 2012).

A	B	min (A, B)	max (A, B)	1 – A
0	0	0	0	1
0	1	0	1	1
1	0	0	1	0
1	1	1	1	0

Moreover, as there is a function behind the truth table, values other than 1 and 0 are also included. In Figure 5.7, the truth table is converted to a plot of two fuzzy sets applied together to create one fuzzy set. The upper part of the figure shows plots matching the preceding two-valued truth tables. The lower part of the figure simulates how the operations work over a continuously varying range of truth values A and B according to the fuzzy operations defined.

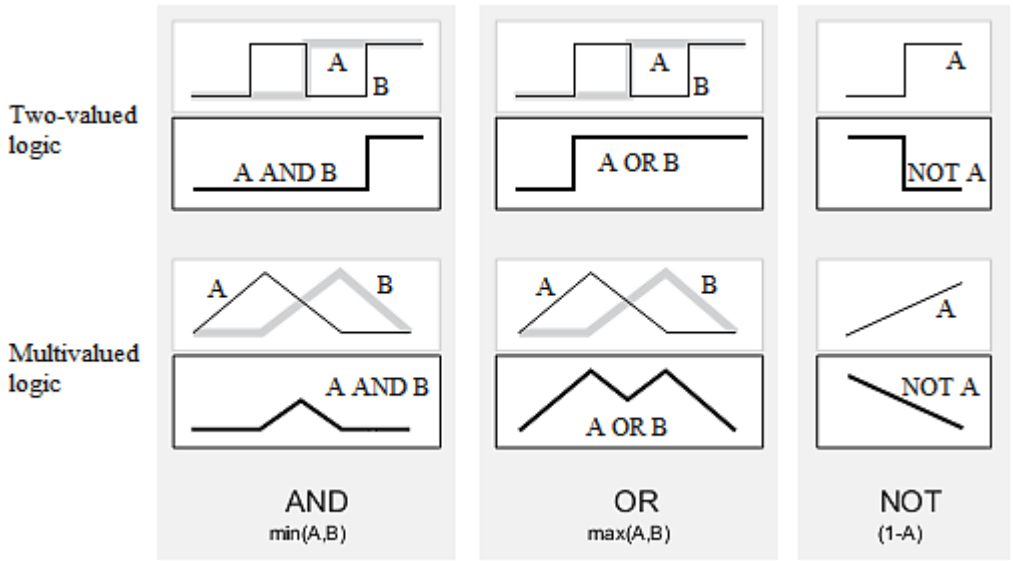

Figure 5.7 Plotted standard truth table (The MathWorks, Inc., 2012).

In addition to the classical operators, customized operators such as fuzzy intersection, fuzzy union and fuzzy complement can be used.

5.1.4. If – Then Rules

If-then rules are used to express the conditional statements containing fuzzy logic. A single fuzzy if-then rule has the form below:

$$\text{If x is A, then y is B} \tag{54}$$

Above, A and B are linguistic values defined by fuzzy sets on input spaces X and Y, respectively. The if-part of the rule "x is A" is called the antecedent or premise, while the then-part of the rule "y is B" is called the consequent or conclusion. An example of such a rule might be

If service is good, then tip is average.

In general, the input to an if-then rule is the current value for the input variable (in this case, service) and the output is an entire fuzzy set (in this case, average). Interpreting an if-then rule involves firstly evaluating the antecedent (which involves fuzzifying the input and applying any necessary fuzzy operators) and secondly applying that result to the consequent (known as implication). In the case of two-valued or binary logic if the premise is true, then the conclusion is also true. If the antecedent is true to some degree of membership, then the consequent is also true to that same degree:

In binary logic, premise and consequent are together either true or false. However, in fuzzy logic, partial antecedent provides partial implication. The antecedent of a rule can have multiple parts:

If sky is dark and storm is robust and barometer is falling, then...

In the case above, all parts of the antecedent are calculated simultaneously and resolved to a single number by using logical operators. The consequent of a rule can also have multiple parts:

If temperature is cold, then warm water is opened and cold water is closed.

In this case all consequents are affected equally by the result of the antecedent. The consequent is affected by the antecedent in this way: the consequent specifies a fuzzy set to be assigned to the output. The implication function then modifies that fuzzy set to the degree specified by the antecedent. An example with truncation is shown in Figure 5.8.

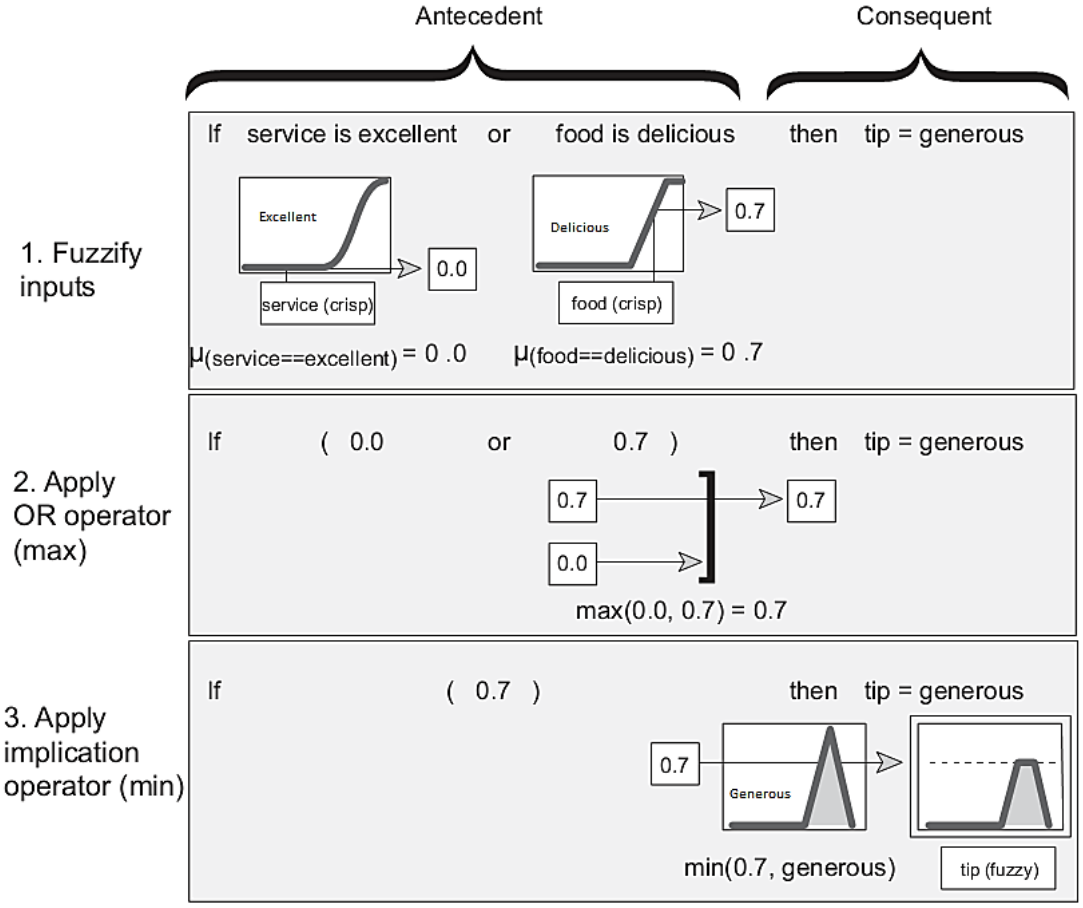

Figure 5.8 An example of if-then rule (The MathWorks, Inc., 2012).

To sum up, if-then rule is a three-part process (The MathWorks, Inc., 2012):

- Fuzzify inputs: Resolve all fuzzy statements in the antecedent to a degree of membership between 0 and 1. If the antecedent consists of only one part, then the degree of support for the rule is degree of membership.
- Apply fuzzy operator to multiple part antecedents: If the antecedent consists of multiple parts, apply fuzzy logic operators and resolve the antecedent to a single number between 0 and 1. Then, this number is the degree of support.
- Apply implication method: Use the degree of support for the entire rule to figure the output fuzzy set. An entire fuzzy set is assigned to the output by the consequent of a fuzzy rule. This fuzzy set is described by a membership function specifying the qualities of the consequent. If the antecedent is only partially true (i.e., it is assigned to a value less than 1), then the output fuzzy set is trimmed according to the implication method.

The output of each rule is a fuzzy set and these sets are then aggregated into a single output fuzzy set. Finally the resulting set is defuzzified or resolved to a single number. As a result, membership functions, logical operations and if-then rules constitute the process of fuzzy inference.

5.1.5. Sugeno Type Fuzzy Inference

The Sugeno output membership functions are either linear or constant. A typical rule in a Sugeno fuzzy model has the form

$$\text{If Input 1} = x \text{ and Input 2} = y, \text{ then Output is } z = ax + by + c \tag{55}$$

For a zero-order Sugeno model, the output level z is a constant (a = b = 0). The output level z_i of each rule is weighted by the firing strength w_i of the rule. For instance, for an AND rule with Input 1 = x and Input 2 = y, the firing strength is

$$w_i = \text{AndMethod}\,(F_1(x), F_2(y)) \tag{56}$$

where $F_{1,2}(.)$ are the membership functions for Inputs 1 and 2.

The final output of the system is the weighted average of all rule outputs, computed as

$$\text{Final Output} = \frac{\sum_{i=1}^{N} w_i z_i}{\sum_{i=1}^{N} w_i} \tag{57}$$

where N is the number of rules. A Sugeno rule operates as shown in Figure 5.9.

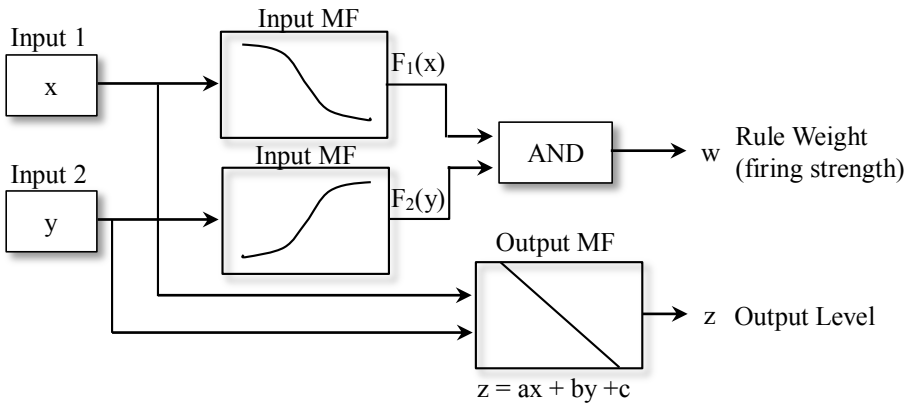

Figure 5.9 Sugeno rule process (The MathWorks, Inc., 2012).

5.1.6. Anfis

The acronym anfis derives its name from adaptive neuro-fuzzy inference system. Anfis applies fuzzy inference techniques to data modeling. Fuzzy inference can be applied to a system where input/output data for modeling were collected.

The neuro-adaptive learning method works similarly to that of neural networks. Neuro-adaptive learning techniques provide a method for the fuzzy modeling procedure to learn information about a data set. Anfis computes the membership function parameters that best allow the associated fuzzy inference system to track the given input/output data.

Using a given input/output data set, anfis constructs a fuzzy inference system (FIS) whose membership function parameters are tuned (adjusted) using either a back propagation algorithm alone or in combination with a least squares type of method. This adjustment allows the defined fuzzy systems to learn from the data they are modeling.

In this study, anfis function of MATLAB R2010b (The MathWorks, Inc., 2010) was used with the following properties:

- A single-output Sugeno-type fuzzy inference system using a grid partition on the data used as initial conditions (initialization of the membership function parameters) for anfis training.
- The number of membership functions is 6; the input membership function type is 'Gaussian bell'; and the output membership function type is 'linear'.
- Since a large number of rules (more than 250) in the FIS is created when the membership functions are greater than 6, MATLAB may run out of memory.

5.2. Model Validation

Model validation is the process by which the input vectors from input/output data sets on which the FIS was not trained, are presented to the trained FIS model, to see how well the FIS model predicts the corresponding data set output values. When the results are evaluated by anfis, the following error rates in Table 5.4 are obtained:

Table 5.4 Root means square errors (RMSE) of the derived equations.

	Training Error	**Checking Error**
Equation (45)	$2.7767*10^{-5}$	0.016389
Equation (50)	$1.6746*10^{-4}$	0.034070

When a data matrix composed of input and output columns is given anfis, anfis generates its own output column based on the training by the data matrix and the process described in this chapter. Then, anfis compares its output column to the original output column by using RMSE. RMSE may be defined like that:

$$\mathrm{RMSE} = \sqrt{\frac{1}{N} * \sum_{k=1}^{N} (t_k - a_k)^2} \tag{58}$$

where t_k is the output of the training data; a_k is the output generated by anfis; and N is the number of the output data.

Training error shows RMSE between the output of the regression equation and the output generated by anfis. Similarly, checking error shows RMSE between the output of Phase2 and the output generated by anfis. Since Equation (45) produces less checking error, it is the most truthful equation in this study.

CHAPTER 6

LINING SUPPORT DESIGN

6.1. Lining Thickness Calculation

Assuming that p_i is equal to $p_{sc\,max}$ in Equation (28) in Elastic Theory and inserting Equation (48) into Equation (28), t_c becomes

$$t_c = r\left(\sqrt{\frac{f_c}{f_c - 2p_i}} - 1\right) \tag{59}$$

Inserting Equation (48) into Equation (59) gives

$$t_c = r\left(\sqrt{\frac{f_c}{f_c - 0.0322 * \sigma_{ci} + 0.001436 * \sigma_{ci} * GSI - z * (0.013014 - 0.008748 * k2)}} - 1\right) \tag{60}$$

In the following section, a software program utilizing Equation (60) is explained.

6.2. Lining Thickness Estimator "Shaft 2D"

A user friendly object-oriented software package was developed by the author of this study in MATLAB R2010b (The MathWorks, Inc., 2010) to overcome the tiresome shaft lining thickness calculations. The package allows users to enter and change inputs any time at input window and see the design of liner along shaft depth. This software is a Windows Standalone Application using Equation (59). It has the interface shown in Figure 6.1.

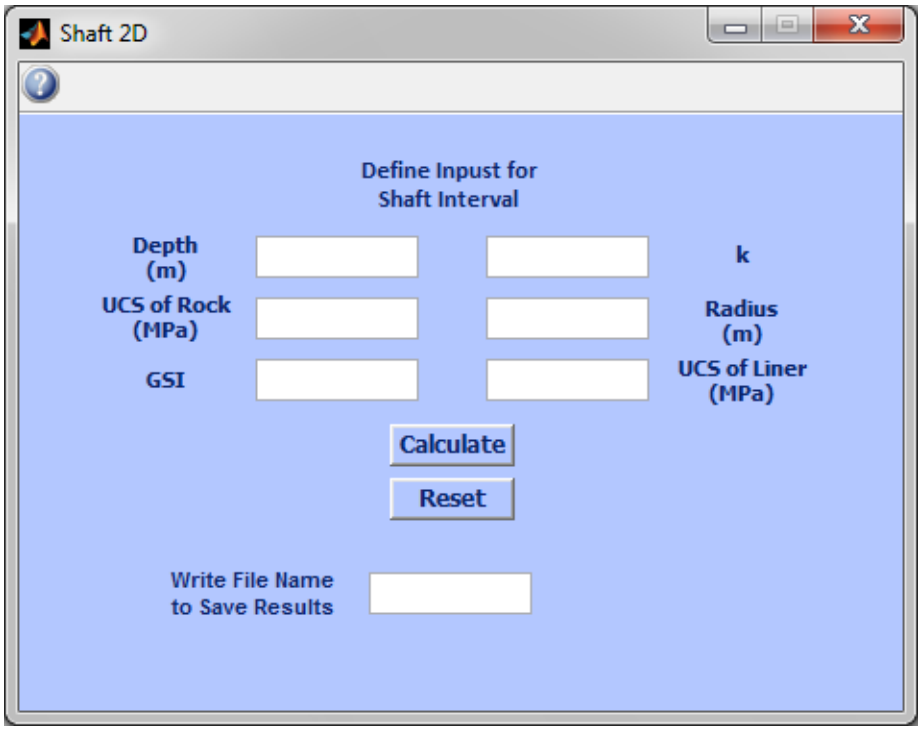

Figure 6.1 Interface of lining thickness calculator "Shaft 2D".

This program takes the following inputs:

- Depth takes an interval in meters. Along this interval, properties of the rock are fixed. For instance, if an interval from 60 m to 85 m is asked, it must be entered as 60:85.
- UCS of Rock indicates uniaxial compressive strength of intact rock in MPa for the asked interval. It must be entered as a single number, for instance, 25.
- GSI indicates geologic strength index for the asked interval. It must be entered as a single number, for instance, 30.
- k is ratio of horizontal stresses or horizontal and vertical stresses for the asked interval. It must be entered as a single number, for instance, 2.
- Radius takes radius of the shaft in meter. It must be entered as a single number, for instance, 3.
- UCS of Liner indicates uniaxial compressive strength of lining in MPa for the asked interval. It must be entered as a single number, for instance, 35.
- The results can be saved to an Excel (Microsoft Corporation) file if a name is written. The file is found in the same folder where the program exists.
- The software is capable of taking different interval properties along a shaft depth. Multiple inputs must be separated by a comma, for example, 60:85,85:110 or 25,30.

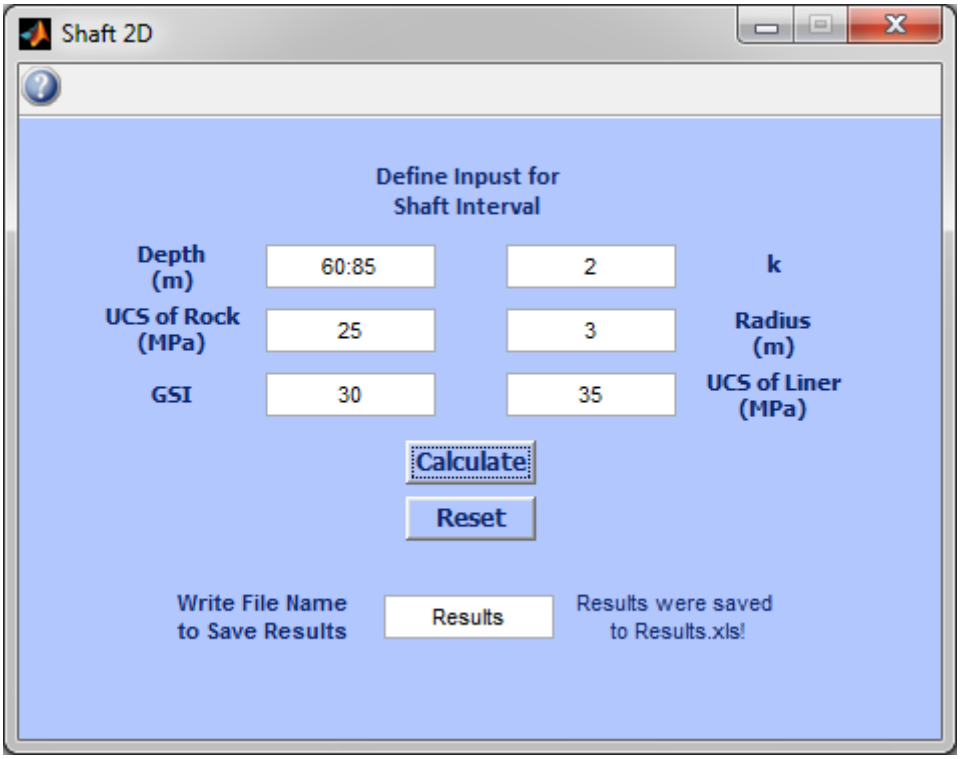

Figure 6.2 Example inputs for the software.

Table 6.1 The saved results of the query in Figure 6.2.

Interval (m)	UCS of Liner (MPa)	Top Thickness (cm)	Bottom Thickness (cm)
60-85	35	7	10

In the example above, the shaft interval starts at 60 m and ends at 85 m. Thickness of the lining is 7 cm at 60 m and 10 cm at 85 m. Since it is not practical to change lining thickness so often for short intervals, the software is designed to change the lining thickness at every 25 m interval, giving the maximum thickness at that interval as the lining thickness. Additionally, the practical thicknesses defined in Rules of Thumb are taken into account. When the following inputs were added to the previous inputs, lining thickness is shown in Figure 6.3.

- Depth: 85 m to 110 m
- UCS of Rock: 30 MPa
- GSI: 25
- k: 2
- Radius: 3 m
- UCS of Liner: 35 MPa

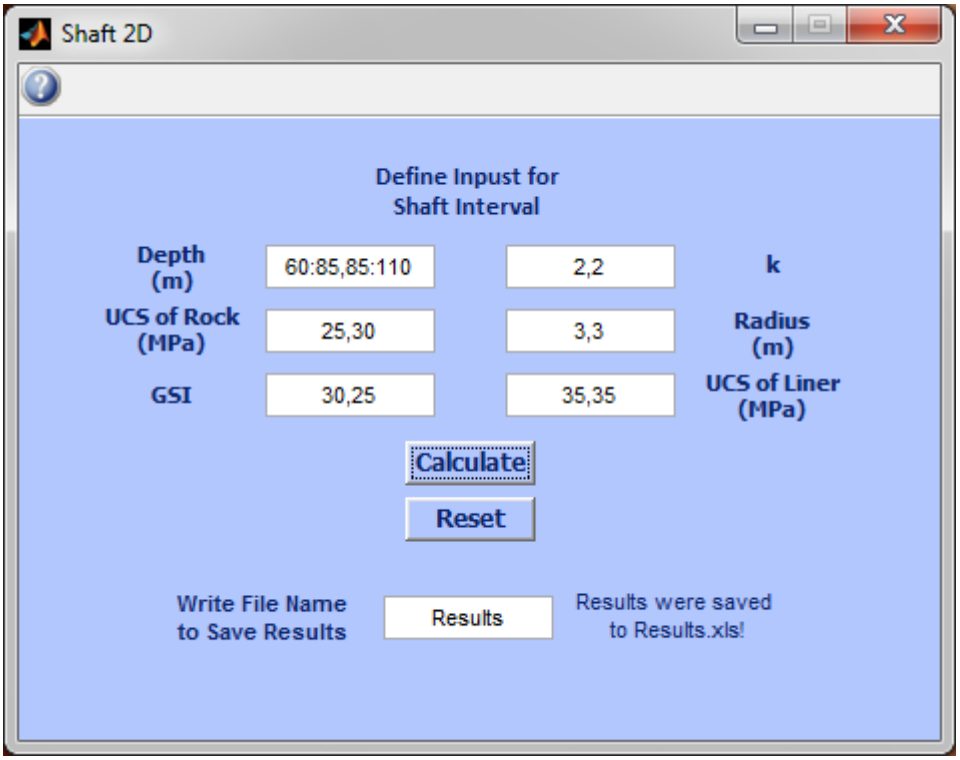

Figure 6.3 An example for multiple intervals.

Table 6.2 Results for multiple inputs in Figure 6.3.

Interval (m)	UCS of Liner (MPa)	Thicknesss (cm)	Lining Type
60-85	35	10	Shotcrete
85-110	35	15	Shotcrete

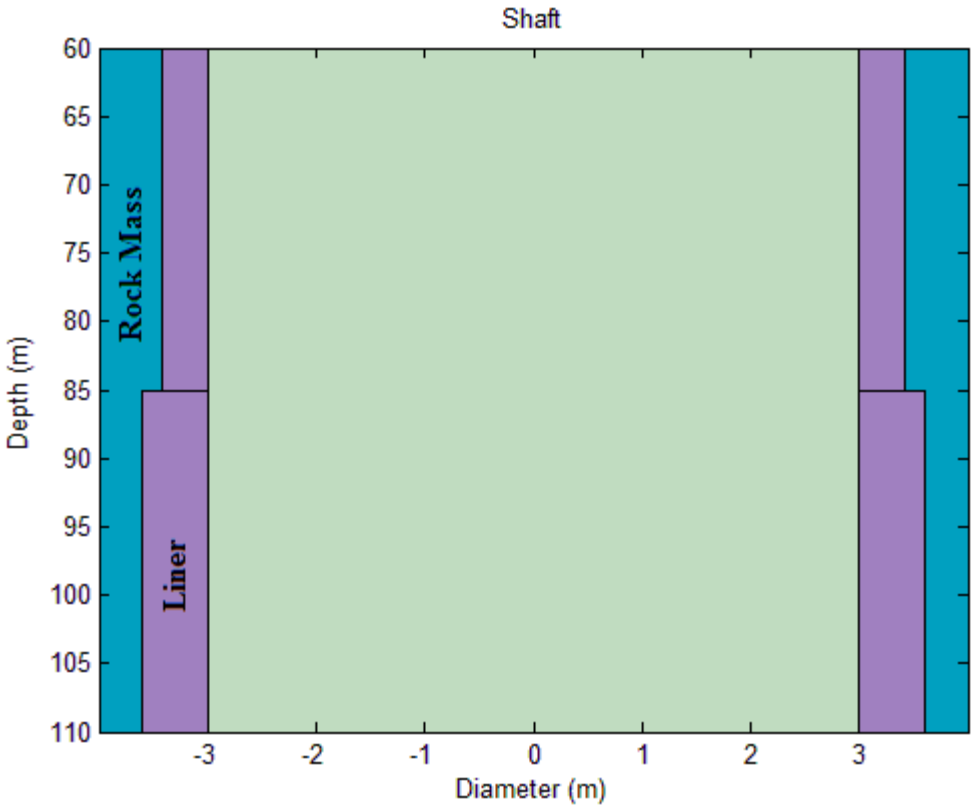

Figure 6.4 Graph of the lining for the previous example. Not scaled.

6.3. Flowchart of the Program

The flowchart of the program shows the rough procedure of the software Shaft 2D. Firstly, the software needs the parameters to estimate p_i; secondly, p_i is compared to f_c; and thirdly, t_c is estimated. The interval where t_c takes place determines the lining type of the shaft.

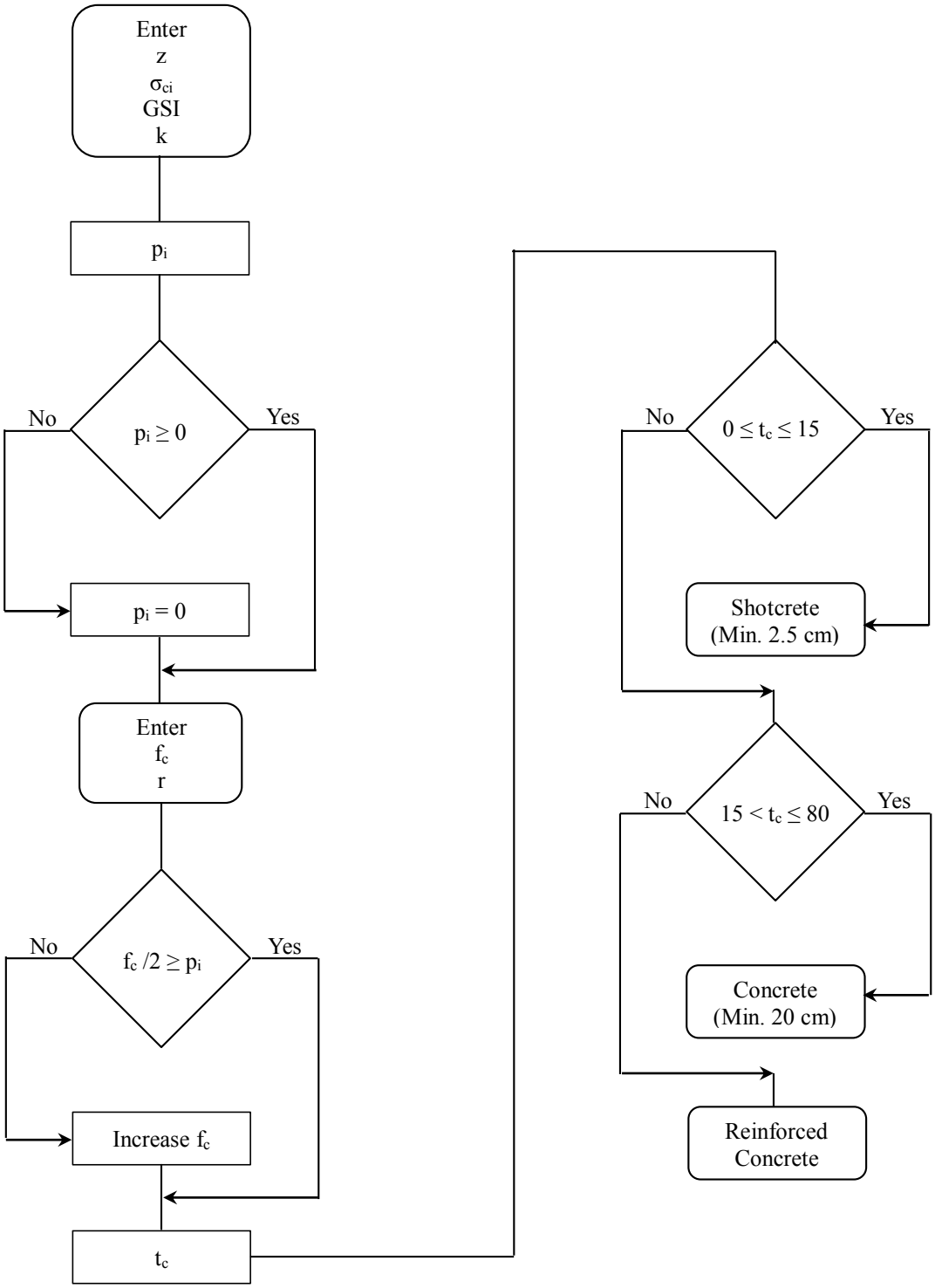

Figure 6.5 Flowchart of the developed program.

6.4. Manual Calculation

This section gives a hand calculation of lining thickness. The first example has the following inputs:

z = 60 to 75 m, σ_{ci} = 30 MPa, GSI = 30, k = 2, r = 3 m, f_c = 25 MPa.

Putting the inputs for 60 and 75 m into Equation (45) gives

$$p_i = 30 * \left(0.0161 - 0.000718 * 30 + 0.241 * \frac{0.027 * 60}{30} + 0.162 * \frac{2 * 0.027 * 60}{30}\right) \approx 0.75 \text{ MPa}$$

$$p_i = 30 * \left(0.0161 - 0.000718 * 30 + 0.241 * \frac{0.027 * 75}{30} + 0.162 * \frac{2 * 0.027 * 75}{30}\right) \approx 0.98 \text{ MPa}$$

Then putting p_i's into Equation (59) yields

$$t_c = 3 * \left(\sqrt{\frac{25}{25 - 2 * 0.75}} - 1\right) \approx 9.5 \text{ cm}$$

$$t_c = 3 * \left(\sqrt{\frac{25}{25 - 2 * 0.98}} - 1\right) \approx 12.5 \text{ cm}$$

Because of practical reasons, the lining thickness is chosen as 12.5 cm for 60 – 75 m interval.

6.5. Case Study Comparisons

Comparison of the results to the case studies may provide verification for this study. Although a survey on the literature provides real data from the field, there may be some deficiencies in these data. Since all the inputs for the software do not exist in the case below, some values were assumed and compared afterwards. The following values are given by Emir and Önce (2002) for a 3.25 m shaft radius in the GLI deep coal zone.

Table 6.3 Data from the borehole measurements of GLI deep coal zone.

Rock	Claystone	Marn	Marn
z (m)	36 to 62	124 to 250	250 to 390
σ_{ci} (MPa)	12.6	11.2	11.2
γ (MN/m^3)	0.021	0.021	0.021
ϕ (°)	40 (Assumed)	38	38
s (Hoek-Brown cons.)	0.0013	0.0031	0.0054
GSI (Equation (42))	40	48	53

Table 6.4 Stress ratio around the shaft and strength of the concrete.

k (Assumed)	1	1	1
f_c (MPa)	30	30	30

Table 6.5 Pressure on the lining for the intervals in Table 6.3.

Rock	Claystone	Marn	Marn
Shaft 2D (MPa)	0.233 to 0.516	1.144 to 2.515	2.474 to 3.998
Kopex (MPa)	0.610 to 1.054	1.612 to 3.250	3.250 to 5.070
Protodjakonow (MPa)	0.164 to 0.283	0.619 to 1.249	1.249 to 1.948

Table 6.6 Comparison of lining thicknesses.

Rock	Claystone	Marn	Marn
z (m)	36 to 62	124 to 250	250 to 390
Shaft 2D (cm)	3 to 6	13 to 31	31 to 54
Heise (cm)	3 to 6	12 to 27	27 to 43
Arıoğlu (cm)	5 to 12	26 to 61	60 to 102
Haynes (cm)	14 to 17	23 to 37	37 to 52
Emir and Önce (cm)	30	30	30

Above, all the methods uses the outer pressure interval provided by Shaft 2D in Table 6.5. In Table 6.6, the minimum and the maximum thicknesses and the lining type are not taken into account to make an accurate evaluation. It is seen that Shaft 2D provides the minimum lining thicknesses when compared to the others. However, in each method, the thicknesses are mostly affected by the depth. The thicknesses spread out from each other as the depth increases.

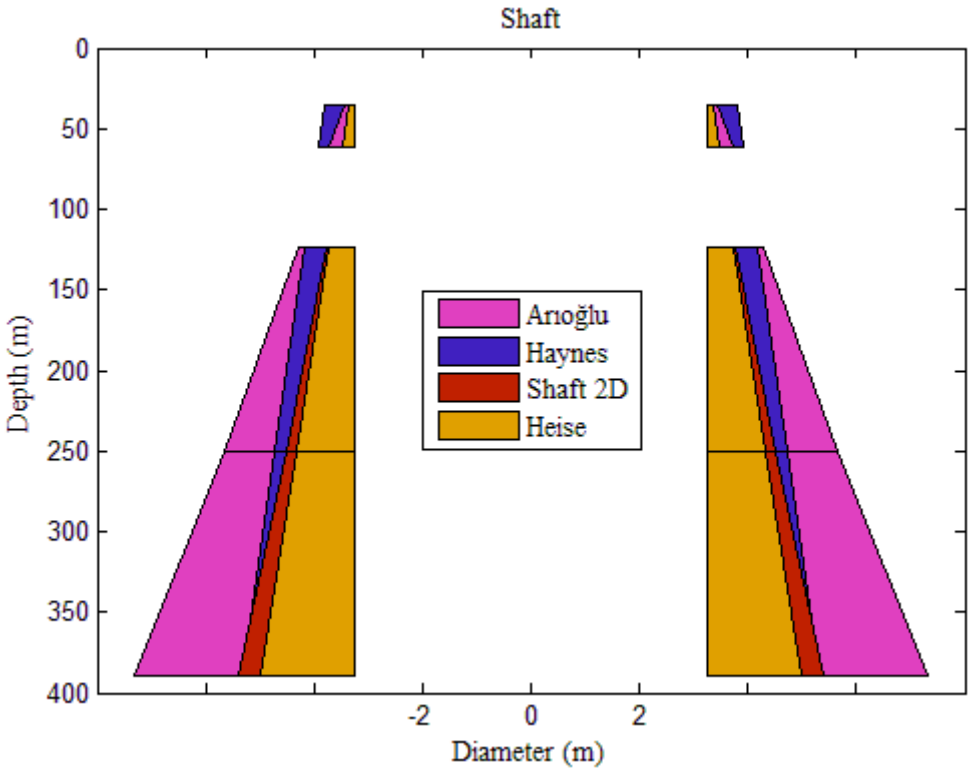

Figure 6.6 Comparison of the thicknesses in Table 6.6. Not scaled.

Figure 6.6 shows that "Shaft 2D" or Equation (48) locates between other methods. Increase in depth makes all the methods to give greater thicknesses but each method has a different reaction to the depth. While Haynes' and Heise's methods have steeper angles, "Shaft 2D"s and Arıoğlu's methods have less slope.

CHAPTER 7

CONCLUSIONS AND RECOMMENDATIONS

Although numerical studies done by using a software let users define so many parameter of shaft and surrounding rock mass, the estimation of support pressure is a challenging problem since it depends on many parameters. Therefore, the parameters chosen to estimate a support pressure equation should be closely related to support pressure and well represent shaft geometry and surrounding rock mass. However, there will be always bias and overdesign in the estimated equation. Moreover, when these parameters or their values change, support pressure equation will also change. Therefore, verifications and limits of numerical studies must be taken into account. It can be concluded that the support pressure equation derived in this study is valid for rock masses with the following properties:

Compressive strength: 25 to 200 MPa
Geological strength index: 20 to 80
Stress ratio for horizontal stresses: 0.5 to 2
Depth: 25 to 600 m

The numerical modeling by means of Phase2 used in this study aims at giving suitable lining thickness for circular shafts in different rock masses. For that reason, 2D shaft sections with different variables in Hoek-Brown medium were modeled. Results of the models lead to the followings:

- Increase in uniaxial compressive strength of intact rock causes support pressure to decrease.
- Increase in geological strength index causes support pressure to decrease.
- Increase in depth causes support pressure to increase.
- Increase in horizontal to vertical stress ratio causes support pressure to behave like a curve.

A number of regression analyses were made to get a proper function of support pressure. Firstly, a linear equation was obtained with regression constant of 74.6. Secondly, a non-linear equation was obtained.

In this study, the following lining thickness formula by Lamé is used to determine the thickness of the liner with varying strength where p_i comes from Equation (48).

$$t_c = r\left(\sqrt{\frac{f_c}{f_c - 2p_i}} - 1\right)$$

where t_c is thickness of liner; r is radius of shaft; f_c is uniaxial compressive strength of liner; and p_i is defined as

$$p_i = \sigma_{ci} * (0.0161 - 0.000718 * GSI) + z * (0.006507 + 0.004374 * k2)$$

Table 7.1 gives approximate support properties of shotcrete and concrete for circular openings under hydrostatic loading for perfect symmetry. The supports are assumed to act over the entire surface of the opening walls (Hoek, Kaiser, & Bawden, 1995). The equations above can be better used with the properties below:

Table 7.1 Support characteristics of shotcrete and concrete for circular openings.

	28 Day Old Shotcrete					**28 Day Old Concrete**				
Excavation Diameter (m)	4	6	8	10	12	4	6	8	10	12
Max. Support Pressure (MPa)	0.86	0.58	0.43	0.35	0.29	4.86	3.33	2.53	2.04	1.71
Thickness (mm)	50					300				
Strength (MPa)	35					35				
Stiffness (MPa)	21000					21000				

The sensitivity analysis of Equation (48) shows that p_i is most sensitive to σ_z because it has the greatest coefficient in the linear equation. However, since σ_{ci} is multiplied by GSI, their total effect is greater than that of σ_z. This result can be observed in Figure 4.3, Figure 4.4 and Figure 4.5.

When the outputs of Equation (45) and Equation (50) evaluated by the fuzzy logic system anfis, it is seen that the former has a less error. However, these error rates may always be updated by changing the parameters of anfis, if desired. Nonetheless, it seems that Equation (45) will always have a less error rate than Equation (50) because the latter is a weak match for the outputs of Phase2.

The developed software "Shaft 2D" is the easy way to calculate the lining thickness given by Equation (60). It takes inputs through its interface and gives the results by saving and visualizing. It can be used as a Windows Standalone Application. Although the software uses Equation (60) to calculate lining thickness, it includes some assumptions such as a range for parameters, types of lining thicknesses, as 25 m depth interval or accepting k2 as k.

The followings are recommended after this study:

- Analytical solution of support pressure inside circular shafts for non-hydrostatic stress state with Hoek-Brown failure criterion was not given so far. Therefore, to overcome this, numerical studies are carried out but closed form solutions may be developed in the future.
- Software capable of simulations provide an excessive help to make numerical studies. However, these studies need to be supported with data from fields.
- The lining design carried out in this study does not take into account the shaft collar design, ground water loading conditions, loading from heavy geological conditions (faults, shear zones etc.), form of topography, structures and other openings around shafts. Considerations of these factors will improve the quality of shaft lining design.
- The dependency of software using numerical methods such as finite difference, finite element, boundary element or distinct element methods on the number and position of nodes, elements and meshes affects the results notably. Therefore, models with higher number of nodes and meshes in an infinite field will produce more realistic results.
- Other lining methods such as timbers, steels, rock bolts, meshes should also be considered in the future studies.
- The effect of the varying shaft radius with the displacement boundary control for the boundaries of the shaft section should also be thought.
- More detailed studies on non-linear responses of support pressure may cause better models.

REFERENCES

Arıoğlu, E. (1970). Maden Kuyularının Kaplamalarına Gelen Radyal Basıncın Hesabı ve Kaplama Kalınlığının Tesbiti. *İTÜ Dergisi*, pp. 36-41.

Arıoğlu, E. (1982). Maden Kuyusu Kaplama Kalınlığının Boyutlandırılmasına Rasyonel Bir Yaklaşım. *7. Türkiye Madencilik Bilimsel ve Teknik Kongresi* (pp. 367-383). Ankara: TMMOB Maden Mühendisleri Odası.

Brady, B. G., & Brown, E. T. (2005). *Rock Mechanics for Underground Mining.* New York: Kluwer Academic Publishers.

Emir, E., & Önce, G. (2002). Sayısal Modelleme ile G.L.İ. Derin Linyit Sahası için Kuyu Kaplama Kalınlığının Belirlenmesi. *Madencilik*, pp. 22-30.

Harrison, J. P., & FREng, J. A. (2000). *Engineering Rock Mechanics: Part 2.* Oxford: Pergamon.

Hoek, E. (2012). *Rock Mass Properties.* Retrieved 2012, from Hoek's Corner: http://www.rocscience.com/education/hoeks_corner

Hoek, E. (2012). *Shotcrete Support.* Retrieved from Hoek's Corner: http://www.rocscience.com/education/hoeks_corner

Hoek, E., Carranza-Torres, C., & Corkum, B. (2002). Hoek-Brown Failure Criterion – 2002 Edition. *5. North American Rock Mechanics Symposium*, (pp. 267-273). Toronto.

Hoek, E., Kaiser, P., & Bawden, W. (1995). *Support of Underground Excavations in Hard Rock.* Rotterdam: Balkema.

Kendorski, F. S., & Hambley, D. F. (1992). Other Applications of Geomechanics. In H. L. Hartman, *SME Mining Engineering Handbook* (pp. 972-988). Colorado: Society for Mining, Metallurgy, and Exploration, Inc.

Kopex Corporation. (1998). *Geological Section and Pressure Diagram of Kozlu Shaft.* Kopex Corporation.

Öztürk, H. (2000). *Prediction of Broken Zone Radius and Lining Thickness around Circular Mine Shafts.* Ankara: METU.

Pariseau, W. G. (1992). Rock Mechanics. In H. L. Hartman, *SME Mining Engineering Handbook* (pp. 829-847). Colorado: Society for Mining, Metallurgy, and Exploration, Inc.

The MathWorks, Inc. (2012, September). Fuzzy Logic Toolbox™ User's Guide. USA.

Theodoridis, S., & Koutroumbas, K. (2009). *Pattern Recognition.* Oxford: Academic Press.

Unrug, K. F. (1992). Construction of Development Openings. In H. L. Hartman, *SME Mining Engineering Handbook* (pp. 1580-1645). Colorado: Society for Mining, Metallurgy, and Exploration, Inc.

Vergne, J. d. (2003). *The Hard Rock Miner's Handbook, Edition 3.* Ontario: McIntosh Engineering.

APPENDIX A

ESTIMATION OF MATERIAL CONSTANTS

This section shows the estimation of E_i and m_i. Hoek (2012) recommends the following equation when no direct value of Ei is available.

$$E_i = MR \times \sigma_{ci} \tag{61}$$

To estimate E_i and m_i, from the following rock groups were benefited (Hoek, 2012).

Table A.1 E_i when σ_{ci} is 25 MPa. E_i was rounded off to 12500.

σ_{ci} (MPa)	**Rock**	**MR**
5 – 25	Chalk	1000
5 – 25	Rocksalt (Halite – NaCl)	?
5 – 25	Potash (Slyvite – KCl)	?
5 – 25	Gypsum	350
5 – 25	Anhydrite	350
25 – 50	Claystone	250 ± 50
25 – 50	Coal	?
25 – 50	Concrete	?
25 – 50	Schist	675 ± 425
25 – 50	Shale	200 ± 50
25 – 50	Siltstone	375 ± 25
Average of 5 – 25	1700 / 3 = 567	
Average of 25 – 50	1500 / 4 = 375	
Average of 5 – 50	3200 / 7 = 457	
E_i (MPa)	457 * 25 = 11425	
Weighted Average	(1700*3 + 1500*4)/(3*3+4*4) = 444	
E_i (MPa)	444 * 25 = 11100	

Table A.2 E_i when σ_{ci} is 50 MPa. E_i was rounded off to 25000.

σ_{ci} (MPa)	Rock	MR
25 – 50	Claystone	250 ± 50
25 – 50	Coal	?
25 – 50	Concrete	?
25 – 50	Schist	675 ± 425
25 – 50	Shale	200 ± 50
25 – 50	Siltstone	375 ± 25
50 – 100	Limestone	700 ± 100
50 – 100	Marble	850 ± 150
50 – 100	Phyllite	550 ± 250
50 – 100	Sandstone	275 ± 75
50 – 100	Schist	675 ± 425
50 – 100	Shale	200 ± 50
Average of 25 – 50	1500 / 4 = 375	
Average of 50 – 100	3250 / 6 = 542	
Average of 25 – 100	4750 / 10 = 475	
E_i (MPa)	50 * 475 = 23750	
Weighted Average	(1500*4 + 3250*6)/(4*4+6*6) = 490	
E_i (MPa)	50 * 490 = 24500	

Table A.3 E_i when σ_{ci} is 100 MPa. E_i was rounded off to 50000.

σ_{ci} (MPa)	Rock	MR
50 – 100	Limestone	700 ± 100
50 – 100	Marble	850 ± 150
50 – 100	Phyllite	550 ± 250
50 – 100	Sandstone	275 ± 75
50 – 100	Schist	675 ± 425
50 – 100	Shale	200 ± 50
100 – 250	Amphibolite	450 ±50
100 – 250	Sandstone	275 ± 75
100 – 250	Basalt	350 ± 100
100 – 250	Gabbro	450 ± 50
100 – 250	Gneiss	525 ± 225
100 – 250	Granodiorite	425 ± 25
100 – 250	Limestone	700 ± 100
100 – 250	Marble	850 ± 150
100 – 250	Rhyolite	400 ± 100
100 – 250	Tuff	300 ± 100
Average of 50 – 100	3250 / 6 = 542	
Average of 100 – 250	4725 / 10 = 473	
Average of 50 – 250	7975 / 16 = 498	
E_i (MPa)	100 * 498 = 49800	
Weighted Average	(3250*6 + 4725*10)/(6*6+10*10) = 491	
E_i (MPa)	100 * 491 = 49100	

Table A.4 E_i when σ_{ci} is 200 MPa. E_i was rounded off to 100000.

σ_{ci} (MPa)	Rock	MR
100 – 250	Amphibolite	450 ±50
100 – 250	Sandstone	275 ± 75
100 – 250	Basalt	350 ± 100
100 – 250	Gabbro	450 ± 50
100 – 250	Gneiss	525 ± 225
100 – 250	Granodiorite	425 ± 25
100 – 250	Limestone	700 ± 100
100 – 250	Marble	850 ± 150
100 – 250	Rhyolite	400 ± 100
100 – 250	Tuff	300 ± 100
Average of 100 – 250	4725 / 10 = 473	
E_i (MPa)	200 * 473 = 94600	

Table A.5 m_i when σ_{ci} is 25 MPa. m_i was rounded off to 7.

σ_{ci} (MPa)	Rock	m_i
5 – 25	Chalk	7 ± 2
5 – 25	Rocksalt (Halite – NaCl)	?
5 – 25	Potash (Slyvite – KCl)	?
5 – 25	Gypsum	8 ± 2
5 – 25	Anhydrite	12 ± 2
25 – 50	Claystone	4 ± 2
25 – 50	Coal	?
25 – 50	Concrete	?
25 – 50	Schist	10 ± 3
25 – 50	Shale	6 ± 2
25 – 50	Siltstone	7 ± 2
Average of 5 – 25	27 / 3 = 9	
Average of 25 – 50	27 / 4 = 6.75	
Average of 5 – 50	54 / 7 = 7.71	
Weighted Average	(27*3 + 27*4)/(3*3+4*4) = 7.56	

Table A.6 m_i when σ_{ci} is 50 MPa. m_i was rounded off to 14.

σ_{ci} (MPa)	Rock	m_i
25 – 50	Claystone	4 ± 2
25 – 50	Coal	?
25 – 50	Concrete	?
25 – 50	Schist	10 ± 3
25 – 50	Shale	6 ± 2
25 – 50	Siltstone	7 ± 2
50 – 100	Limestone	10 ± 3
50 – 100	Marble	9 ± 3
50 – 100	Phyllite	7 ± 3
50 – 100	Sandstone	17 ± 4
50 – 100	Schist	10 ± 3
50 – 100	Shale	6 ± 2
Average of 25 – 50	27 / 4 = 6.75	
Average of 50 – 100	59 / 6 = 9.83	
Average of 25 – 100	86 / 10 = 8.6	
Weighted Average	(27*4 + 59*6)/(4*4+6*6) = 8.88	

Table A.7 m_i when σ_{ci} is 100 MPa. m_i was rounded off to 21.

σ_{ci} (MPa)	Rock	m_i
50 – 100	Limestone	10 ± 3
50 – 100	Marble	9 ± 3
50 – 100	Phyllite	7 ± 3
50 – 100	Sandstone	17 ± 4
50 – 100	Schist	10 ± 3
50 – 100	Shale	6 ± 2
100 – 250	Amphibolite	26 ± 6
100 – 250	Sandstone	17 ± 4
100 – 250	Basalt	25 ± 5
100 – 250	Gabbro	27 ± 3
100 – 250	Gneiss	28 ± 5
100 – 250	Granodiorite	29 ± 3
100 – 250	Limestone	10 ± 3
100 – 250	Marble	9 ± 3
100 – 250	Rhyolite	25 ± 5
100 – 250	Tuff	13 ± 5
Average of 50 – 100	59 / 6 = 9.83	
Average of 100 – 250	209 / 10 = 20.9	
Average of 50 – 250	268 / 16 = 16.75	
Weighted Average	(59*6 + 209*10)/(6*6+10*10) = 17.97	

Table A.8 m_i when σ_{ci} is 200 MPa. m_i was rounded off to 28.

σ_{ci} (MPa)	Rock	m_i
100 – 250	Amphibolite	26 ± 6
100 – 250	Sandstone	17 ± 4
100 – 250	Basalt	25 ± 5
100 – 250	Gabbro	27 ± 3
100 – 250	Gneiss	28 ± 5
100 – 250	Granodiorite	29 ± 3
100 – 250	Limestone	10 ± 3
100 – 250	Marble	9 ± 3
100 – 250	Rhyolite	25 ± 5
100 – 250	Tuff	13 ± 5
Average of 100 – 250	209 / 10 = 20.9	

The following estimates of rock strength are helpful to approximate E_i and m_i of intact rock (Hoek, Rock Mass Properties, 2012).

Table A.9 Field estimate of strength of rock types.

Strength	Rock	Explanation of Strength
> 250 MPa	Fresh basalt, Chert, Diabase, Gneiss, Granite, Quartzite	Specimen can only be chipped with a geological hammer.
100 – 250 MPa	Amphibolite, Sandstone, Basalt, Gabbro, Gneiss, Granodiorite, Limestone, Marble, Rhyolite, Tuff	Specimen requires many blows of a geological hammer to fracture it.
50 – 100 MPa	Limestone, Marble, Phyllite, Sandstone, Schist, Shale	Specimen requires more than one blow of a geological hammer to fracture it.
25 – 50 MPa	Claystone, Coal, Concrete, Schist, Shale, Siltstone	Cannot be scraped or peeled with a pocket knife, specimen can be fractured with a single blow from a geological hammer.
5 – 25 MPa	Chalk, Rocksalt, Potash	Can be peeled with a pocket knife with difficulty, shallow indentation made by firm blow with point of a geological hammer.
1 – 5 MPa	Highly weathered or altered rock	Crumbles under firm blows with point of a geological hammer, can be peeled by a pocket knife.
0.25 – 1 MPa	Stiff fault gouge	Indented by thumbnail.

APPENDIX B

RESULTS OF NUMERICAL MODELING

Table B.1 First quarter of the results.

Model	σ_{ci} (MPa)	GSI	σ_z (MPa)	σ_{h1} (MPa)	σ_{h2} (MPa)	k1	k2	p_i (MPa)
1	25	20	2.7	2.7	1.35	1	0.5	1.42
2	25	20	8.1	8.1	4.05	1	0.5	5.73
3	25	20	16.2	16.2	8.1	1	0.5	13.96
4	25	20	2.7	2.7	2.7	1	1	1.22
5	25	20	8.1	8.1	8.1	1	1	4.92
6	25	20	16.2	16.2	16.2	1	1	11.23
7	25	20	2.7	2.7	4.05	1	1.5	2.47
8	25	20	8.1	8.1	12.15	1	1.5	8.94
9	25	20	16.2	16.2	24.3	1	1.5	18.93
10	25	20	2.7	2.7	5.4	1	2	3.31
11	25	20	8.1	8.1	16.2	1	2	15.49
12	25	20	16.2	16.2	32.4	1	2	NA
13	25	40	2.7	2.7	1.35	1	0.5	1.02
14	25	40	8.1	8.1	4.05	1	0.5	4.44
15	25	40	16.2	16.2	8.1	1	0.5	10.35
16	25	40	2.7	2.7	2.7	1	1	0.75
17	25	40	8.1	8.1	8.1	1	1	3.75
18	25	40	16.2	16.2	16.2	1	1	9.3
19	25	40	2.7	2.7	4.05	1	1.5	1.71
20	25	40	8.1	8.1	12.15	1	1.5	7.7
21	25	40	16.2	16.2	24.3	1	1.5	18.24
22	25	40	2.7	2.7	5.4	1	2	2.8
23	25	40	8.1	8.1	16.2	1	2	13.29
24	25	40	16.2	16.2	32.4	1	2	18.9
25	25	60	2.7	2.7	1.35	1	0.5	0.55
26	25	60	8.1	8.1	4.05	1	0.5	3.57
27	25	60	16.2	16.2	8.1	1	0.5	8.4
28	25	60	2.7	2.7	2.7	1	1	0.36
29	25	60	8.1	8.1	8.1	1	1	2.64
30	25	60	16.2	16.2	16.2	1	1	7.28
31	25	60	2.7	2.7	4.05	1	1.5	1.05
32	25	60	8.1	8.1	12.15	1	1.5	5.89
33	25	60	16.2	16.2	24.3	1	1.5	15.12
34	25	60	2.7	2.7	5.4	1	2	1.9
35	25	60	8.1	8.1	16.2	1	2	9.62
36	25	60	16.2	16.2	32.4	1	2	19.98
37	25	80	2.7	2.7	1.35	1	0.5	0
38	25	80	8.1	8.1	4.05	1	0.5	2.03
39	25	80	16.2	16.2	8.1	1	0.5	6.83
40	25	80	2.7	2.7	2.7	1	1	0
41	25	80	8.1	8.1	8.1	1	1	1.32
42	25	80	16.2	16.2	16.2	1	1	4.97
43	25	80	2.7	2.7	4.05	1	1.5	0.14
44	25	80	8.1	8.1	12.15	1	1.5	3.85
45	25	80	16.2	16.2	24.3	1	1.5	11.46
46	25	80	2.7	2.7	5.4	1	2	0.76
47	25	80	8.1	8.1	16.2	1	2	6.83
48	25	80	16.2	16.2	32.4	1	2	18.9

Table B.2 Second quarter of the results.

Model	σ_{ci} (MPa)	GSI	σ_z (MPa)	σ_{h1} (MPa)	σ_{h2} (MPa)	k1	k2	p_i (MPa)
49	50	20	2.7	2.7	1.35	1	0.5	0.85
50	50	20	8.1	8.1	4.05	1	0.5	4.12
51	50	20	16.2	16.2	8.1	1	0.5	9.3
52	50	20	2.7	2.7	2.7	1	1	0.63
53	50	20	8.1	8.1	8.1	1	1	3.13
54	50	20	16.2	16.2	16.2	1	1	7.95
55	50	20	2.7	2.7	4.05	1	1.5	1.41
56	50	20	8.1	8.1	12.15	1	1.5	6.52
57	50	20	16.2	16.2	24.3	1	1.5	15.9
58	50	20	2.7	2.7	5.4	1	2	2.34
59	50	20	8.1	8.1	16.2	1	2	9.37
60	50	20	16.2	16.2	32.4	1	2	19.8
61	50	40	2.7	2.7	1.35	1	0.5	0.4
62	50	40	8.1	8.1	4.05	1	0.5	2.61
63	50	40	16.2	16.2	8.1	1	0.5	7.44
64	50	40	2.7	2.7	2.7	1	1	0.28
65	50	40	8.1	8.1	8.1	1	1	1.91
66	50	40	16.2	16.2	16.2	1	1	5.56
67	50	40	2.7	2.7	4.05	1	1.5	0.75
68	50	40	8.1	8.1	12.15	1	1.5	4.44
69	50	40	16.2	16.2	24.3	1	1.5	12.07
70	50	40	2.7	2.7	5.4	1	2	1.35
71	50	40	8.1	8.1	16.2	1	2	7.44
72	50	40	16.2	16.2	32.4	1	2	17.58
73	50	60	2.7	2.7	1.35	1	0.5	0.07
74	50	60	8.1	8.1	4.05	1	0.5	1.48
75	50	60	16.2	16.2	8.1	1	0.5	4.95
76	50	60	2.7	2.7	2.7	1	1	0.01
77	50	60	8.1	8.1	8.1	1	1	1.03
78	50	60	16.2	16.2	16.2	1	1	3.58
79	50	60	2.7	2.7	4.05	1	1.5	0.31
80	50	60	8.1	8.1	12.15	1	1.5	2.75
81	50	60	16.2	16.2	24.3	1	1.5	8.54
82	50	60	2.7	2.7	5.4	1	2	0.66
83	50	60	8.1	8.1	16.2	1	2	4.95
84	50	60	16.2	16.2	32.4	1	2	14.47
85	50	80	2.7	2.7	1.35	1	0.5	0
86	50	80	8.1	8.1	4.05	1	0.5	0.26
87	50	80	16.2	16.2	8.1	1	0.5	2.57
88	50	80	2.7	2.7	2.7	1	1	0
89	50	80	8.1	8.1	8.1	1	1	0
90	50	80	16.2	16.2	16.2	1	1	1.65
91	50	80	2.7	2.7	4.05	1	1.5	0
92	50	80	8.1	8.1	12.15	1	1.5	1.08
93	50	80	16.2	16.2	24.3	1	1.5	5.1
94	50	80	2.7	2.7	5.4	1	2	0
95	50	80	8.1	8.1	16.2	1	2	2.57
96	50	80	16.2	16.2	32.4	1	2	9.47

Table B.3 Third quarter of the results.

Model	σ_{ci} (MPa)	GSI	σ_z (MPa)	σ_{h1} (MPa)	σ_{h2} (MPa)	k1	k2	p_i (MPa)
97	100	20	2.7	2.7	1.35	1	0.5	0.42
98	100	20	8.1	8.1	4.05	1	0.5	2.44
99	100	20	16.2	16.2	8.1	1	0.5	6.78
100	100	20	2.7	2.7	2.7	1	1	0.31
101	100	20	8.1	8.1	8.1	1	1	1.8
102	100	20	16.2	16.2	16.2	1	1	5.1
103	100	20	2.7	2.7	4.05	1	1.5	0.74
104	100	20	8.1	8.1	12.15	1	1.5	4.08
105	100	20	16.2	16.2	24.3	1	1.5	10.99
106	100	20	2.7	2.7	5.4	1	2	1.3
107	100	20	8.1	8.1	16.2	1	2	6.78
108	100	20	16.2	16.2	32.4	1	2	17.76
109	100	40	2.7	2.7	1.35	1	0.5	0.13
110	100	40	8.1	8.1	4.05	1	0.5	1.22
111	100	40	16.2	16.2	8.1	1	0.5	4.05
112	100	40	2.7	2.7	2.7	1	1	0.08
113	100	40	8.1	8.1	8.1	1	1	0.87
114	100	40	16.2	16.2	16.2	1	1	2.93
115	100	40	2.7	2.7	4.05	1	1.5	0.28
116	100	40	8.1	8.1	12.15	1	1.5	2.24
117	100	40	16.2	16.2	24.3	1	1.5	7.06
118	100	40	2.7	2.7	5.4	1	2	0.57
119	100	40	8.1	8.1	16.2	1	2	4.05
120	100	40	16.2	16.2	32.4	1	2	12.13
121	100	60	2.7	2.7	1.35	1	0.5	0
122	100	60	8.1	8.1	4.05	1	0.5	0.46
123	100	60	16.2	16.2	8.1	1	0.5	2.18
124	100	60	2.7	2.7	2.7	1	1	0
125	100	60	8.1	8.1	8.1	1	1	0.27
126	100	60	16.2	16.2	16.2	1	1	1.5
127	100	60	2.7	2.7	4.05	1	1.5	0
128	100	60	8.1	8.1	12.15	1	1.5	1.06
129	100	60	16.2	16.2	24.3	1	1.5	4.14
130	100	60	2.7	2.7	5.4	1	2	0.1
131	100	60	8.1	8.1	16.2	1	2	2.18
132	100	60	16.2	16.2	32.4	1	2	7.66
133	100	80	2.7	2.7	1.35	1	0.5	0
134	100	80	8.1	8.1	4.05	1	0.5	0
135	100	80	16.2	16.2	8.1	1	0.5	0.35
136	100	80	2.7	2.7	2.7	1	1	0
137	100	80	8.1	8.1	8.1	1	1	0
138	100	80	16.2	16.2	16.2	1	1	0
139	100	80	2.7	2.7	4.05	1	1.5	0
140	100	80	8.1	8.1	12.15	1	1.5	0
141	100	80	16.2	16.2	24.3	1	1.5	1.54
142	100	80	2.7	2.7	5.4	1	2	0
143	100	80	8.1	8.1	16.2	1	2	0.35
144	100	80	16.2	16.2	32.4	1	2	3.76

Table B.4 Fourth quarter of the results.

Model	σ_{ci} (MPa)	GSI	σ_z (MPa)	σ_{h1} (MPa)	σ_{h2} (MPa)	k1	k2	p_i (MPa)
145	200	20	2.7	2.7	1.35	1	0.5	0.19
146	200	20	8.1	8.1	4.05	1	0.5	1.31
147	200	20	16.2	16.2	8.1	1	0.5	4.03
148	200	20	2.7	2.7	2.7	1	1	0.14
149	200	20	8.1	8.1	8.1	1	1	0.96
150	200	20	16.2	16.2	16.2	1	1	2.97
151	200	20	2.7	2.7	4.05	1	1.5	0.36
152	200	20	8.1	8.1	12.15	1	1.5	2.31
153	200	20	16.2	16.2	24.3	1	1.5	6.87
154	200	20	2.7	2.7	5.4	1	2	0.66
155	200	20	8.1	8.1	16.2	1	2	4.03
156	200	20	16.2	16.2	32.4	1	2	11.61
157	200	40	2.7	2.7	1.35	1	0.5	0
158	200	40	8.1	8.1	4.05	1	0.5	0.49
159	200	40	16.2	16.2	8.1	1	0.5	1.93
160	200	40	2.7	2.7	2.7	1	1	0
161	200	40	8.1	8.1	8.1	1	1	0.34
162	200	40	16.2	16.2	16.2	1	1	1.37
163	200	40	2.7	2.7	4.05	1	1.5	0.06
164	200	40	8.1	8.1	12.15	1	1.5	0.99
165	200	40	16.2	16.2	24.3	1	1.5	3.61
166	200	40	2.7	2.7	5.4	1	2	0.19
167	200	40	8.1	8.1	16.2	1	2	1.93
168	200	40	16.2	16.2	32.4	1	2	6.63
169	200	60	2.7	2.7	1.35	1	0.5	0
170	200	60	8.1	8.1	4.05	1	0.5	0
171	200	60	16.2	16.2	8.1	1	0.5	0.7
172	200	60	2.7	2.7	2.7	1	1	0
173	200	60	8.1	8.1	8.1	1	1	0
174	200	60	16.2	16.2	16.2	1	1	0.43
175	200	60	2.7	2.7	4.05	1	1.5	0
176	200	60	8.1	8.1	12.15	1	1.5	0.19
177	200	60	16.2	16.2	24.3	1	1.5	1.64
178	200	60	2.7	2.7	5.4	1	2	0
179	200	60	8.1	8.1	16.2	1	2	0.7
180	200	60	16.2	16.2	32.4	1	2	3.44
181	200	80	2.7	2.7	1.35	1	0.5	0
182	200	80	8.1	8.1	4.05	1	0.5	0
183	200	80	16.2	16.2	8.1	1	0.5	0
184	200	80	2.7	2.7	2.7	1	1	0
185	200	80	8.1	8.1	8.1	1	1	0
186	200	80	16.2	16.2	16.2	1	1	0
187	200	80	2.7	2.7	4.05	1	1.5	0
188	200	80	8.1	8.1	12.15	1	1.5	0
189	200	80	16.2	16.2	24.3	1	1.5	0
190	200	80	2.7	2.7	5.4	1	2	0
191	200	80	8.1	8.1	16.2	1	2	0
192	200	80	16.2	16.2	32.4	1	2	0.53

APPENDIX C

RESTRICTED SUPPORT PRESSURES

Table C.1 First half of p_i restricted to (0-4) MPa.

Row	σ_{ci} (MPa)	GSI	σ_z (MPa)	σ_{h1} (MPa)	σ_{h2} (MPa)	k1	k2	p_i (MPa)
1	25	20	2.7	2.7	2.7	1	1	1.22
2	25	20	2.7	2.7	4.05	1	1.5	2.47
3	25	40	2.7	2.7	1.35	1	0.5	1.02
4	25	40	2.7	2.7	2.7	1	1	0.75
5	25	40	8.1	8.1	8.1	1	1	3.75
6	25	40	2.7	2.7	4.05	1	1.5	1.71
7	25	60	2.7	2.7	1.35	1	0.5	0.55
8	25	60	8.1	8.1	4.05	1	0.5	3.57
9	25	60	2.7	2.7	2.7	1	1	0.36
10	25	60	8.1	8.1	8.1	1	1	2.64
11	25	60	2.7	2.7	4.05	1	1.5	1.05
12	25	60	2.7	2.7	5.4	1	2	1.9
13	25	80	8.1	8.1	4.05	1	0.5	2.03
14	25	80	8.1	8.1	8.1	1	1	1.32
15	25	80	2.7	2.7	4.05	1	1.5	0.14
16	25	80	8.1	8.1	12.15	1	1.5	3.85
17	25	80	2.7	2.7	5.4	1	2	0.76
18	50	20	2.7	2.7	1.35	1	0.5	0.85
19	50	20	2.7	2.7	2.7	1	1	0.63
20	50	20	8.1	8.1	8.1	1	1	3.13
21	50	20	2.7	2.7	4.05	1	1.5	1.41
22	50	20	2.7	2.7	5.4	1	2	2.34
23	50	40	2.7	2.7	1.35	1	0.5	0.4
24	50	40	8.1	8.1	4.05	1	0.5	2.61
25	50	40	2.7	2.7	2.7	1	1	0.28
26	50	40	8.1	8.1	8.1	1	1	1.91
27	50	40	2.7	2.7	4.05	1	1.5	0.75
28	50	40	2.7	2.7	5.4	1	2	1.35
29	50	60	2.7	2.7	1.35	1	0.5	0.07
30	50	60	8.1	8.1	4.05	1	0.5	1.48
31	50	60	2.7	2.7	2.7	1	1	0.01
32	50	60	8.1	8.1	8.1	1	1	1.03
33	50	60	16.2	16.2	16.2	1	1	3.58
34	50	60	2.7	2.7	4.05	1	1.5	0.31
35	50	60	8.1	8.1	12.15	1	1.5	2.75
36	50	60	2.7	2.7	5.4	1	2	0.66
37	50	80	8.1	8.1	4.05	1	0.5	0.26
38	50	80	16.2	16.2	8.1	1	0.5	2.57
39	50	80	16.2	16.2	16.2	1	1	1.65
40	50	80	8.1	8.1	12.15	1	1.5	1.08
41	50	80	8.1	8.1	16.2	1	2	2.57
42	100	20	2.7	2.7	1.35	1	0.5	0.42
43	100	20	8.1	8.1	4.05	1	0.5	2.44
44	100	20	2.7	2.7	2.7	1	1	0.31
45	100	20	8.1	8.1	8.1	1	1	1.8

Table C.2 Second half of p_i restricted to (0-4) MPa.

Row	σ_{ci} (MPa)	GSI	σ_z (MPa)	σ_{h1} (MPa)	σ_{h2} (MPa)	k1	k2	p_i (MPa)
46	100	20	2.7	2.7	4.05	1	1.5	0.74
47	100	20	2.7	2.7	5.4	1	2	1.3
48	100	40	2.7	2.7	1.35	1	0.5	0.13
49	100	40	8.1	8.1	4.05	1	0.5	1.22
50	100	40	2.7	2.7	2.7	1	1	0.08
51	100	40	8.1	8.1	8.1	1	1	0.87
52	100	40	16.2	16.2	16.2	1	1	2.93
53	100	40	2.7	2.7	4.05	1	1.5	0.28
54	100	40	8.1	8.1	12.15	1	1.5	2.24
55	100	40	2.7	2.7	5.4	1	2	0.57
56	100	60	8.1	8.1	4.05	1	0.5	0.46
57	100	60	16.2	16.2	8.1	1	0.5	2.18
58	100	60	8.1	8.1	8.1	1	1	0.27
59	100	60	16.2	16.2	16.2	1	1	1.5
60	100	60	8.1	8.1	12.15	1	1.5	1.06
61	100	60	2.7	2.7	5.4	1	2	0.1
62	100	60	8.1	8.1	16.2	1	2	2.18
63	100	80	16.2	16.2	8.1	1	0.5	0.35
64	100	80	16.2	16.2	24.3	1	1.5	1.54
65	100	80	8.1	8.1	16.2	1	2	0.35
66	100	80	16.2	16.2	32.4	1	2	3.76
67	200	20	2.7	2.7	1.35	1	0.5	0.19
68	200	20	8.1	8.1	4.05	1	0.5	1.31
69	200	20	2.7	2.7	2.7	1	1	0.14
70	200	20	8.1	8.1	8.1	1	1	0.96
71	200	20	16.2	16.2	16.2	1	1	2.97
72	200	20	2.7	2.7	4.05	1	1.5	0.36
73	200	20	8.1	8.1	12.15	1	1.5	2.31
74	200	20	2.7	2.7	5.4	1	2	0.66
75	200	40	8.1	8.1	4.05	1	0.5	0.49
76	200	40	16.2	16.2	8.1	1	0.5	1.93
77	200	40	8.1	8.1	8.1	1	1	0.34
78	200	40	16.2	16.2	16.2	1	1	1.37
79	200	40	2.7	2.7	4.05	1	1.5	0.06
80	200	40	8.1	8.1	12.15	1	1.5	0.99
81	200	40	16.2	16.2	24.3	1	1.5	3.61
82	200	40	2.7	2.7	5.4	1	2	0.19
83	200	40	8.1	8.1	16.2	1	2	1.93
84	200	60	16.2	16.2	8.1	1	0.5	0.7
85	200	60	16.2	16.2	16.2	1	1	0.43
86	200	60	8.1	8.1	12.15	1	1.5	0.19
87	200	60	16.2	16.2	24.3	1	1.5	1.64
88	200	60	8.1	8.1	16.2	1	2	0.7
89	200	60	16.2	16.2	32.4	1	2	3.44
90	200	80	16.2	16.2	32.4	1	2	0.53

APPENDIX D

REGRESSION ANALYSIS DETAILS

The following explanations ease to understand the statistical results of the regressions by Minitab 16.

- Predictor lists variables in a regression equation. For instance, constant, σ_{ci}, GSI etc.
- Coef gives coefficients of predictors. It is 1 for the constant.
- SE Coef gives the standard deviation of the estimate of a regression coefficient. It measures how precisely the data can estimate the coefficient's unknown value. Its value is always positive and smaller values indicate a more precise estimate.
- T is calculated by dividing the coefficient (Coef) by its standard error (SE Coef).
- P is used to determine whether a factor is significant; it is typically compared against an alpha value of 0.05. If the p-value is lower than 0.05, then the factor is significant.
- S is standard deviation of the data.
- R-Sq means percentage of response variable variation that is explained by its relationship with one or more predictor variables. In general, the higher the R^2, the better the model fits your data. R^2 is always between 0 and 100 %. It is also known as the coefficient of determination or a multiple determination (in a multiple regression).
- R-Sq (adj) is percentage of response variable variation that is explained by its relationship with one or more predictor variables, adjusted for the number of predictors in the model. This adjustment is important because the R^2 for any model will always increase when a new term is added. A model with more terms may appear to have a better fit simply because it has more terms. However, some increases in R^2 may be due to chance alone.

Analysis of Variance Table:

The main output from an analysis of variance study is arranged in a table and it lists the sources of variation, their degrees of freedom, the total sum of squares, and the mean squares. The analysis of variance table also includes the F-statistics and p-values. These are used to determine whether the predictors or factors are significantly related to the response.

- Source indicates the source of variation, either from the factor, the interaction, or the error. The total is a sum of all the sources.
- DF indicates degrees of freedom from each source. If a factor has three levels, the degree of freedom is 2 (n-1). If you have a total of 30 observations, the degrees of freedom total is 29 (n – 1).
- SS indicates sum of squares between groups (factor) and the sum of squares within groups (error).
- MS (mean squares) are found by dividing the sum of squares by the degrees of freedom.
- F is calculated by dividing the factor MS by the error MS; this ratio can be compared against a critical F found in a table.
- P is used to determine whether a factor is significant; typically compared against an alpha value of 0.05. If the p-value is lower than 0.05, then the factor is significant. P-value for each coefficient tests the null hypothesis that the coefficient is equal to zero (no effect). Therefore, low p-values suggest the predictor is a meaningful addition to the model.
- Unusual observations (outliers) list observations that have a disproportionate impact on a regression. Influential observations, also known as unusual observations, are important to identify because they can produce misleading results. For example, a significant coefficient may appear to be non-significant.
- Standardized residuals are helpful in detecting outliers. The standardized residual equals the value of a residual, divided by an estimate of its standard deviation. Standardized residuals greater than 2 and less than -2 are usually considered large and Minitab labels these observations with an 'R' in the table of unusual observations and the table of fits and residuals.

The statistical results of the linear regression are given below:

Regression Analysis: p_i/σ_{ci} versus GSI; σ_z/σ_{ci}; σ_{h2}/σ_{ci}

The regression equation is
$p_i/\sigma_{ci} = 0.0161 - 0.000718 \times GSI + 0.241 \times \sigma_z/\sigma_{ci} + 0.162 \times \sigma_{h2}/\sigma_{ci}$

Predictor	Coef	SE Coef	T	P
Constant	0.016080	0.004532	3.55	0.001
GSI	−0.0007183	0.0001074	−6.69	0.000
σ_z/σ_{ci}	0.24082	0.03415	7.05	0.000
σ_{h2}/σ_{ci}	0.16173	0.03234	5.00	0.000

S = 0.0167660 R-Sq = 74.6% R-Sq(adj) = 73.7%

Analysis of Variance:

Source	DF	SS	MS	F	P
Regression	3	0.070865	0.023622	84.03	0.000
Residual Error	86	0.024174	0.000281		
Total	89	0.095039			

Source	DF	Seq SS
GSI	1	0.002427
σ_z/σ_{ci}	1	0.061410
σ_{h2}/σ_{ci}	1	0.007028

Unusual Observations:

Obs	GSI	p_i/σ_{ci}	Fit	SE Fit	Residual	St Resid
2	20.0	0.09880	0.05392	0.00415	0.04488	2.76R
5	40.0	0.15000	0.11777	0.00636	0.03223	2.08RX
8	60.0	0.14280	0.07721	0.00653	0.06559	4.25RX
12	60.0	0.07600	0.03393	0.00356	0.04207	2.57R
13	80.0	0.08120	0.06284	0.00675	0.01836	1.20 X
14	80.0	0.05280	0.08904	0.00489	−0.03624	2.26R
16	80.0	0.15400	0.11524	0.00756	0.03876	2.59RX
38	80.0	0.05140	0.06284	0.00675	−0.01144	−0.75 X
39	80.0	0.03300	0.08904	0.00489	−0.05604	−3.49R

R denotes an observation with a large standardized residual.
X denotes an observation whose X value gives it large leverage.

The statistical results of the non-linear regressions are given below:

Polynomial Regression Analysis: p_i/σ_{ci} versus GSI

The regression equation is
$p_i/\sigma_{ci} = 7.516 - 9.077 \times \log10(GSI) + 2.745 \times (\log10(GSI))^2$

S = 0.0131632 R-Sq = 97.6% R-Sq(adj) = 92.9%

Analysis of Variance:

Source	DF	SS	MS	F	P
Regression	2	0.0071972	0.0035986	20.77	0.153
Error	1	0.0001733	0.0001733		
Total	3	0.0073705			

Sequential Analysis of Variance:

Source	DF	SS	F	P
Linear	1	0.0000309	0.01	0.935
Quadratic	1	0.0071663	41.36	0.098

Regression Analysis: p_i/σ_{ci} versus σ_z/σ_{ci}

The regression equation is
$p_i/\sigma_{ci} = 0.2033 + 0.1528 \times \log10(\sigma_z/\sigma_{ci})$

S = 0.0155892 R-Sq = 93.4% R-Sq(adj) = 90.1%

Analysis of Variance:

Source	DF	SS	MS	F	P
Regression	1	0.0068844	0.0068844	28.33	0.034
Error	2	0.0004860	0.0002430		
Total	3	0.0073705			

Polynomial Regression Analysis: pi/σci versus σh2/σci

The regression equation is
$p_i/\sigma_{ci} = 0.2225 + 0.2272 \times \log10(\sigma_{h2}/\sigma_{ci}) + 0.0410 \times (\log10(\sigma_{h2}/\sigma_{ci}))^2$

S = 0.0277883 R-Sq = 89.5% R-Sq(adj) = 68.6%

Analysis of Variance:

Source	DF	SS	MS	F	P
Regression	2	0.0065983	0.0032991	4.27	0.324
Error	1	0.0007722	0.0007722		
Total	3	0.0073705			

Sequential Analysis of Variance:

Source	DF	SS	F	P
Linear	1	0.0065715	16.45	0.056
Quadratic	1	0.0000268	0.03	0.883

APPENDIX E

RESULTS OF CLASSIFICATION

Table E.1 The data of the 1st class.

Model	p_i (MPa)	σ_{ci} (MPa)	GSI	σ_z (MPa)	σ_{h1} (MPa)	σ_{h2} (MPa)	Class
97	0.42	100	20	2.7	2.7	1.35	1
98	2.44	100	20	8.1	8.1	4.05	1
99	6.78	100	20	16.2	16.2	8.1	1
100	0.31	100	20	2.7	2.7	2.7	1
101	1.8	100	20	8.1	8.1	8.1	1
102	5.1	100	20	16.2	16.2	16.2	1
103	0.74	100	20	2.7	2.7	4.05	1
104	4.08	100	20	8.1	8.1	12.15	1
105	10.99	100	20	16.2	16.2	24.3	1
106	1.3	100	20	2.7	2.7	5.4	1
107	6.78	100	20	8.1	8.1	16.2	1
108	17.76	100	20	16.2	16.2	32.4	1
109	0.13	100	40	2.7	2.7	1.35	1
110	1.22	100	40	8.1	8.1	4.05	1
111	4.05	100	40	16.2	16.2	8.1	1
112	0.08	100	40	2.7	2.7	2.7	1
113	0.87	100	40	8.1	8.1	8.1	1
114	2.93	100	40	16.2	16.2	16.2	1
115	0.28	100	40	2.7	2.7	4.05	1
116	2.24	100	40	8.1	8.1	12.15	1
117	7.06	100	40	16.2	16.2	24.3	1
118	0.57	100	40	2.7	2.7	5.4	1
119	4.05	100	40	8.1	8.1	16.2	1
120	12.13	100	40	16.2	16.2	32.4	1
121	0	100	60	2.7	2.7	1.35	1
122	0.46	100	60	8.1	8.1	4.05	1
123	2.18	100	60	16.2	16.2	8.1	1
124	0	100	60	2.7	2.7	2.7	1
125	0.27	100	60	8.1	8.1	8.1	1
126	1.5	100	60	16.2	16.2	16.2	1
127	0	100	60	2.7	2.7	4.05	1
128	1.06	100	60	8.1	8.1	12.15	1
129	4.14	100	60	16.2	16.2	24.3	1
130	0.1	100	60	2.7	2.7	5.4	1
131	2.18	100	60	8.1	8.1	16.2	1
132	7.66	100	60	16.2	16.2	32.4	1
133	0	100	80	2.7	2.7	1.35	1
134	0	100	80	8.1	8.1	4.05	1
135	0.35	100	80	16.2	16.2	8.1	1
136	0	100	80	2.7	2.7	2.7	1
137	0	100	80	8.1	8.1	8.1	1
138	0	100	80	16.2	16.2	16.2	1
139	0	100	80	2.7	2.7	4.05	1
140	0	100	80	8.1	8.1	12.15	1
141	1.54	100	80	16.2	16.2	24.3	1
142	0	100	80	2.7	2.7	5.4	1
143	0.35	100	80	8.1	8.1	16.2	1
144	3.76	100	80	16.2	16.2	32.4	1

Table E.2 The data of the 2nd class.

Model	p_i (MPa)	σ_{ci} (MPa)	GSI	σ_z (MPa)	σ_{h1} (MPa)	σ_{h2} (MPa)	Class
25	0.55	25	60	2.7	2.7	1.35	2
26	3.57	25	60	8.1	8.1	4.05	2
27	8.4	25	60	16.2	16.2	8.1	2
28	0.36	25	60	2.7	2.7	2.7	2
29	2.64	25	60	8.1	8.1	8.1	2
30	7.28	25	60	16.2	16.2	16.2	2
31	1.05	25	60	2.7	2.7	4.05	2
32	5.89	25	60	8.1	8.1	12.15	2
33	15.12	25	60	16.2	16.2	24.3	2
34	1.9	25	60	2.7	2.7	5.4	2
35	9.62	25	60	8.1	8.1	16.2	2
36	19.98	25	60	16.2	16.2	32.4	2
37	0	25	80	2.7	2.7	1.35	2
38	2.03	25	80	8.1	8.1	4.05	2
39	6.83	25	80	16.2	16.2	8.1	2
40	0	25	80	2.7	2.7	2.7	2
41	1.32	25	80	8.1	8.1	8.1	2
42	4.97	25	80	16.2	16.2	16.2	2
43	0.14	25	80	2.7	2.7	4.05	2
44	3.85	25	80	8.1	8.1	12.15	2
45	11.46	25	80	16.2	16.2	24.3	2
46	0.76	25	80	2.7	2.7	5.4	2
47	6.83	25	80	8.1	8.1	16.2	2
48	18.9	25	80	16.2	16.2	32.4	2
73	0.07	50	60	2.7	2.7	1.35	2
74	1.48	50	60	8.1	8.1	4.05	2
75	4.95	50	60	16.2	16.2	8.1	2
76	0.01	50	60	2.7	2.7	2.7	2
77	1.03	50	60	8.1	8.1	8.1	2
78	3.58	50	60	16.2	16.2	16.2	2
79	0.31	50	60	2.7	2.7	4.05	2
80	2.75	50	60	8.1	8.1	12.15	2
81	8.54	50	60	16.2	16.2	24.3	2
82	0.66	50	60	2.7	2.7	5.4	2
83	4.95	50	60	8.1	8.1	16.2	2
84	14.47	50	60	16.2	16.2	32.4	2
85	0	50	80	2.7	2.7	1.35	2
86	0.26	50	80	8.1	8.1	4.05	2
87	2.57	50	80	16.2	16.2	8.1	2
88	0	50	80	2.7	2.7	2.7	2
89	0	50	80	8.1	8.1	8.1	2
90	1.65	50	80	16.2	16.2	16.2	2
91	0	50	80	2.7	2.7	4.05	2
92	1.08	50	80	8.1	8.1	12.15	2
93	5.1	50	80	16.2	16.2	24.3	2
94	0	50	80	2.7	2.7	5.4	2
95	2.57	50	80	8.1	8.1	16.2	2
96	9.47	50	80	16.2	16.2	32.4	2

Table E.3 The data of the 3rd class. For classification, p_i of the 12th model was taken as 21.

Model	p_i (MPa)	σ_{ci} (MPa)	GSI	σ_z (MPa)	σ_{h1} (MPa)	σ_{h2} (MPa)	Class
3	13.96	25	20	16.2	16.2	8.1	3
6	11.23	25	20	16.2	16.2	16.2	3
8	8.94	25	20	8.1	8.1	12.15	3
9	18.93	25	20	16.2	16.2	24.3	3
11	15.49	25	20	8.1	8.1	16.2	3
12	21	25	20	16.2	16.2	32.4	3
15	10.35	25	40	16.2	16.2	8.1	3
18	9.3	25	40	16.2	16.2	16.2	3
21	18.24	25	40	16.2	16.2	24.3	3
23	13.29	25	40	8.1	8.1	16.2	3
24	18.9	25	40	16.2	16.2	32.4	3
54	7.95	50	20	16.2	16.2	16.2	3
57	15.9	50	20	16.2	16.2	24.3	3
60	19.8	50	20	16.2	16.2	32.4	3
69	12.07	50	40	16.2	16.2	24.3	3
72	17.58	50	40	16.2	16.2	32.4	3

Table E.4 The data of the 4th class.

Model	p_i (MPa)	σ_{ci} (MPa)	GSI	σ_z (MPa)	σ_{h1} (MPa)	σ_{h2} (MPa)	Class
145	0.19	200	20	2.7	2.7	1.35	4
146	1.31	200	20	8.1	8.1	4.05	4
147	4.03	200	20	16.2	16.2	8.1	4
148	0.14	200	20	2.7	2.7	2.7	4
149	0.96	200	20	8.1	8.1	8.1	4
150	2.97	200	20	16.2	16.2	16.2	4
151	0.36	200	20	2.7	2.7	4.05	4
152	2.31	200	20	8.1	8.1	12.15	4
153	6.87	200	20	16.2	16.2	24.3	4
154	0.66	200	20	2.7	2.7	5.4	4
155	4.03	200	20	8.1	8.1	16.2	4
156	11.61	200	20	16.2	16.2	32.4	4
157	0	200	40	2.7	2.7	1.35	4
158	0.49	200	40	8.1	8.1	4.05	4
159	1.93	200	40	16.2	16.2	8.1	4
160	0	200	40	2.7	2.7	2.7	4
161	0.34	200	40	8.1	8.1	8.1	4
162	1.37	200	40	16.2	16.2	16.2	4
163	0.06	200	40	2.7	2.7	4.05	4
164	0.99	200	40	8.1	8.1	12.15	4
165	3.61	200	40	16.2	16.2	24.3	4
166	0.19	200	40	2.7	2.7	5.4	4
167	1.93	200	40	8.1	8.1	16.2	4
168	6.63	200	40	16.2	16.2	32.4	4
169	0	200	60	2.7	2.7	1.35	4
170	0	200	60	8.1	8.1	4.05	4
171	0.7	200	60	16.2	16.2	8.1	4
172	0	200	60	2.7	2.7	2.7	4
173	0	200	60	8.1	8.1	8.1	4
174	0.43	200	60	16.2	16.2	16.2	4
175	0	200	60	2.7	2.7	4.05	4
176	0.19	200	60	8.1	8.1	12.15	4
177	1.64	200	60	16.2	16.2	24.3	4
178	0	200	60	2.7	2.7	5.4	4
179	0.7	200	60	8.1	8.1	16.2	4
180	3.44	200	60	16.2	16.2	32.4	4
181	0	200	80	2.7	2.7	1.35	4
182	0	200	80	8.1	8.1	4.05	4
183	0	200	80	16.2	16.2	8.1	4
184	0	200	80	2.7	2.7	2.7	4
185	0	200	80	8.1	8.1	8.1	4
186	0	200	80	16.2	16.2	16.2	4
187	0	200	80	2.7	2.7	4.05	4
188	0	200	80	8.1	8.1	12.15	4
189	0	200	80	16.2	16.2	24.3	4
190	0	200	80	2.7	2.7	5.4	4
191	0	200	80	8.1	8.1	16.2	4
192	0.53	200	80	16.2	16.2	32.4	4

Table E.5 The data of the 5th class.

Model	p_i (MPa)	σ_{ci} (MPa)	GSI	σ_z (MPa)	σ_{h1} (MPa)	σ_{h2} (MPa)	Class
1	1.42	25	20	2.7	2.7	1.35	5
2	5.73	25	20	8.1	8.1	4.05	5
4	1.22	25	20	2.7	2.7	2.7	5
5	4.92	25	20	8.1	8.1	8.1	5
7	2.47	25	20	2.7	2.7	4.05	5
10	3.31	25	20	2.7	2.7	5.4	5
13	1.02	25	40	2.7	2.7	1.35	5
14	4.44	25	40	8.1	8.1	4.05	5
16	0.75	25	40	2.7	2.7	2.7	5
17	3.75	25	40	8.1	8.1	8.1	5
19	1.71	25	40	2.7	2.7	4.05	5
20	7.7	25	40	8.1	8.1	12.15	5
22	2.8	25	40	2.7	2.7	5.4	5
49	0.85	50	20	2.7	2.7	1.35	5
50	4.12	50	20	8.1	8.1	4.05	5
51	9.3	50	20	16.2	16.2	8.1	5
52	0.63	50	20	2.7	2.7	2.7	5
53	3.13	50	20	8.1	8.1	8.1	5
55	1.41	50	20	2.7	2.7	4.05	5
56	6.52	50	20	8.1	8.1	12.15	5
58	2.34	50	20	2.7	2.7	5.4	5
59	9.37	50	20	8.1	8.1	16.2	5
61	0.4	50	40	2.7	2.7	1.35	5
62	2.61	50	40	8.1	8.1	4.05	5
63	7.44	50	40	16.2	16.2	8.1	5
64	0.28	50	40	2.7	2.7	2.7	5
65	1.91	50	40	8.1	8.1	8.1	5
66	5.56	50	40	16.2	16.2	16.2	5
67	0.75	50	40	2.7	2.7	4.05	5
68	4.44	50	40	8.1	8.1	12.15	5
70	1.35	50	40	2.7	2.7	5.4	5
71	7.44	50	40	8.1	8.1	16.2	5

APPENDIX F

COMPARISON OF REGRESSION EQUATIONS

Table F.1 Comparison of p_i/σ_{ci} by Phase2 to that of the regression equations.

Row	p_i/σ_{ci} by Phase2	pi/σ_{ci} by Eq. 45	pi/σ_{ci} by Eq. 50	Row	p_i/σ_{ci} by Phase2	pi/σ_{ci} by Eq. 45	pi/σ_{ci} by Eq. 50
1	0.049	0.045	0.032	**46**	0.007	0.015	0.007
2	0.099	0.054	0.054	**47**	0.013	0.017	0.000
3	0.041	0.022	0.000	**48**	0.001	-0.004	0.002
4	0.030	0.031	0.002	**49**	0.012	0.013	0.000
5	0.150	0.118	0.012	**50**	0.001	-0.002	0.001
6	0.068	0.040	0.003	**51**	0.009	0.020	0.001
7	0.022	0.008	0.000	**52**	0.029	0.053	0.004
8	0.143	0.077	0.019	**53**	0.003	0.000	0.000
9	0.014	0.017	0.005	**54**	0.022	0.027	0.001
10	0.106	0.104	0.034	**55**	0.006	0.003	0.000
11	0.042	0.025	0.008	**56**	0.005	-0.001	-0.001
12	0.076	0.034	0.011	**57**	0.022	0.025	0.004
13	0.081	0.063	0.065	**58**	0.003	0.006	0.002
14	0.053	0.089	0.114	**59**	0.015	0.038	0.012
15	0.006	0.011	0.028	**60**	0.011	0.012	0.004
16	0.154	0.115	0.146	**61**	0.001	-0.012	0.000
17	0.030	0.020	0.036	**62**	0.022	0.019	0.005
18	0.017	0.019	-0.004	**63**	0.004	0.011	0.014
19	0.013	0.024	0.000	**64**	0.015	0.037	0.060
20	0.063	0.067	0.080	**65**	0.004	0.004	0.018
21	0.028	0.028	0.003	**66**	0.038	0.050	0.073
22	0.047	0.032	0.006	**67**	0.001	0.006	0.090
23	0.008	0.005	0.000	**68**	0.007	0.015	0.006
24	0.052	0.040	0.001	**69**	0.001	0.007	0.069
25	0.006	0.009	0.000	**70**	0.005	0.018	0.002
26	0.038	0.053	0.004	**71**	0.015	0.034	0.012
27	0.015	0.014	0.000	**72**	0.002	0.008	0.052
28	0.027	0.018	0.000	**73**	0.012	0.021	-0.001
29	0.001	-0.010	-0.001	**74**	0.003	0.009	0.038
30	0.030	0.025	0.004	**75**	0.002	0.000	0.000
31	0.000	-0.005	0.000	**76**	0.010	0.013	0.000
32	0.021	0.038	0.012	**77**	0.002	0.004	0.000
33	0.072	0.104	0.034	**78**	0.007	0.020	0.001
34	0.006	-0.001	0.000	**79**	0.000	-0.006	0.003
35	0.055	0.051	0.018	**80**	0.005	0.007	0.000
36	0.013	0.004	0.001	**81**	0.018	0.027	0.001
37	0.005	0.011	0.014	**82**	0.001	-0.005	0.002
38	0.051	0.063	0.065	**83**	0.010	0.010	0.000
39	0.033	0.089	0.114	**84**	0.004	-0.001	-0.001
40	0.022	0.037	0.060	**85**	0.002	0.006	0.002
41	0.051	0.050	0.073	**86**	0.001	-0.007	0.000
42	0.004	0.010	0.030	**87**	0.008	0.012	0.004
43	0.024	0.028	-0.007	**88**	0.004	-0.004	0.000
44	0.003	0.013	0.017	**89**	0.017	0.019	0.005
45	0.018	0.034	0.012	**90**	0.003	0.004	0.018

APPENDIX G

SOME PHASE2 MODELS

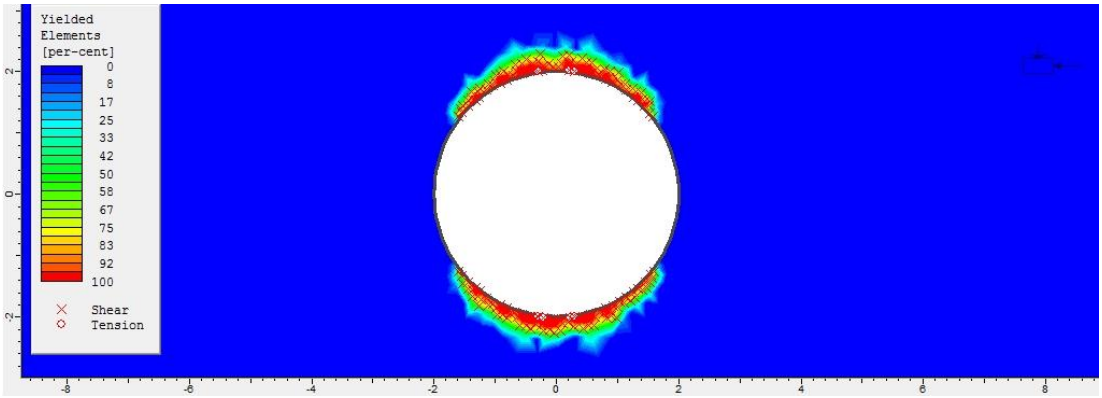

Figure G.1 The result (yielded elements) of model 25 without p_i.

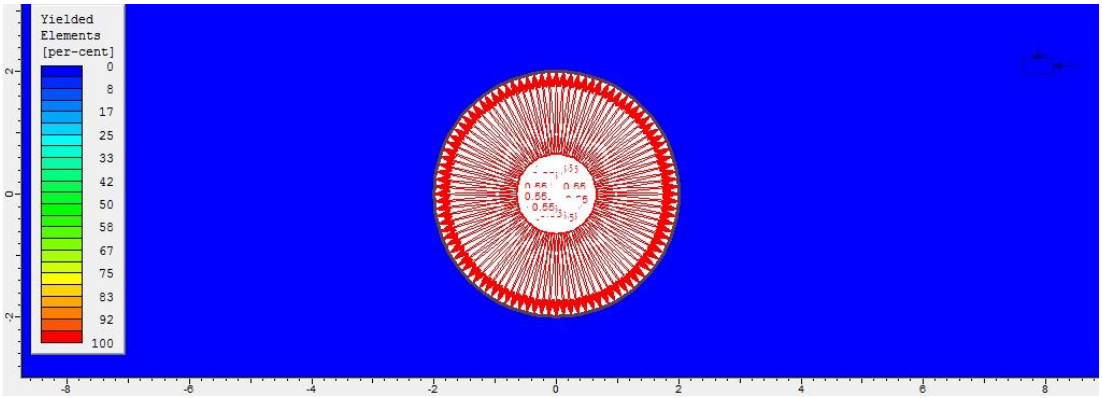

Figure G.2 The result (yielded elements) of model 25 with p_i of 0.55 MPa.

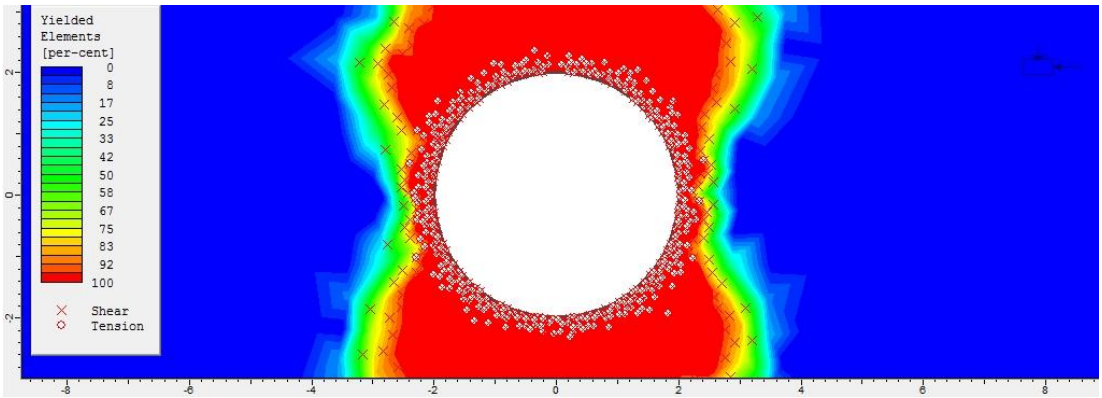

Figure G.3 The result (yielded elements) of model 72 without p_i.

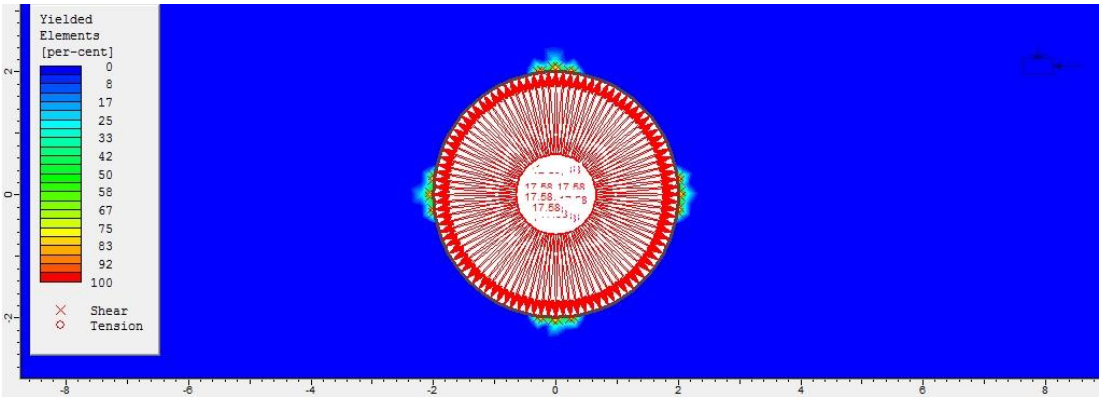

Figure G.4 The result (yielded elements) of model 72 with p_i of 17.58 MPa.

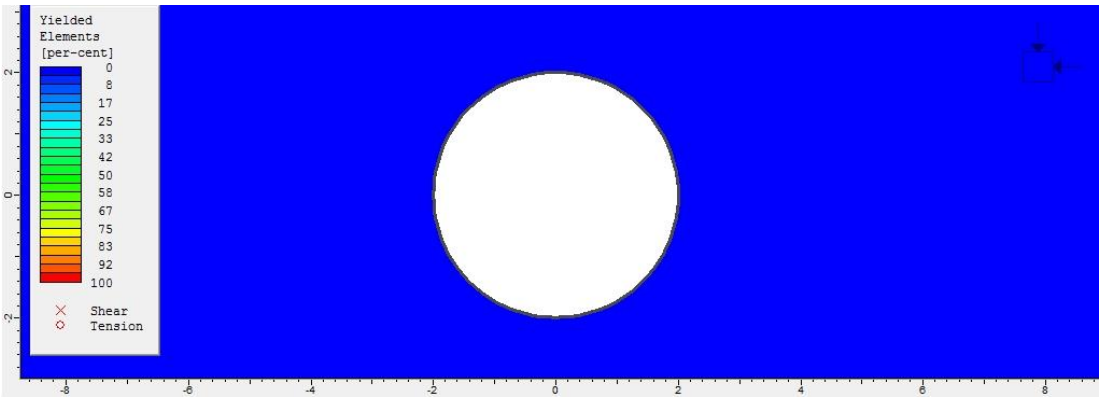

Figure G.5 The result (yielded elements) of model 138 without p_i.